SISSA
Scuola
Internazionale
Superiore di
Studi Avanzati

Physics Area - PhD course in
Astroparticle Physics

Phenomenological Aspects of Gravity beyond General Relativity

Candidate:
Lotte ter Haar

Advisor:
Enrico Barausse

Co-advisor:
Stefano Liberati

Academic Year 2021-22

Abstract

In the last decades, a large family of gravity theories beyond General Relativity has been proposed to address issues such as the nature of the cosmological acceleration, or the non-renormalizability of Einstein's theory. Alongside technical developments in the field of precision gravitational-wave astronomy, it is important to also deepen our theoretical knowledge about gravity. To assess whether these modified theories of gravity are viable, we should explore their phenomenology and gravitational-wave signatures. The work presented in this thesis touches upon two approaches in the field of modified gravity, which are adding a scalar degree of freedom in the gravitational sector or breaking Lorentz invariance. Some of the theories in the particularly popular class of scalar-tensor theories exhibit a so-called screening mechanism. We study the kinetic screening mechanism of a scalar-tensor theory with first-order derivative self-interactions (k-essence) in neutron stars. Then, we present a generalization of khronometric theory (which is the infrared limit of Hořava gravity) by applying the degeneracy program that was used to derive Degenerate Higher-Order Scalar-Tensor (DHOST) theories.

Publications

The research presented in this thesis is largely based on the following publications produced in scientific collaborations during my doctoral studies at the Scuola Internazionale Superiore di Studi Avanzati (SISSA):

- Chapter 3 and Chapter 4:
  - L. ter Haar, M. Bezares, M. Crisostomi, E. Barausse, and C. Palenzuela, "Dynamics of Screening in Modified Gravity," *Phys. Rev. Lett.* **126** no. 9, (2021) 091102, arXiv:2009.03354 [gr-qc].
  - M. Bezares, L. ter Haar, M. Crisostomi, E. Barausse, and C. Palenzuela, "Kinetic screening in nonlinear stellar oscillations and gravitational collapse," *Phys. Rev. D* **104** no. 4, (2021) 044022, arXiv:2105.13992 [gr-qc].
  - M. Bezares, R. Aguilera-Miret, L. ter Haar, M. Crisostomi, C. Palenzuela, and E. Barausse, "No Evidence of Kinetic Screening in Simulations of Merging Binary Neutron Stars beyond General Relativity," *Phys. Rev. Lett.* **128** no. 9, (2022) 091103, arXiv:2107.05648 [gr-qc].
- Chapter 5:
  - E. Barausse, M. Crisostomi, S. Liberati, and L. ter Haar, "Degenerate Hořava gravity," *Class. Quant. Grav.* **38** no. 10, (2021) 105007, arXiv:2101.00641 [hep-th].

Acknowledgements

First of all, I would like to thank Enrico for his active supervision, support, and constant encouragement which has been incredibly helpful throughout the course of my PhD. I am grateful to him for the scientific discussions we had, patiently teaching me the things I did not know yet and inspiring me to think critically along the way. I would also like to thank Stefano for sharing his knowledge and experiences with me, and showing me the importance of creative thinking. My deepest gratitude to both of them for giving me the opportunity to learn a great deal about physics, and the art of doing science. I would also like to express my gratitude to Prof. Claudia de Rham and Prof. Shinji Mukohyama for their careful reading of this thesis and useful comments to improve it.

I would also like to thank my colleagues in the GRAMS group for stimulating discussions and doing science together: Miguel, Marco, Sebastian, Mario, Nicola, Aron, Sourabh, Marcelo, Memo, Mateja, and Alexandru. A special thanks to Miguel for introducing me to the field of Numerical Relativity, and without whom many of the projects presented in this thesis would not have been possible. His positive attitude and constant willingness to help has made it an absolute pleasure to work with him. I also had the pleasure of working with Marco, whose insightful comments and intuitive approach in science have taught me a lot. Thank you to my external collaborators Carlos and Ricard as well.

These years would not have been the same without the amazing people I encountered in SISSA and Trieste, and who have turned into incredibly warm, loyal and supportive friends. I am infinitely thankful to Matteo, Nata, Miguel, Anto, Thanh, Giulio, Tommi, Gabri, Andrea, Valentina, Lara, Hasti, Farida, Titou, Riki, Memo, Alessandro, Oleg, Renata, Raquel, Kate, Linda, and Aybüke. Thank you for making me laugh, making me feel at home, and having conversations that always gave me

something to think about; for studying together, helping me when I asked, and making sure I drank enough coffee/limoncello; for learning Go with me, battling lockdown together, cooking incredible food, learning how to climb with me, and going on trips all over Italy together. Thinking of the countless joyous moments we shared brings a smile to my face. I look forward to the future encounters we will have, wherever in the world this may be.

Door naar Italië te verhuizen heb ik veel goede vrienden in Nederland achtergelaten. Hun support was echter zelfs op grote afstand voelbaar, velen van jullie heb ik ook in Triëst mogen verwelkomen, en ik kijk er altijd weer naar uit om jullie in Nederland te zien. Annanina, Melodi, Eva, Ruth, Karlijn, Hannah, Marion, Maaike, Tom en Thomas, bedankt voor alles. Ik wil vooral Mirte en Marieke bedanken, die als geen ander begrijpen hoe verwarrend natuurkunde kan zijn en welke uitdagingen dit vak te bieden heeft. Bedankt voor jullie onvoorwaardelijke steun, en waardevolle vriendschap.

Ik wil graag mijn diepe dankbaarheid uitspreken naar mijn ouders en zusjes, voor de steun die ik altijd heb gevoeld in mijn keuzes, en de aanmoediging wanneer het even niet mee zat. Lieve mam, pap, Anna, Floor, Sara en Mijntje, ik ben ontzettend dankbaar voor alles dat jullie voor me gedaan hebben. Fede, thank you for being an endless source of love and happiness, and never failing to cheer me up. Your faith in me makes me feel strong and supported, and I could not be more grateful for having you by my side.

Contents

Introduction

Although General Relativity is one of the most successful theories in physics, exploring gravity beyond Einstein's theory remains an important endeavour. With the recent detection of gravitational waves, we have now entered the era of precision gravitational-wave astronomy, which opens a new experimental window to probe the strong-field regime. To test the basic principles of General Relativity, it is necessary to deepen also our theoretical knowledge about gravity alongside these technical developments. Throughout the years, an extended variety of alternative theories of gravity has been proposed. A particularly popular branch concerns the field of scalar-tensor theories, in which a scalar degree of freedom is added to the gravitational sector. Alternatively, one can give up Lorentz invariance by selecting a preferred frame, which is for instance the case in Hořava gravity. In this work, we explore both of these directions.

Some scalar-tensor theories exhibit a so-called screening mechanism, which hides scalar fluctuations on small scales, but allows for deviations beyond. Screening mechanisms allow these theories to pass Solar-System tests, and are therefore crucial for their viability. Not much work has been done yet to study their workings in the strong-field/highly dynamical regime, which is the regime of interest for gravitational-wave observations. In this thesis, we aim to do precisely this, and investigate the kinetic screening mechanism of a scalar-tensor theory with first-order derivative self-interactions in neutron stars.

Whereas scalar-tensor theories are usually cosmologically motivated and aim to explain the origin of dark energy, other branches in the field of modified gravity were introduced due to theoretical objections to General Relativity. Einstein's theory is non-renormalizable, and therefore only predictive in the low energy regime. Lorentz-violating theories, such as Hořava gravity, attempt to address this issue. The form

of the action of these theories is constrained to avoid propagation of Ostrogradski modes. This is for instance the case for khronometric theory, which is the infrared limit of Hořava gravity. We apply the degeneracy program that was used to derive Degenerate Higher-Order Scalar-Tensor (DHOST) theories, and investigate whether this theory is unique.

Outline: In Chapter 1, we introduce the theory of General Relativity, and discuss its main solutions, e.g. compact objects (black holes and neutron stars), and gravitational waves. We summarize what classical tests the theory has passed, and how it is currently tested in gravitational-wave observatories. We also give a brief overview of modern cosmology. In Chapter 2, we motivate studies of gravity beyond General Relativity, and describe two branches in more detail, namely scalar-tensor theories and Lorentz-violating theories of gravity. In Chapter 3 and 4, we study a scalar-tensor theory named k-essence, and explore its screening mechanism (k-mouflage). We present static k-mouflage stars and their properties in Chapter 3, whereas Chapter 4 describes their dynamics (both in isolation and in binaries). In Chapter 5, we present a generalization of khronometric theory—which avoids the propagation of Ostrogradski modes by means of a suitable degeneracy condition—and study its phenomenology.

Notation and conventions: Throughout this thesis, we adopt the metric signature $(-+++)$. We present our work mostly in natural units where $\hbar = c = 1$, but sometimes use geometrized units for which $G = c = 1$. In Chapter 3 and 4, we differentiate between Einstein and Jordan frame quantities by using tilded symbols for the latter. In some sections, we use the short-hand notation $\varphi_\mu = \nabla_\mu \varphi$ and $\varphi_{\mu\nu} = \nabla_\mu \nabla_\nu \varphi$.

1 Fundamentals of Gravity

The direct detection of gravitational waves has offered us new opportunities to probe unknown physics, also in the field of gravity. More than ever, the question whether we correctly understand the nature of gravity and the Universe is a relevant one. In this chapter, we consider both the theoretical and observational foundation of the study of gravity. In Section 1.1, we discuss our modern interpretation of gravity and introduce the theory of General Relativity. We present compact object solutions and explain how General Relativity has been tested through observation. In Section 1.2, we describe the theory underlying gravitational-wave astrophysics, and give an overview of present and future gravitational-wave detectors. In Section 1.3, we briefly summarize the current status of modern cosmology, and discuss the problem of dark energy. This chapter provides a review of the most important topics that appear in this thesis, and is based on standard textbooks and lecture notes written by Carroll [5], Wald [6], Will [7], Misner, Thorne, and Wheeler [8], Maggiore [9], Reall [10], Tong [11], Rezzolla [12], and Baumann [13][1].

1.1 General Relativity

In 1915, Einstein wrote down the theory of General Relativity, and revolutionized our way of describing gravity. He did not interpret gravity as a force, but understood that a proper theory of gravity should be geometric. To this day, gravity is still most accurately described by General Relativity. In this section, we discuss how our understanding of gravity has changed throughout the years, describe compacts objects in this theory, and present some of the precision tests that General Relativity has passed.

[1] This list is by no means complete, and merely lists some of the author's favourites.

1.1.1 From Newton to Einstein

Understanding Special and General Relativity means accepting that our intuitive notions about the nature of space and time are simply not correct. To fully grasp why it is crucial to rewire the way we think about these concepts, we will first show where Newton's theory of gravity fails. In Newtonian gravity, the interaction between the gravitational field and matter is described by the Poisson equation

$$\nabla^2\Phi = 4\pi G\rho \,, \tag{1.1.1}$$

relating the gravitational potential Φ to the mass density ρ and Newton's gravitational constant G. The Green's function solution to the Poisson equation is

$$\Phi(\mathbf{x},t) = -G\int \mathrm{d}^3x' \frac{\rho(\mathbf{x}',t)}{|\mathbf{x}-\mathbf{x}'|} \,, \tag{1.1.2}$$

which for a point mass of mass M simplifies to $\Phi = -GM/r$. The acceleration is then given by the gradient of the potential, $\mathbf{a} = -\nabla\Phi$, and can be plugged into Newton's second law to find the famous inverse-square law of gravity as presented in his *Principia* [14]

$$\mathbf{F} = -\frac{GMm}{r^2}\mathbf{e}_r \,, \tag{1.1.3}$$

describing the gravitational force between two bodies of masses M and m separated by a vector $\mathbf{r} = r\mathbf{e}_r$.

Although Newton's universal law of gravity accurately describes much of what we see on Earth or in the Solar System, it has some serious flaws as well. The most disturbing feature of describing gravity in this manner is that any change in the mass density ρ propagates instantaneously through space. A similar problem was found in Coulomb's law of electrostatics, leading Maxwell to introduce his equations of electrodynamics, in which electric and magnetic fields propagate. Not much later, Michelson and Morley conducted their well-known experiment that served not only as strong evidence against the—at the time—popular belief light propagated through an aether, but also led to the surprising conclusion that the speed of light c is constant in every direction. Clearly, the Galilean transformations through which one transforms between reference frames in Newtonian gravity are inconsistent with this observation. One has to use Lorentz transformations, that mix space and time coordinates, instead, and it turned out that the Maxwell equations were in fact Lorentz invariant.

These scientific findings inspired Einstein in 1905 to write down his theory of Special Relativity, where he assumes the following two postulates

1. *Principle of relativity: The laws of physics take the same form in every inertial frame of reference,*

2. *Invariance of the speed of light: Light is always propagated in vacuum with a definite velocity c that is independent of the state of motion of the emitting body,*

and regards the relationship between space and time.

To understand better the consequences of Special Relativity and to introduce some geometric concepts that will be useful later when we introduce General Relativity, we compare its causal structure to that of Newtonian gravity[2]. In both theories, we can consider space and time to be composed of *events*, with every event being a point of space at an instant of time. All events are characterized by four numbers: three for the spatial position and one for the time. This is what we can think of as *spacetime*, which in General Relativity is described in a more mathematically precise manner as a four-dimensional manifold. The critical difference in the causal structure of Newtonian gravity and Special Relativity becomes clear when one considers the notion of *simultaneity*. In Newtonian gravity, there is a natural and observer-independent way of defining events happening at the same time, these events together define a three-dimensional set.

In Special Relativity, however, the notion of simultaneity is subtler and not absolute. We can define two intertial observers, e.g. observers moving in a non-accelerated manner, and let each of them label events in spacetime. When observer O' is moving with a velocity v in the x-direction of observer O, we relate their respective labelling through the following Lorentz transformations:

$$t' = \gamma \left(t - \frac{vx}{c^2} \right) \ , \tag{1.1.4}$$

$$x' = \gamma \left(x - vt \right) \ , \tag{1.1.5}$$

$$y' = y \ , \tag{1.1.6}$$

$$z' = z \ , \tag{1.1.7}$$

[2]We follow Wald's [6] explanation in the next two paragraphs.

where c is the speed of light and $\gamma = 1/\sqrt{1-(v/c)^2}$ is the Lorentz factor. A fundamental point in Special Relativity is that there are no preferred inertial observers, meaning the notion of time and space (and intervals thereof) are not absolute[3]. Thus, there are no absolute three-dimensional surfaces like in Newtonian gravity, the causal relation of an event p to other events is rather described by a *light cone*. Events that lie on the boundary of the future light cone of p can only be reached by a light signal emitted from p (similarly for the past light cone). There are also events that are neither in the future nor past of p, these are said to be spacelike related to the event. Observers can still define events to occur simultaneously, but their definition will depend on their motion, and different observers will disagree on the simultaneity of events. Lastly, we point out an absolute and observer-independent quantity in spacetime, one that truly measures its intrinsic structure, which is the spacetime interval

$$\mathrm{d}s^2 = -c^2\mathrm{d}t^2 + \mathrm{d}x^2 + \mathrm{d}y^2 + \mathrm{d}z^2 \ , \tag{1.1.8}$$

and describes the *Minkowski metric* $\eta_{\mu\nu} = \mathrm{diag}(-1,+1,+1,+1)$.

General Relativity was born out of a need to introduce the concept of relativity in gravity, but its development took a different road than Special Relativity and takes its origin in what is called the *weak equivalence principle*. It had been known for a long time that objects with different masses fall at the same rate, or more formally put, the inertial mass m_I and gravitational mass m_G have been measured in experiments to be practically equal [15]

$$\frac{m_I}{m_G} = 1 \pm 10^{-15} \ . \tag{1.1.9}$$

However, the interpretation of these masses is different: m_G is the source for the gravitational field, whereas m_I characterizes the dynamical response of an object to any forces, and in Newtonian gravity there is no reason for their values to be so fine-tuned. Instead, the weak equivalence principle takes this equality to be exact

$$m_I = m_G \ , \tag{1.1.10}$$

and the universality of free-fall a fundamental property of the gravitational field. In General Relativity, this principle is extended by means of a thought experiment conducted by Einstein (which he himself referred to as his "happiest thought"). The

[3]This leads to counter-intuitive phenomena such as time dilation, Lorentz contraction, and the twin paradox.

experiment goes as follows: Imagine you are confined in a box, unable to observe what is happening outside of the box, and are challenged to determine the laws of physics. You have been given two test particles, with which you could for instance measure the gravitational field. Indeed, you drop the two particles, and they fall in the same way, confirming what you know about gravity. Here comes the catch though: Imagine now there is no gravitational field, but that instead the box itself is moving with an acceleration $\mathbf{a} = -\mathbf{g}$. Surprisingly, your observations would be exactly the same as before. Einstein correctly understood that, in regions of spacetime where the gravitational field is homogeneous, there is no way to distinguish between being in a gravitational field or uniformly accelerated frame. Said differently, in small enough regions of spacetime, the laws of physics are those of Special Relativity, and it is impossible to detect gravity by means of *local* experiments. This insight is what we call the *Einstein equivalence principle*[4]. The fact that the gravitational field manifests itself differently in local and global regions of spacetime hints at an even deeper understanding of gravity. Reminiscent of curved manifolds in geometry, where a globally curved manifold seems flat locally, Einstein concluded that General Relativity must be a geometric theory and that gravity should not be interpreted as a force but rather as the curvature of spacetime.

We leave out a discussion on differential geometry in this work, and jump to the mathematical description of General Relativity (note that from now on we take $c = 1$, unless stated otherwise explicitly). At the centre of the theory are the Einstein field equations, but before we present those we introduce some definitions. Just like in Special Relativity, we can define a metric $g_{\mu\nu}(\mathbf{x})$ through the invariant spacetime interval

$$\mathrm{d}s^2 = g_{\mu\nu}(\mathbf{x})\mathrm{d}x^\mu \mathrm{d}x^\nu \ , \tag{1.1.11}$$

where $g_{\mu\nu} \to \eta_{\mu\nu}$ locally. The line element (1.1.11) is invariant under coordinate transformations, making sure General Relativity respects *general covariance* or *diffeomorphism invariance*. The amount of curvature of a spacetime is quantified by the Riemann tensor

$$R^\rho{}_{\sigma\mu\nu} = \partial_\mu \Gamma^\rho_{\nu\sigma} - \partial_\nu \Gamma^\rho_{\mu\sigma} + \Gamma^\rho_{\mu\lambda}\Gamma^\lambda_{\nu\sigma} - \Gamma^\rho_{\nu\lambda}\Gamma^\lambda_{\mu\sigma} \ , \tag{1.1.12}$$

whose contractions with the metric $R_{\mu\nu}$ and R are called the Ricci tensor and scalar,

[4]There are additional variants of equivalence principles that include the self-gravity of spatially-extended objects, but those will not be discussed here.

respectively, and where

$$\Gamma^{\sigma}_{\mu\nu} = \frac{1}{2} g^{\sigma\rho} \left(\partial_\mu g_{\nu\rho} + \partial_\nu g_{\rho\mu} - \partial_\rho g_{\mu\nu} \right) \ , \tag{1.1.13}$$

is the Christoffel symbol, also referred to as the Levi-Civita connection. The Einstein equations are then

$$G_{\mu\nu} = 8\pi G T_{\mu\nu} \ , \tag{1.1.14}$$

where the Einstein tensor $G_{\mu\nu} = R_{\mu\nu} - \frac{1}{2} R g_{\mu\nu}$ describes the geometry of the spacetime, and the energy-momentum tensor $T_{\mu\nu}$ describes the matter sector. The action that yields these equations is the Einstein-Hilbert action, e.g.

$$S_{EH} = \frac{1}{16\pi G} \int \mathrm{d}^4 x \sqrt{-g} \ R \ . \tag{1.1.15}$$

From the Einstein field equations it is also understood that it is matter that is sourcing the curvature of spacetime. When one considers the contracted Bianchi identity $\nabla_\mu G^{\mu\nu} = 0$, which leads to $\nabla_\mu T^{\mu\nu} = 0$, it becomes clear that this interaction goes both ways and that spacetime in turn influences the evolution of matter[5]. In general, the Einstein equations are not easy to solve, and it took years for most solutions to be found. The next sections will be devoted to present a few of them.

1.1.2 Black Holes

We start by presenting some vacuum solutions, e.g. solutions for which matter is absent. Rewriting the Einstein equations (1.1.14) as

$$R_{\mu\nu} = 8\pi G \left(T_{\mu\nu} - \frac{1}{2} T g_{\mu\nu} \right) \ , \tag{1.1.16}$$

it is clear that vacuum solutions are those for which the Ricci tensor vanishes

$$R_{\mu\nu} = 0 \ . \tag{1.1.17}$$

The first vacuum solution was actually found shortly after the development of General Relativity, which was by Schwarzschild in 1916. He presented a spherically symmetric static solution called the Schwarzschild metric, which in polar coordinates $\{t, r, \theta, \phi\}$ takes the form

$$\mathrm{d}s^2 = -\left(1 - \frac{2GM}{r}\right) \mathrm{d}t^2 + \left(1 - \frac{2GM}{r}\right)^{-1} \mathrm{d}r^2 + r^2 \mathrm{d}\Omega^2 \ , \tag{1.1.18}$$

[5] Or, to quote Wheeler, "matter tells spacetime how to curve, spacetime tells matter how to move."

where $\mathrm{d}\Omega^2 = \mathrm{d}\theta^2 + \sin^2\theta \mathrm{d}\phi^2$ is the metric on a unit two-sphere. The constant M is interpreted as the mass of the gravitating object. In the absence of matter this object is referred to as a *black hole*, but it should be noted that the Schwarzschild solution describes the spacetime in the exterior of any spherical body such as a star.

Some observations about this metric are in place. First, it turns out this is the unique spherically symmetric vacuum solution to the Einstein equations: this result is known as *Birkhoff's theorem*. Then, there are two radii of interest in this metric, which are at $r = 0$ and $r = 2GM$. The first one represents a *singularity*, a missing point in the manifold where curvature becomes infinite[6] and the metric is not well-defined. Also at $r = 2GM$ the metric seems singular, but this apparent singularity can be removed by choosing appropriate coordinates, such as Eddington-Finkelstein coordinates. Instead, this radius represents a point of no return: any particle or object following a trajectory at $r < 2GM$ is unable to cross this so-called *event horizon* and escape to infinity. Said differently, at the event horizon the gravitational field is so strong that one's escape velocity would need to exceed the speed of light. A black hole can then be defined as a region of spacetime that is separated from infinity by an event horizon. Lastly, one can check how the Schwarzschild metric is related to the Minkowski metric. As expected, we recover Minkowski space when $M \to 0$, but we find that for $r \to \infty$ the same is true. This property of the metric is known as *asymptotic flatness*.

We now generalize the Schwarzschild solution by giving up on spherical symmetry, and look for axial symmetric static solutions instead. It took quite some years for this solution to be discovered, but it was finally introduced by Kerr in 1963. The Kerr metric he wrote down looks like this in Boyer-Lindquist coordinates $\{t, r, \theta, \phi\}$[7]:

$$\begin{aligned}\mathrm{d}s^2 = &-\left(1 - \frac{2Mr}{\Sigma}\right)\mathrm{d}t^2 - \frac{4aMr}{\Sigma}\sin^2\theta \mathrm{d}t\mathrm{d}\phi + \frac{\Sigma}{\Delta}\mathrm{d}r^2 + \Sigma \mathrm{d}\theta^2 \\ &+ \left(r^2 + a^2 + \frac{2Mr}{\Sigma}a^2 \sin^2\theta\right)\sin^2\theta \mathrm{d}\phi^2 \,, \end{aligned} \tag{1.1.19}$$

[6]The quantity that becomes infinite is the Kretschmann scalar given by $\mathcal{K} = R_{abcd}R^{abcd}$.

[7]Note that these are not the same as the polar coordinates we used for the Schwarzschild solution: if we keep the angular momentum per unit mass a fixed but let $M \to 0$, we do recover flat space but not in polar coordinates.

with

$$\Delta \equiv r^2 - 2Mr + a^2\,, \qquad \Sigma \equiv r^2 + a^2\cos^2\theta \qquad \text{and} \qquad a \equiv J/M\,, \tag{1.1.20}$$

where J is the angular momentum of the black hole. Just like a Schwarzschild black hole, Kerr black holes possess a singularity and event horizon. As a consistency check, one can check that this metric collapses to the Schwarzschild one for $a \to 0$. Although until now we have assumed the vacuum solutions do not carry any electric or magnetic charges Q and P, this does not necessarily have to be the case. The metrics describing charged black holes are derived by replacing $2GM \to 2GM - G(Q^2 + P^2)/r$ in the Schwarzschild, respectively Kerr, solution to obtain the Reissner-Nordström metric for non-rotating, charged black holes, respectively Kerr-Newman metric for rotating, charged black holes.

In terms of intrinsic properties of the black hole, these metrics cannot be generalized any further. Therefore, any black hole in General Relativity is uniquely characterized by only three parameters: its mass, its angular momentum and its charge. This is what we call a *no-hair theorem*. As we will see later, no-hair theorems also exist for theories beyond General Relativity. This also means that for astrophysical black holes—and for instance mergers leading to a new black hole—all higher multipoles will be radiated away, and the resulting black hole will relax to a stable, axisymmetric (Kerr or Kerr-Newman) state.

1.1.3 Neutron Stars

We already mentioned that the exterior solution for any spherical body, including stars, is the Schwarzschild solution. This leaves us with the task of describing the interior of such objects. The following derivation can be found in standard text books (see e.g. [5]), and will only be described briefly. We take a general spherically symmetric static ansatz for the metric

$$\mathrm{d}s^2 = -\alpha(r)^2\mathrm{d}t^2 + a(r)^2\mathrm{d}r^2 + r^2\mathrm{d}\Omega^2\,, \tag{1.1.21}$$

where $a(r)$ and $\alpha(r)$ are functions depending only on r, and consider a non-zero energy-momentum tensor, modelling the star as a perfect fluid

$$T_{\mu\nu} = (\rho + p)\,u_\mu u_\nu + p g_{\mu\nu}\,, \tag{1.1.22}$$

where ρ and p, the energy density and the pressure respectively, are functions of r, and u_μ is the four-velocity. The four-velocity will be pointed in the same direction as the Killing vector associated with the static symmetry of our set-up, meaning it will be timelike. Normalizing it to $u^\mu u_\mu = -1$, we have $u_\mu = (-\alpha, 0, 0, 0)$. We now plug in these elements in the Einstein equations (1.1.14), and obtain three independent relations. By considering the conservation of the energy-momentum tensor, e.g. $\nabla_\mu T^{\mu\nu} = 0$, and identifying

$$\alpha(r) = e^{\Phi(r)} \,, \qquad a(r) = \left(1 - \frac{2m(r)}{r}\right)^{-1/2} \,, \tag{1.1.23}$$

we can write down a differential equation for m, Φ and p:

$$\frac{dm}{dr} = 4\pi r^2 \rho \,, \tag{1.1.24}$$

$$\frac{d\Phi}{dr} = \frac{m + 4\pi r^3 p}{r(r-2m)} \,, \tag{1.1.25}$$

$$\frac{dp}{dr} = -\frac{(\rho + p)(Gm + 4\pi G r^3 p)}{r(r - 2Gm)} \,. \tag{1.1.26}$$

Equation (1.1.26) is the *Tolman-Oppenheimer-Volkoff equation* of hydrostatic equilibrium. To be able to solve this system of coupled ordinary differential equations, we need to close it with an equation relating the pressure p and energy density ρ, a so-called *equation of state*. Since the conditions in astrophysical systems are so different from the ones on Earth, we generally do not know the exact relation between these quantities. Nevertheless, we know that by good approximation they obey a polytropic equation of state

$$p = K\rho_0^\Gamma \,, \qquad p = (\Gamma - 1)\rho_0 \epsilon \,, \tag{1.1.27}$$

where K is a constant of proportionality, ρ_0 the baryonic density, ϵ the specific internal energy, and $\Gamma = (n+1)/n$ with n the polytropic index, whose values depend on the type of star that is being modelled. Now that the system is complete it can be solved, which is a task generally performed numerically. A similar approach is taken to describe stellar solutions in theories beyond General Relativity (see Chapter 3).

Neutron stars are the most compact stars we know to exist in our Universe, with a typical mass of $\sim 1.4\ M_\odot$ and radius of ~ 10 km. The formation and evolution of massive stars are complex processes, which depend mostly on their initial mass

and metallicity (see [16] for details). Stars with an initial mass greater than 8 $M_\odot$ have the potential to form a neutron star through a supernova explosion (stars with a lower initial mass may evolve in e.g. a white dwarf). After the supernova explosion, the core collapses to a remnant, which we call a neutron star. However, if the initial mass of the star is above 25 $M_\odot$, the material ejected by the supernova explosion can fall back on the core, causing the star to evolve to a black hole through a so-called fallback process. Direct collapse to black holes is possible for stars with initial masses between 40–100 $M_\odot$. Other interesting objects are pulsars, which are rapidly rotating and highly magnetized neutron stars, that due to a misalignment of their magnetic and rotation axis emit radio pulses from their magnetic poles (the beams can only be detected if they are directed towards the Earth, this is called the "lighthouse" effect) [17–19].

1.1.4 Testing Gravity

Since its introduction, General Relativity has been tested in a multitude of ways. In this section, we will only briefly discuss a few of these tests, see [7] for a more detailed review. The classical tests are done in the weak-field regime[8], with experiments taking place in our Solar System. The standard tool in this regime to compare predictions from different theories of gravity is the parametrized post-Newtonian (PPN) formalism. It is based on the post-Newtonian (PN) expansion, which assumes slow motion and weak gravity, allowing an expansion of the Einstein equations in terms of v/c. By doing this, one finds that the leading order in the expansion gives Newtonian gravity, whereas the higher order terms describe relativistic corrections. The PPN formalism is a theory-agnostic version of this expansion that explicitly parametrizes how any general theory of gravity can be different from Newtonian gravity.

Corrections are generally controlled by ten dimensionless parameters, a more detailed treatment of these can be found in Appendix B. The two most relevant ones for a popular branch of modified gravity models, scalar-tensor theories (see Section 2.2), are

[8] Whether an object is weakly- or strongly-gravitating can be quantified by its compactness. The compactness is a dimensionless parameter that for weakly-gravitating bodies of mass M and radius R takes the value $C = GM/R \ll 1$.

γ and β, that appear in the metric functions at first and second order, respectively [20]:

$$g_{tt}(r) = -1 + \frac{2GM}{r} - 2\left(\beta - \gamma\right)\left(\frac{GM}{r}\right)^2 + \mathcal{O}\left(r^{-3}\right) \ , \tag{1.1.28}$$

$$g_{rr}(r) = 1 + 2\gamma\frac{GM}{r} + \mathcal{O}\left(r^{-2}\right) \ . \tag{1.1.29}$$

In these expressions, we are working in polar coordinates and expanding around a spherically symmetric body of mass M. The parameter γ can be physically interpreted as the amount of spatial curvature induced by a unit mass, whereas β represents the non-linearity of the gravitational potential at the first post-Newtonian order (1PN). In General Relativity both of these parameters are unity, which is consistent with the strongest experimental constraints: $|\gamma - 1| = (2.1 \pm 2.3) \times 10^{-5}$ and $|\beta - 1| = (0.3 \pm 1.3) \times 10^{-4}$ [21, 22]. However, in alternative theories of gravity these parameters might be different from one.

The classical tests used in Solar-System experiments to determine the PPN parameters include the perihelion precession of Mercury, deflection of light, Shapiro time-delay and the Nordtvedt effect. The anomalous orbit of Mercury had been known since the 1850s, but remained unexplained until the introduction of General Relativity. Einstein himself computed the precession of Mercury's orbit in his theory, and predicted an anomalous rate of $43.0\,''$/century[9] [23]. This is in excellent agreement with observation, and provided the first successful prediction of General Relativity. Combined with measurements of γ by the Cassini experiment, this effect can be used to constrain β. The parameter γ can be constrained by using another test proposed by Einstein in 1911 [24], namely the deflection of light (and the Shapiro time-delay effect, discussed in the next paragraph). The bending of light by the Sun (or any massive object) due to curved spacetime is probably one of the most famous predictions by the theory, and was experimentally confirmed in 1919 by Sir Arthur Eddington and collaborators during a Solar eclipse [25]. In the PPN formalism, a light ray passing the Sun at an impact parameter b is deflected by an angle [7]

$$\delta\theta = \frac{1}{2}\left(1 + \gamma\right)\frac{4M_\odot}{b}\left(\frac{1 + \cos\theta_0}{2}\right) \ , \tag{1.1.30}$$

with θ_0 the angle between the Earth-Sun line and the path of the photons, and $M_\odot$ the solar mass. This effect has now been measured in several experiments and used

[9] We use $''$ to denote arcseconds.

to constrain γ [26], with a value of $|\gamma - 1| \simeq 2 \times 10^{-4}$ being obtained with Very-Long-Baseline Interferometry (VLBI) techniques collecting light coming from quasars bent by the Sun [27]. In VLBI, observations from different telescopes on Earth or in space are cross-correlated, which results in a telescope with a much larger effective size. This dramatically improves the angular resolution with respect to observations performed with just one telescope, and makes VLBI a very powerful tool.

When light passes a massive object, its trajectory is not only bent, it is also slowed down from the perspective of an observer far away from the sources—this is the Shapiro time-delay effect. It was first predicted in 1964, by Irwin Shapiro, who also proposed an observational test for the effect [28]. He suggested to bounce radio pulses off the surface of Venus and Mercury, and measure the time for the signal to arrive back, predicting there should be a measurable time delay due to the presence of the Sun given by [7]:

$$\delta t = 2(1+\gamma) M_\odot \frac{4 d_p d_E}{b^2} \,, \tag{1.1.31}$$

where d_p (d_E) is the distance between the Sun and the planet (Earth). These tests were successfully performed in 1966–1967, measuring the predicted time-delay. More recent studies use artificial satellites rather than planets to reflect the radar signals, which has resulted in the strongest bound on γ so far by the Cassini spacecraft [21]. The last classical test we will discuss here is based on the Nordtvedt effect, which refers to the possible violation of the strong equivalence principle [29, 30]. This principle is a combination of the Einstein equivalence principle and an extension of the weak equivalence principle to objects with non-negligible self-gravity. Although General Relativity satisfies these conditions, many alternative theories of gravity violate it, by for instance predicting a space-dependent gravitational constant. Ignoring preferred-frame effects, the Nordtvedt effect is parametrized by [7]

$$\eta = 4\beta - \gamma - 3 \,. \tag{1.1.32}$$

The Nordtvedt effect would result in a polarization of the Moon's orbit in the direction of the Sun. It is classically tested by continuously monitoring the Earth-Moon distance through reflecting laser pulses on a mirror placed on the surface of the Moon during the Apollo 11 mission, an approach still adopted by the Lunar Laser Ranging experiment to this day [22].

More recently, we have also started testing General Relativity in regions with a strong gravitational field, such as around compact objects[10]. Historically, we have used binary pulsars to probe strong gravity. The discovery of the Hulse-Taylor binary led to the first indirect detection of gravitational waves (see the next section) [31], proving their existence as predicted by General Relativity. Nowadays, there is an additional channel to test General Relativity in the strong-field regime, which is through the LIGO/Virgo observations of black hole and neutron star binary coalescences [32–37]. These are violent events that produce a distinct gravitational-wave signal, that allows for precision tests in the gravitational sector [38–42]. Gravitational waves can be used to study gravity in a theory-agnostic way through parametrized tests, inspiral-merger-ringdown (IMR) consistency tests, or gravitational-wave propagation tests (see [43] for a review). Parametrized tests are model-independent and modify the General Relativistic waveform template in a general manner. The parameters associated to these deviations can then be constrained with parameter estimation techniques. These tests can be easily applied to some modified gravity models, as the mapping between these parameters and their theoretical constants is known. Then, in IMR consistency tests, one checks whether the physical properties—e.g. the mass and spin of the remnant black hole—of the system as extracted from different parts of the gravitational-wave signal coincide. Lastly, we can explore whether there are any deviations from General Relativity in the propagation of gravitational waves, for instance by extracting the (modified) dispersion relation of the graviton.

Long before the first detection of gravitational waves, we have been observing compact objects in the electromagnetic spectrum. Electromagnetic tests are important because they allow us to probe much larger systems than those observed by the LIGO/Virgo observatories. A way to test gravity in the strong-field regime is by detecting X-ray radiation coming from the accretion disks of black holes [44], which can be observed both around stellar-mass and super-massive black holes. Super-massive black holes are also being probed in the radio spectrum. In 2017, the first direct observations of black holes were made by a network of radio telescopes called the Einstein Horizon Telescope (EHT), which took the famous image of M87* [45], and the recently published image of Sgr A* (the black hole in the centre of our Milky Way) [46]. The images capture the black hole shadow, a dark region caused by gravi-

[10]Black holes have a compactness between $0.5 \leq C \leq 1$, whereas for neutron stars the compactness can range between $C \sim 0.1 - 0.3$.

tational light bending and photon capture at the event horizon. Although not precise enough yet, in the future the technique of black hole imaging might contribute to precision measurements of the gravitational field.

1.2 Gravitational-Wave Astrophysics

Another interesting vacuum solution to the Einstein equations that we have not touched upon yet are gravitational waves. Einstein already predicted the existence of gravitational waves in General Relativity, but it took almost a century for them to be detected. Finally, on 14 September, 2015, gravitational waves were observed, which revolutionized the field of astrophysics, allowing us now to probe the Universe both with electromagnetic and gravitational-wave observations. In this section, we will introduce the theoretical foundations of gravitational waves, and then discuss the present and future gravitational-wave observatories.

1.2.1 Gravitational Waves

We will introduce the notion of gravitational waves by considering the linearized Einstein equations, meaning we consider linear perturbations over a flat background metric[11]

$$g_{\mu\nu} = \eta_{\mu\nu} + h_{\mu\nu} \ , \tag{1.2.1}$$

with $|h_{\mu\nu}| << 1$, e.g. the gravitational field is weak and can be regarded as a perturbation on top of the Minkowski metric, and work at leading order in the perturbations. With some straightforward tensor algebra, one can then derive the linearized Einstein equations:

$$\partial^\sigma \partial_\nu h_{\sigma\mu} + \partial^\sigma \partial_\mu h_{\sigma\nu} - \partial_\mu \partial_\nu h - \Box h_{\mu\nu} + \eta_{\mu\nu}(\Box h - \partial^\rho \partial^\lambda h_{\rho\lambda}) = 16\pi G T_{\mu\nu} \ , \tag{1.2.2}$$

where $\Box \equiv \eta^{\alpha\beta}\partial_\alpha \partial_\beta$ is the flat-space d'Alembertian. For future convenience we also define $\bar{h}_{\mu\nu} = h_{\mu\nu} - \frac{1}{2} h \eta_{\mu\nu}$.

The decomposition (1.2.1) of the metric into a Minkowski background plus a perturbation is not unique. Under an infinitesimal coordinate change $x^\mu \to x^\mu + \xi^\mu(x)$, the

[11] If one omits the weak-field approximation and considers the full non-linear equations instead, this treatment is complicated considerably. However, with more rigorous methods one can find that the results are the same as in this section.

change in the metric, $\delta g_{\mu\nu} = -(\partial_\mu \xi_\nu + \partial_\nu \xi_\mu)$, can be interpreted as a transformation of the perturbation $h_{\mu\nu}$, e.g. $h_{\mu\nu} \to h_{\mu\nu} - \partial_\mu \xi_\nu - \partial_\nu \xi_\mu$, which for $\bar{h}_{\mu\nu}$ becomes

$$\bar{h}_{\mu\nu} \to \bar{h}_{\mu\nu} - \partial_\mu \xi_\nu - \partial_\nu \xi_\mu + \eta_{\mu\nu} \partial^\sigma \xi_\sigma \, . \tag{1.2.3}$$

Much like the electromagnetic tensor in Maxwell's theory, $F_{\mu\nu} = \partial_\mu A_\nu - \partial_\nu A_\mu$, is invariant under the gauge transformation $A_\mu \to A_\mu + \partial_\mu \lambda$, the linearized Riemann tensor is invariant under the gauge transformation (1.2.3). The usual procedure in electromagnetism is to impose a gauge condition, for instance the Lorentz gauge $\partial^\mu A_\mu = 0$, and find the solutions to the Maxwell equations. Similarly, in linearized General Relativity we can pick the Lorenz gauge[12]

$$\partial^\mu \bar{h}_{\mu\nu} = 0 \, , \tag{1.2.4}$$

in which the linearized Einstein equations (1.2.2) take on the relatively simple form

$$\Box \bar{h}_{\mu\nu} = -16\pi G T_{\mu\nu} \, , \tag{1.2.5}$$

which is a wave equation sourced by the energy-momentum tensor.

First, we take a look at the freely-propagating degrees of freedom of the gravitational field, e.g. solutions to the vacuum equation, $\Box \bar{h}_{\mu\nu} = 0$. A plane-wave solution reads

$$\bar{h}_{\mu\nu} = \mathrm{Re}\left(H_{\mu\nu} e^{i k_\sigma x^\sigma} \right) \, , \tag{1.2.6}$$

where $H_{\mu\nu}$ is a complex polarization matrix, and k^σ is the (real) wave vector. By plugging in this solution, we see that k^σ is a null vector, telling us that gravitational waves propagate at the speed of light. We can now study this solution, and determine how many degrees of freedom the gravitational field actually propagates. Naively, one would say that there are ten degrees of freedom (from the symmetric polarization matrix), however, we should not forget about the gauge symmetry of the theory. The Lorenz gauge implies

$$k^\mu H_{\mu\nu} = 0 \, , \tag{1.2.7}$$

which means that the polarization is transverse to the direction of propagation, and only six degrees of freedom are left. It turns out we have further freedom in our choice of gauge, which becomes clear by taking a closer look at the solutions for ξ_μ . The gauge transformation (1.2.3) leaves the solution in the Lorenz gauge if

$$\Box \xi_\mu = 0 \, . \tag{1.2.8}$$

[12] This gauge goes by many other names, such as 'De Donder' or 'harmonic' gauge.

A solution of the form $\xi_\mu = \lambda_\mu e^{ik_\sigma x^\sigma}$ transforms the polarization matrix as

$$H_{\mu\nu} = H_{\mu\nu} - i\left(k_\mu\lambda_\nu + k_\nu\lambda_\mu - \eta_{\mu\nu}k^\sigma\lambda_\sigma\right) \ . \tag{1.2.9}$$

We can choose λ_μ such that

$$H_{0\mu} = 0 \qquad \text{and} \qquad H^\mu{}_\mu = 0 \ , \tag{1.2.10}$$

a choice we refer to as the *transverse traceless gauge*. These five conditions are not independent of each other and can be combined to constrain the four components of λ_μ[13]. Finally, we find there are $10 - 4 - 4 = 2$ independent polarizations. The polarization matrix for a plane wave travelling in the x^3 direction reads

$$H_{\mu\nu} = \begin{pmatrix} 0 & 0 & 0 & 0 \\ 0 & H_+ & H_\times & 0 \\ 0 & H_\times & -H_+ & 0 \\ 0 & 0 & 0 & 0 \end{pmatrix} \ , \tag{1.2.11}$$

with H_+ and $H_\times$ describing the two polarizations of the wave.

Of course, gravitational waves can also be generated by sources. We go back to the linearized Einstein equation (1.2.2), take $T_{\mu\nu}$ to be nonzero, and derive a formula that describes the rate at which gravitational waves are emitted from a system of masses, the so-called *quadrupole formula*. We assume the energy-momentum tensor is sourced by non-relativistic matter, and write down a solution for $\bar{h}_{\mu\nu}$ in terms of the "retarded Green's function" far away from this source:

$$\bar{h}_{\mu\nu}(t, \mathbf{x}) \approx 4G \int \mathrm{d}^3y \, \frac{T_{\mu\nu}(t_r, \mathbf{y})}{|\mathbf{x} - \mathbf{y}|} \ , \tag{1.2.12}$$

where $t_r = t - |\mathbf{x} - \mathbf{y}|$ is the retarded time, which appears because the gravitational field at $(t, \mathbf{x})$ is influenced by a sum of the events on the past light cone. Since we are evaluating the gravitational field far away from the source, we can Taylor expand in small values for $|\mathbf{y}|$ and write (1.2.12) as

$$\bar{h}_{\mu\nu}(t, \mathbf{x}) \approx \frac{4G}{r} \int \mathrm{d}^3y \, T_{\mu\nu}(t - r, \mathbf{y}) \ , \tag{1.2.13}$$

[13]More precisely, we can impose $H^\mu{}_\mu = 0$, then $H_{0i} = 0$ as well by choosing λ_μ, and lastly by using (1.2.7) we show that $H_{00} = 0$.

with $r = |\mathbf{x}|$. The quadrupole formula is then given by the spatial components of this tensor[14], which—by using conservation of the energy-momentum tensor $T_{\mu\nu}$—can be written as:

$$\bar{h}_{ij}(t, \mathbf{x}) = \frac{2G}{r} \frac{d^2 I_{ij}}{dt^2}(t_r) \ . \tag{1.2.14}$$

with the *quadrupole moment*

$$I_{ij}(t_r) = \int \mathrm{d}^3 y \, T^{00}(t_r, \mathbf{y}) y_i y_j \ . \tag{1.2.15}$$

It is now clear that gravitational waves are produced as a consequence of an accelerating mass quadrupole moment (similar to electromagnetic waves being produced by an accelerating dipole moment). Monopolar and dipolar radiation are absent in General Relativity. Whereas absence of the first can be interpreted as a consequence of Birkhoff's theorem, the second is a consequence of the conservation of linear momentum.

For future convenience, we would like to point out how gravitational waves are parametrized in the *Newman-Penrose null tetrad formalism* [47]. In this formalism, the tensors in the theory are projected onto a null tetrad basis $(l^\mu, n^\mu, m^\mu, \bar{m}^\mu)$, consisting of two real null vectors and a complex-conjugate pair. With these vectors a bunch of Newman-Penrose scalars can be defined, such as the Weyl scalars $\Psi_0 \, , \ldots , \, \Psi_4$ [48], which are projections of the Weyl tensor (the trace-free parts of the Riemann tensor)

$$C_{\rho\sigma\mu\nu} = R_{\rho\sigma\mu\nu} - \frac{2}{(n-2)} \left(g_{\rho[\mu} R_{\nu]\sigma} - g_{\sigma[\mu} R_{\nu]\rho} \right) + \frac{2}{(n-1)(n-2)} g_{\rho[\mu} g_{\nu]\sigma} R \tag{1.2.16}$$

on the null tetrad (n is the number of dimensions). In the transverse traceless gauge the outgoing gravitational radiation if captured by Ψ_4 for which

$$\Psi_4 = C_{\rho\sigma\mu\nu} \bar{m}^\rho n^\sigma \bar{m}^\mu n^\nu \qquad \rightarrow \qquad \Psi_4^{\mathrm{TT}} = -\ddot{H}_+ + i \ddot{H}_\times \ . \tag{1.2.17}$$

Note that $\Psi_1 \, , \ldots , \, \Psi_3$ vanish, and that Ψ_0 encodes the ingoing gravitational radiation (whether Ψ_0 or Ψ_4 is zero depends on the direction of the gravitational wave). Although in General Relativity the outgoing radiative degrees of freedom are simply

[14] The other components describe the conserved quantities inside the region we are studying:

$$\bar{h}_{00}(t, \mathbf{x}) \approx \frac{4G}{r} E \ , \qquad E \equiv \int \mathrm{d}^3 y \, T_{00}(t - r, \mathbf{y}) \ ,$$
$$\bar{h}_{0i}(t, \mathbf{x}) \approx -\frac{4G}{r} P_i \ , \qquad P_i \equiv -\int \mathrm{d}^3 y \, T_{0i}(t - r, \mathbf{y}) \ ,$$

but hold no information about the propagating degrees of freedom.

encoded in Ψ_4 , scalar-tensor theories (those will be described in Chapter 2) allow for an additional scalar (breathing) radiative mode[15]. This scalar mode is encoded in

$$\Phi_{22} = R_{\mu\nu} n^\mu n^\nu \ , \tag{1.2.18}$$

which is one of the Ricci scalars in the formalism.

1.2.2 Present and Future Detectors

For many years, the possibility of gravitational waves actually existing in nature and to be detectable was met with skepticism[16]. Nevertheless, in 1974, their existence was confirmed through (indirect) detection by the discovery of the Hulse-Taylor binary [31]. One of the stars in this binary neutron star system is a pulsar, and emits a radio pulse every 59 ms. This was used to accurately measure the period of the binary, which becomes smaller over time. The binary's orbital decay turned out to be in excellent agreement with the quadrupole formula, providing the first strong experimental evidence for gravitational waves. The first direct detection came decades later with the historic observation of a gravitational wave produced during the merger of a distant black hole binary system on 14 September, 2015 (see Figure 1). Since then, there have been numerous gravitational-wave detections mainly done by the Laser Interferometer Gravitational-Wave Observatory (LIGO) and Virgo collaboration, whose observatories are located in Hanford and Livingston (United States), and Cascina (Italy), respectively.

Gravitational waves are detected by highly-sensitive laser interferometers. Until now, all of the gravitational-wave detections have been made by L-shaped, ground-based observatories, in which a split laser beam is travelling back and forth through the two identical arms, and reflected by mirrors at either ends. The basic principle is that if a gravitational wave is travelling perpendicular to the plane of the detector, it will shorten one arm while lengthening the other. The difference in length can be derived from an interference pattern emerging from the interferometer, which can then be related to the characteristic strain of the gravitational wave. Even though the LIGO and Virgo detectors have seemingly long arms (4 km and 3 km, respectively), if they would have been regular Michelson interferometers, they would still

[15] Note that both modes need to be evaluated in the Jordan frame, also defined in Chapter 2.
[16] Even Einstein himself did not believe them to be physical near the end of his life [49].

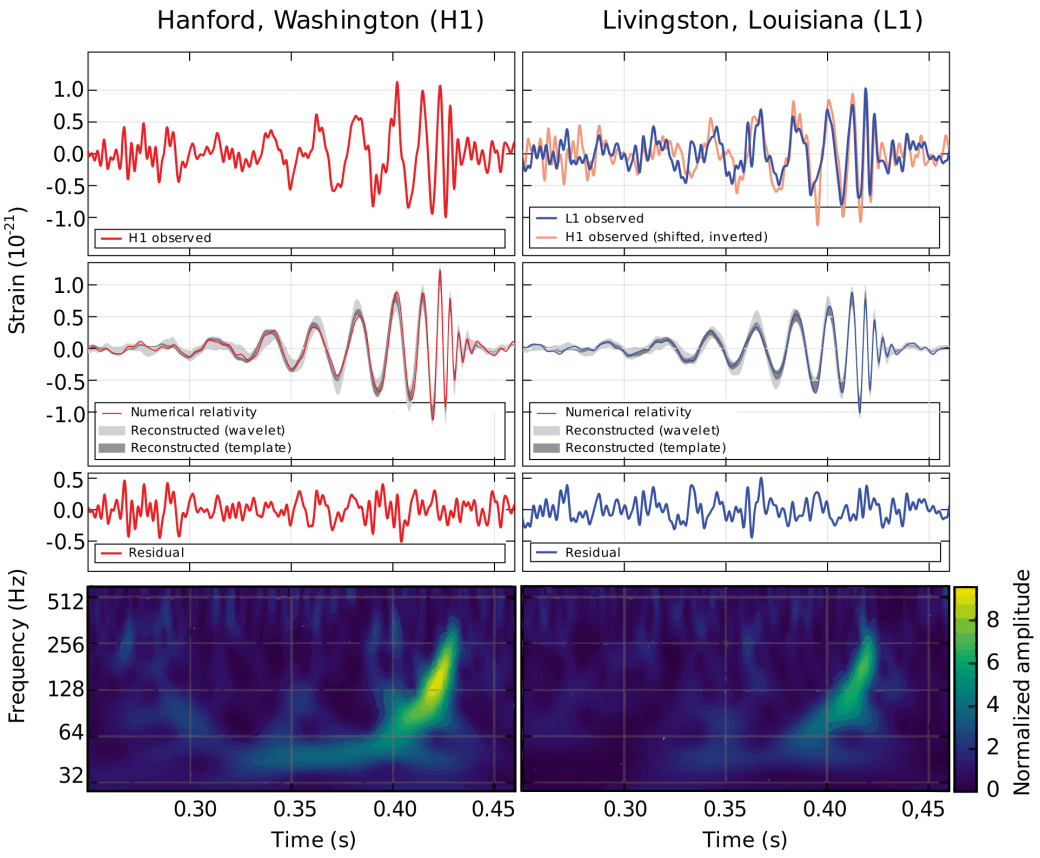

Figure 1: The first direct detection of gravitational waves (GW150914) by the LIGO observatories on 14 September, 2015 [32].

have been too short to detect gravitational waves. This issue is resolved by the inclusion of Fabry-Perot cavities, which are created by placing additional mirrors near the beam splitter. The laser beam can now bounce back and forth between these mirrors and the mirrors at the end of the arms, increasing the effective arm length in the detectors to roughly 1200 km. Another issue in these detectors, namely the limited initial power of the laser beam, is addressed by power recycling mirrors. These mirrors continually reflect the laser beam coming from the interferometer back into the instrument, which greatly boosts its power. This advanced engineering design makes these interferometers the most sensistive ones every constructed (see Figure 2 for the sensitivity curves of several current and future detectors).

All events detected so far are categorized as compact binary coalescences. From the

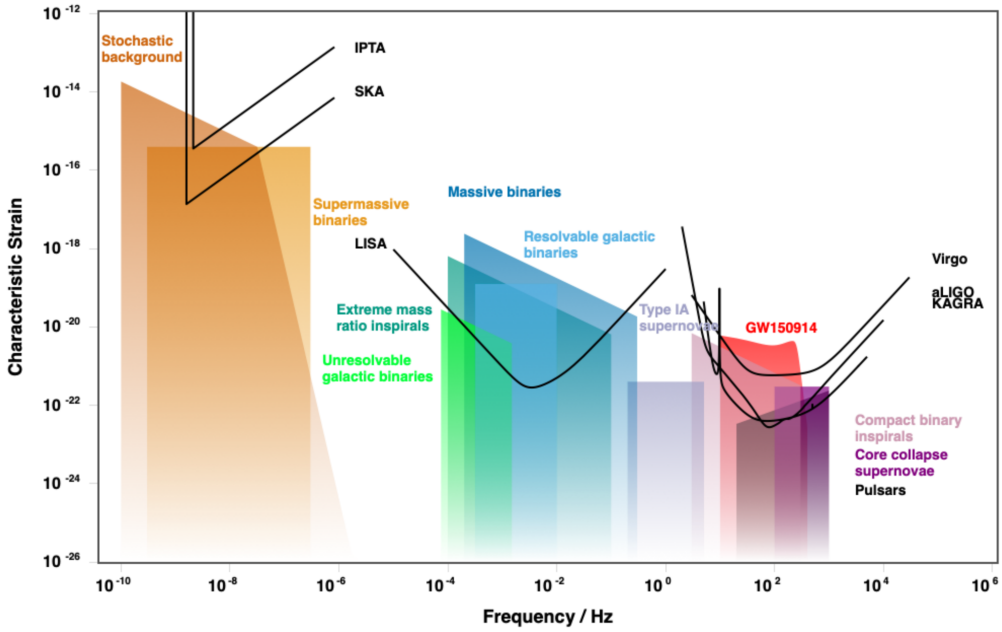

Figure 2: This plot shows the sensitivity curves for several gravitational-wave observatories as a function of the frequency and characteristic strain. The characteristic strain $h_c(f)$ for a frequency f is defined as $[h_c(f)]^2 = 4f^2|\tilde{h}(f)|^2$, where $\tilde{h}(f)$ is the Fourier transform of the signal $h(t)$. The three main branches of gravitational-wave observatories are covered: ground-based (aLIGO, Virgo, KAGRA) and space-borne (LISA) interferometers, and Pulsar Timing Array-based detectors (IPTA, SKA). It also shows the characteristic signal produced by different gravitational-wave sources (this figure has been produced by using the online tool described in [50]).

frequency of the waves, one can deduce the *chirp mass*, defined as

$$\mathcal{M}_c = \frac{(M_1 M_2)^{3/5}}{(M_1 + M_2)^{1/5}} \,, \tag{1.2.19}$$

where M_1 and M_2 are the masses of the two objects. Again, determining this mass (and also other parameters) is not easy. Gravitational-wave signals are typically weak and polluted by noise. One depends on *matched filter techniques*—where the signal is compared to precise waveform templates produced on theoretical grounds—to detect them, after which parameter estimation can be applied to the signal. The templates can be produced both in general relativistic or modified gravity context, which immediately also provides a test of those theories. Thus far, the catalog of events de-

tected by the LIGO/Virgo collaboration is composed of numerous binary black hole mergers, and a couple of binary neutron star and mixed coalescences (e.g. binary systems consisting of a black hole and neutron star). All these detections have been of great scientific importance. Especially the first observation of a binary neutron star merger (GW170817) played an influential role in gravitational-wave astrophysics [33], as it could be cross-correlated with observations of electromagnetic emissions of the merger. This allowed for a comparison between the propagation speeds of gravity and light, which put strong constraints on many modified gravity models [51–56][17]. It also showed that gravitational-wave and electromagnetic observations are complementary, and thus we entered a new era of *multi-messenger gravitational-wave astronomy*.

The potential of gravitational-wave astronomy is directly reflected in the growing number of gravitational-wave detectors. In 2020, the underground Kamioka Gravitational Wave (KAGRA) detector in Hida (Japan) became operational, and is planning to join the LIGO/Virgo collaboration for the next run (O4) in December 2022 [57]. Another detector, proposed by the Indian Initiative in Gravitational-Wave Observations (IndIGO) and based in India, is planned to become operational in 2024. A third-generation of ground-based interferometers with significantly longer arms and aiming to achieve ~ 100 times higher sensitivities than the current generation is also on the way, represented by the Einstein Telescope [58] and Cosmic Explorer [59], and prospected to be operational in the 2030s.

The first space-based interferometric experiments are planned to start in the mid 2030s. Probing gravitational waves in space has the huge advantage of being unaffected by the noisy environment of Earth, such as seismic noise. The main proposed future mission is the realization of the Laser Interferometer Space Antenna (LISA) [60, 61], comprised of three individual spacecrafts arranged in an equilateral triangle with sides 2.5 million km long. With these arm-lengths, they are sensitive to a completely different range of frequencies than the terrestrial detectors, and therefore able to probe new gravitational-wave sources. Other proposed space-based missions include TianQin [62], Taiji [63] and the Deci-hertz Interferometer Gravitational wave Observatory (DECIGO) [64].

[17] These constraints come with some potential caveats, as most of the models considered are not really valid in these regimes.

An alternative approach to detect gravitational waves is by the use of Pulsar Timing Array (PTA) techniques. A passing gravitational wave will cause small fluctuations in the otherwise regular pulsing time of millisecond pulsars. Although requiring a lot of precision, this effect can actually be detected by measuring the time of arrival of radio pulses from a correlated array of stable pulsars. At the moment, this technique is applied by three different collaborations: the Parkes Pulsar Timing Array [65], the North American Nanohertz Observatory for Gravitational Waves (NANOGrav) [66], and the European Pulsar Timing Arrays (EPTA) [67]. Together they constitute the International Pulsar Timing Array (IPTA) [68], which monitors a total of 65 pulsars. The same principle will be used by the Square Kilometre Array (SKA) [69], a radio telescope comprised of hundreds of dishes and hundreds of thousands of low-frequency aperture array telescopes spanning over more than one square kilometre. These missions will probe gravitational waves in the low-frequency regime, coming from a stochastic background or supermassive black hole coalescences.

1.3 Cosmology

General Relativity is applied in the field of cosmology to study the evolution of our Universe. This seems like an incredibly challenging task, but simplifies with the realization that the Universe is *isotropic* and *homogeneous* on large scales, meaning it looks the same at every point in space (for fixed time) and in every direction. The standard model of cosmology—which assumes General Relativity to be the true theory of gravity—is the ΛCDM model, and will be introduced in this section. We will then focus on (the problem of) *dark energy*, the mysterious component responsible for the accelerated expansion of our Universe.

1.3.1 The ΛCDM Model

Isotropy and homogeneity imply that space is maximally symmetric. We can represent the spacetime by time-ordered three-dimensional spatial slices described by the metric

$$\mathrm{d}s^2 = -\mathrm{d}t^2 + a^2(t)\mathrm{d}\ell^2 \,, \tag{1.3.1}$$

where $\mathrm{d}\ell^2 \equiv \gamma_{ij}(\mathbf{x})\mathrm{d}x^i\mathrm{d}x^j$ is the line element on the spatial slices and $a(t)$ the scale factor (tracking the expansion of the Universe). The spatial metric γ_{ij} can take three different forms, depending on its intrinsic curvature, leading to a four-dimensional

metric that looks like

$$\mathrm{d}s^2 = -\mathrm{d}t^2 + a^2(t)\left[\frac{\mathrm{d}r^2}{1-\kappa r^2} + r^2\mathrm{d}\Omega^2\right] . \tag{1.3.2}$$

Here, $\kappa = (-1, 0, +1)$ corresponds to hyperbolic (negative curvature), flat (no curvature), and spherical (positive curvature) spatial slices, respectively. The metric (1.3.2) is called the *Friedmann-Robertson-Walker (FRW) metric* [70, 71].

The next step is to plug the FRW metric in the Einstein equations (1.1.14). Before we do so, we make a slight modification to the equations. We are allowed to add another term to the left-hand side that would still respect the conservation of the energy-momentum tensor and write

$$G_{\mu\nu} + \Lambda g_{\mu\nu} = 8\pi G T_{\mu\nu} , \tag{1.3.3}$$

with Λ a constant called the *cosmological constant*. Einstein originally added this term to the Einstein equations to counter-balance the effect of gravity and create a static Universe. After the discovery of the expansion of the Universe by Hubble and Lemaître [72, 73] he removed it, referring to its original introduction as his "biggest blunder". However, after the discovery that the expansion is accelerating, the cosmological constant regained popularity, and now plays the role of dark energy in the ΛCDM model.

We assume the energy-momentum is sourced by a perfect fluid (1.1.22), which with the preferred $3+1$ foliation collapses to $T_{00} = \rho$ and $T_{ij} = p g_{ij}$. Usually, the cosmological constant is moved to the right-hand side of the equations and interpreted as part of the energy-momentum tensor: $T^{\Lambda}_{\mu\nu} = -(\Lambda/8\pi G) g_{\mu\nu}$. The temporal component of the Einstein equation then gives

$$\left(\frac{\dot{a}}{a}\right)^2 = \frac{8\pi G}{3}\rho - \frac{\kappa}{a^2} , \tag{1.3.4}$$

where the expansion of the Universe is characterized by the Hubble parameter $H \equiv \dot{a}/a$. The spatial parts of the Einstein equations lead to

$$\frac{\ddot{a}}{a} = -\frac{4\pi G}{3}(\rho + 3p) . \tag{1.3.5}$$

These two equations are called the Friedmann equations. From the conservation of the energy-momentum tensor we also obtain the continuity equation

$$\dot{\rho} + 3\frac{\dot{a}}{a}(\rho + p) = 0 . \tag{1.3.6}$$

To close and solve the system of equations, we need to impose an equation of state $w = p/\rho$, with $w = 0$ for matter, $w = 1/3$ for radiation, and $w = -1$ for Λ. From the continuity equation and the equation of state we can derive how every component scales with the scale factor $a(t)$:

$$\rho \propto \begin{cases} a^{-3} & \text{matter} , \\ a^{-4} & \text{radiation} , \\ a^{0} & \Lambda . \end{cases} \tag{1.3.7}$$

Most of the time the Universe is dominated by one component, starting with radiation, then matter, and finally Λ. It is conventional to measure the density of every component nowadays with respect to the critical value, i.e. the density that would correspond to a flat Universe today:

$$\rho_{c,0} = \frac{3H_0^2}{8\pi G} , \tag{1.3.8}$$

where $H_0 \approx 70$ km/sec/Mpc is the Hubble constant (the Hubble parameter measured today). We can then define a dimensionless parameter

$$\Omega_{i,0} \equiv \frac{\rho_{i,0}}{\rho_{c,0}} , \tag{1.3.9}$$

with $i = r, m, \Lambda$ representing the different components. Plugging this into the first Friedmann equation and evaluating it at present time (for which $a(t_0) \equiv 1$), we obtain the constraint

$$1 = \Omega_r + \Omega_m + \Omega_\Lambda + \Omega_\kappa . \tag{1.3.10}$$

The most precise measured values of these parameters come from Cosmic Microwave Background (CMB) power spectra measurements by the Planck collaboration [74]:

$$\Omega_m = 0.3111 \pm 0.0056 , \qquad \Omega_\Lambda = 0.6889 \pm 0.0056 , \qquad \Omega_\kappa = 0.001 \pm 0.002 , \tag{1.3.11}$$

with $\Omega_r \sim 10^{-5} \ll 1$. The matter contribution consists of a baryonic and cold dark matter component, where $\Omega_b \approx 0.05$ and $\Omega_c \approx 0.27$. Thus, the Universe is dominated by its dark components, which are unfortunately the components we know the least about.

The ΛCDM model has made a series of successful predictions, such as the existence of baryonic acoustic oscillations [75] and the CMB polarization [76], but it presents us with some challenges as well [77]. One of these is the tension that appears at 4.4σ

level[18] in the value of the Hubble constant as derived from local measurements of the expansion rate from supernovae ($H_0 \approx 73$ km/sec/Mpc) and early Universe techniques concerning the Cosmic Microwave Background ($H_0 \approx 67$ km/sec/Mpc) [74,79]. Another issue is the tension at 2–3σ level on the value of the σ_8 parameter—which quantifies the magnitude of matter fluctuations, or said differently, the strength of matter clustering—as measured from the anisotropies of the CMB by the Planck satellite and by weak gravitational lensing and galaxy clustering techniques [74, 80]. Today, these tensions are the main motivation for cosmological tests of gravity.

1.3.2 (The Problem of) Dark Energy

We have strong observational evidence that the Universe today is dominated by a dark energy component. It was first discovered in 1998 through measurements of type Ia supernovae by two independent groups, the Supernova Cosmology Project [81–83] and the High-Z Supernova Search Team [84, 85]. Later evidence includes studies of the CMB power spectra, baryon acoustic oscillations, weak gravitational lensing, and the large-scale structure of the Universe [74, 86].

We know dark energy is responsible for the cosmic acceleration and it makes up the majority of the total energy density, but we are still in the dark about its nature. A value of $\Omega_\Lambda \approx 0.7$ is equivalent to an energy density of

$$\rho_\Lambda \approx (10^{-3}\ \text{eV})^4 = 10^{-48}\ \text{GeV}^4\ . \tag{1.3.12}$$

In the previous section we derived that $\rho_\Lambda \propto a^0$, meaning that the energy density stays constant as the volume increases. This in turn means that energy must be produced, and suggests that dark energy might be a property of empty space itself. This type of behavior is actually predicted in quantum field theory, where the ground state energy of the vacuum caused by quantum fluctuations is $T^{\text{vac}}_{\mu\nu} = \rho_{\text{vac}} g_{\mu\nu}$. In modern field theories of elementary particles it is predicted each particle species contributes to the vacuum energy as (we follow [87])

$$\rho_{\text{vac}} \simeq \frac{m^4}{(\hbar/c)^3} + \text{const.}\ , \tag{1.3.13}$$

where m is the mass of the particle, and the constant is arbitrary. This means that at every phase transition, the energy density of the vacuum decreases by $\Delta\rho_{\text{vac}} \simeq$

[18] Note that gravitational waves can be used to potentially break this tension, see e.g. [78].

$m^4(\hbar/c)^{-3}$, corresponding to 10^{60} GeV^4 for the Grand Unified Theory (GUT) transition, 10^{12} GeV^4 for supersymmetry, 10^8 GeV^4 for the electroweak transition, and 10^{-4} GeV for quantum chromodynamics (QCD). We can now assess

$$\begin{aligned}\rho_{\rm vac}(t_{\rm Pl}) &= \rho_{\rm vac}(t_0) + \sum_i \Delta\rho_{\rm vac}(m_i) \\ &\simeq 10^{-48}\ \text{GeV}^4 + 10^{60}\ \text{GeV}^4 = \sum_i \Delta\rho_{\rm vac}(m_i)(1+10^{-108})\ ,\end{aligned} \tag{1.3.14}$$

with $\rho_{\rm vac}(t_{\rm Pl})$ and $\rho_{\rm vac}(t_0) = \rho_\Lambda$ the vacuum energy density at Planck and present times, and m_i represents all the energies corresponding to the phase transitions occurring between $t_{\rm Pl}$ and t_0. We see now that there is a high level of fine-tuning between the values of $\rho_{\rm vac}(t_{\rm Pl})$ and $\sum_i \Delta\rho_{\rm vac}(m_i)$. On top of this, the vacuum energy is radiatively unstable, which would spoil any fine-tuning done at tree level, forcing one to repeat the procedure at every loop level [88]. This is what we call the *cosmological constant problem* [89]. Another theoretical puzzle concerns the question why the dark energy and matter density are so similar in our Universe today. Since they depend differently on the scale factor, there is only a small window in which the transition from a matter-dominated to dark energy-dominated Universe can be observed. However, we as humans seem to be living exactly in this window, referring to this issue as the *coincidence problem*[19].

Alternatives to the cosmological constant have been proposed, such as the *quintessence* models. In these models, the cosmic acceleration is caused by the potential energy of a dynamical scalar field. Another approach is to modify the gravitational dynamics (with respect to General Relativity) on cosmological scales. This is the main philosophy behind *modified gravity* models. We will expand more on these topics in the next chapter.

[19]There are different points of view on whether these issues are truly problems in our modern understanding of the physics of our Universe, see e.g. [90].

2 Alternative Theories of Gravity

A natural consequence of asking ourselves whether we correctly understand the gravitational phenomenon is considering alternatives to General Relativity. Although Einstein's theory has proven to be incredibly successful, there are several motivations for going beyond it. Those will be summarized in Section 2.1. Throughout the years, many theories have been proposed, some more promising than others. In Section 2.2, we focus on the field of scalar-tensor theories. A large subclass of scalar-tensor theories are endowed with a so-called *screening mechanism*, which allows these theories to deviate on cosmological scales while evading constraints in the Solar System. We further explore one type of screening in Chapter 3 and 4. We introduce the topic of Lorentz-violating gravity in Section 2.3, which will be useful before reading Chapter 5.

2.1 Gravity beyond General Relativity

In this section, we motivate the consideration of modified theories of gravity, and briefly summarize ways to modify General Relativity. Moreover, we lay out some basic principles to assess the viability of a modified gravity theory.

2.1.1 Motivations to Modify Gravity

General Relativity has passed every test to date with flying colours, but yet it might not be the final answer to describing gravity on macroscopic scales. Motivation for exploring alternative theories of gravity has been mostly cosmological, e.g. to shed light on long-standing questions concerning the cosmic acceleration and cosmological constant problem (introduced in Section 1.3.2), and to relieve tension on the value of the Hubble constant H_0 and the density fluctuation power spectrum amplitude σ_8 [91].

These models refrain from postulating a mysterious dark sector, but rather change the laws of gravity on cosmological scales to explain observed phenomena. Although General Relativity is indeed well-tested in our Solar System, on larger scales it is less constrained, and a different behavior of gravity in this regime is still allowed.

Gravity used to be relatively untested in the strong-field and highly-dynamical regime, but this changed with the LIGO/Virgo observations [42]. This environment is naturally provided by compact objects, and the full non-linear and dynamical effects in this region can be probed by gravitational waves coming from binaries. We have only recently entered the era of precision (multi-messenger) gravitational-wave astronomy, but gravitational-wave observations already play an important role in verifying General Relativity. No evidence of physics beyond General Relativity has been found yet, motivating the need for so-called *screening mechanisms* in alternative theories of gravity (see Section 2.2.3). Whereas for the inspiral phase analytical methods such as Post-Newtonian theory suffice to construct gravitational waveforms, to model waveforms for the merger and ringdown of the coalescence we have to rely on different techniques. The full evolution equations have to be solved numerically, which has only become possible recently after a series of breakthroughs in the field of Numerical Relativity [92–94]. Clearly, now that we have the tools, it is a good time to parametrize deviations from General Relativity, and to be prepared if they ever do show up in observations.

General Relativity is also subject to theoretical objections: the coupling constant—the gravitational constant—has negative mass dimension, meaning General Relativity is non-renormalizable and therefore ultraviolet incomplete. One could consider adding higher-derivative interactions to render the theory renormalizable, but this generally leads to ghost instabilities (as will be discussed in the next sections). It can therefore only capture quantum effects up to the Planck scale, which is the cut-off scale of General Relativity. Furthermore, General Relativity is incomplete and for instance fails to describe the gravitational field inside a black hole, where curvature diverges in the singularity. Theoretical efforts to address these issues have been made in the field of Quantum Gravity, but experimental data to distinguish between the different proposed theories remains inaccessible.

How then would we modify gravity as described by General Relativity? Let us start

by introducing *Lovelock's theorem* [95, 96]. Assuming the equations of motion for the metric $g_{\mu\nu}$ in vacuum take the form $A^{\mu\nu} = 0$, where $A^{\mu\nu}$ is a symmetric and divergenceless tensor, it states that if $A^{\mu\nu}$ is a function of the metric, and its first and second derivatives only, its most general form in four dimensions is

$$A^{\mu\nu} = aG^{\mu\nu} + bg^{\mu\nu} \,, \tag{2.1.1}$$

where $G^{\mu\nu}$ is the Einstein tensor, and a and b are constants. It therefore follows that the Einstein field equations (including a cosmological constant) are the unique equations of motion upon these assumptions. The most general Lagrangian density we can write down in terms of $g_{\mu\nu}$ in four dimensions leading to the Einstein field equations then takes the form

$$\begin{aligned}\mathcal{L} = \sqrt{-g}\Big[\alpha R - 2\lambda + \beta\epsilon^{\mu\nu\rho\lambda}R^{\alpha\beta}{}_{\mu\nu}R_{\alpha\beta\rho\lambda} \\ + \gamma\left(R^2 - 4R^{\mu}{}_{\nu}R^{\nu}{}_{\mu} + R^{\mu\nu}{}_{\rho\lambda}R^{\rho\lambda}{}_{\mu\nu}\right)\Big] \,,\end{aligned} \tag{2.1.2}$$

where α, λ, β, and γ are constants. Note that the third and fourth term do not contribute to the equations of motion[1].

As a consequence of Lovelock's theorem, one can only write down an alternative theory of gravity by implementing one of the following changes. The first option is to add degrees of freedom, by for instance considering a massive graviton or introducing new fields in the gravitational action. The latter consist of introducing scalar, vector, or tensor (or combinations of these fields) contributions to the gravitational sector, and coupling them non-minimally to the metric. We discuss the family of *scalar-tensor theories* in Section 2.2. Secondly, one can add terms to the gravitational action that are more than second order in derivatives of the metric. While considering higher-order time derivatives, it is important to avoid Ostrogradski instabilities (more on this in Chapter 5). Another class of theories is generated by breaking Lorentz invariance, as is the case for *Hořava gravity* (discussed in Section 2.3).

Other ways to modify gravity (that are not studied in this work) include considering higher-dimensional theories of gravity (also here gravity is modified by including additional degrees of freedom). Generally, these theories introduce additional spatial dimensions, but appear four-dimensional on large scales, with the extra dimensions

[1] For the fourth term, the so-called Gauss-Bonnet term, this is only true in four dimensions, where it reduces to a topological surface term.

being "compactified" on some manifold. Models like these were originally proposed by Kaluza and Klein as an attempt to unify the gravitational and electromagnetic force, and are considered a precursor for string theory. Furthermore, in some modified gravity theories the principle of locality is relaxed, allowing for terms in the equations of motion that might depend on a small region of spacetime or inverse derivative operators.

2.1.2 Requirements of Validity

Once we allow ourselves to relax one or more assumptions that are at the foundation of General Relativity, we find there are many ways to modify gravity. We have already mentioned a few approaches to assess whether a modified theory of gravity is promising or not, such as consistency with observational data, e.g. the theory should be able to pass any of the weak- and strong-field precision tests that General Relativity has already passed. Additionally, we can reduce the number of possible modified theories of gravity by imposing some desirable theoretical properties (a nice discussion on this can be found in [97]). First, the theory must have some limit (continuous or discontinuous) in which its predictions overlap with the ones from General Relativity. This means it should predict stable observed phenomena, such as the existence of black holes, neutron stars, and a viable cosmological scenario.

Another important requirement is that the theory should allow for a well-posed initial value formulation. A given problem modelled by partial differential equations (PDEs) is well-posed if it meets the following three criteria [98]: there exists a solution, the solution is unique, and the solution depends continuously on the initial data. Without this property, the theory loses predictive power. At the level of effective field theories this is not a theoretical requirement, but it is a practical one, as it is fundamental for a successful numerical evolution of the field equations. Usually, it is not trivial to check whether a system of PDEs is well-posed or not, and it is more convenient to check the hyperbolicity of the system. If the field equations are *strongly-hyperbolic*—meaning they can be written as a quasilinear first-order system of PDEs with a principal part (the terms with the highest derivatives) that has real eigenvalues and a complete set of eigenvectors—the system is well-posed and allows for stable numerical evolutions under suitable numerical methods [99–102]. If this is not the case, the system of PDEs is *weakly-hyperbolic* and ill-posed, with solutions that can grow exponentially, leading to unstable numerical evolutions. Strong hyperbolicity of the evolution system of

PDEs is therefore a necessary requirement to numerically evolve field equations in a stable way[2].

Lastly, we would like to avoid any ghost instabilities, and define a physical system with a Hamiltonian bounded from below. To do this, it is necessary to allow no more than two time derivatives in the equations of motion as described by the Ostrogradski theorem [103], or only allow them combined with a set of degeneracy conditions to ensure there is no propagating Ostrogradski mode, as is done in Degenerate Higher-Order Scalar-Tensor (DHOST) theories [104][3].

2.2 Scalar-Tensor Theories

Scalar fields are commonly used in our description of fundamental physics. The Higgs boson plays a huge role in the Standard Model of particle physics, explaining how the other elementary particles are massive, the exponential expansion of spacetime in the early Universe—inflation—is commonly attributed to the existence of the so-called inflaton, and string theory models predict at least one spin-0 mode called the dilaton. It is therefore quite natural to consider a scalar contribution in the gravity sector as well. We define a modified theory of gravity to be any model in which the scalar field couples non-minimally to the metric.

The simplest and one of the most well-known scalar-tensor theories is Fierz-Jordan-Brans-Dicke (FJBD) theory [106–108], described by the action

$$S_{FJBD} = \frac{M_{\rm Pl}^2}{2}\int \mathrm{d}^4x\,\sqrt{-\tilde{g}}\left(\Phi\tilde{R} - \frac{\omega(\Phi)}{\Phi}\tilde{g}^{\mu\nu}\partial_\mu\Phi\partial_\nu\Phi\right) + S_m(\tilde{g}_{\mu\nu},\psi)\ , \tag{2.2.1}$$

where $M_{\rm Pl} = (8\pi G)^{-1/2}$, Φ is the gravitational scalar field, $\omega(\Phi) = \omega_0 = \text{const}$ characterizes the theory (for different scalar-tensor theories this can be a function of Φ), and ψ collectively describes all matter degrees of freedom. An alternative form of this action can be obtained by a conformal transformation of the metric $\tilde{g}_{\mu\nu}$ and

[2] In Section 4.1.2, we explain how to check whether this condition is satisfied.

[3] Note that more-than-second-order equations of motion propagating an Ostrogradski ghost can, however, be dealt with perturbatively, see e.g. [105] (the appearance of the ghost mode is an indication of the breakdown of the regime of validity of the effective field theory).

redefinition of the scalar field

$$g_{\mu\nu} = \Phi(\varphi)\tilde{g}_{\mu\nu} \,, \qquad \frac{\mathrm{d}\log\Phi}{\mathrm{d}\varphi} = \frac{1}{M_{\mathrm{Pl}}}\sqrt{\frac{2}{3+2\omega(\Phi)}} \,. \tag{2.2.2}$$

In these variables, the action takes the form

$$S_{FJBD} = \int \mathrm{d}^4x\,\sqrt{-g}\left(\frac{M_{\mathrm{Pl}}^2}{2}R - \frac{1}{2}g^{\mu\nu}\partial_\mu\varphi\partial_\nu\varphi\right) + S_m\left(\frac{g_{\mu\nu}}{\Phi(\varphi)}, \psi\right) \,. \tag{2.2.3}$$

The different representations of the theory in equations (2.2.1) and (2.2.3) are referred to as the *Jordan* and *Einstein frame*, respectively. In this thesis, we use tilded notation for quantities derived from the Jordan frame metric. Note also that the Ricci scalar in equation (2.2.1) is multiplied by the scalar field Φ, introducing dependence on the local value of the scalar field in the measured value of the gravitational constant. By taking the Newtonian limit of the theory, one can find that Newton's constant G_N as measured by a Cavendish experiment is related to the bare gravitational constant G as it appears in the action (2.2.1) by

$$G_N = \frac{G}{\Phi(\varphi_0)}\frac{4+2\omega_0}{3+2\omega_0} \,, \tag{2.2.4}$$

where φ_0 is the Einstein-frame scalar field at infinity, and $\omega_0 = \omega(\varphi_0)$.

In the Einstein frame, the scalar field is minimally coupled to the metric, and one might wonder if the theory can still be considered a modified gravity theory. Indeed, the field equations describing the evolution of the gravitational field are identical to the Einstein equations plus a massless scalar field. However, it is crucial to realize that by performing this conformal transformation, we introduce couplings between the scalar and matter fields. The behavior of these matter fields is now fundamentally different from matter fields in General Relativity, e.g. they do not follow geodesics of the new metric $g_{\mu\nu}$. We say they are affected by a *fifth force*. The modification of the geodesic equation matches the modification of the field equations in the Jordan frame, or, in other words, the coupling to matter mimics the modification of gravity in the Jordan frame. Numerically, it is usually convenient to work in the Einstein frame, but when interpreting our results we transform back to the physical Jordan frame.

2.2.1 Horndeski and Beyond

The space of scalar-tensor theories is much larger than the example given by FJBD theory in (2.2.1). Horndeski proposed to extend Lovelock's theorem in four dimensions

to General Relativity plus a scalar field, and wrote down the most general action leading to second-order equations of motion for the metric and scalar [109]:

$$S_{HD} = \int \mathrm{d}^4x \sqrt{-g} \left[\sum_{i=2}^{5} \mathcal{L}_i(g_{\mu\nu}, \varphi) + \mathcal{L}_m(g_{\mu\nu}, \psi) \right] , \tag{2.2.5}$$

where

$$\mathcal{L}_2 = K(\varphi, X) , \tag{2.2.6}$$

$$\mathcal{L}_3 = G_3(\varphi, X)\Box\varphi , \tag{2.2.7}$$

$$\mathcal{L}_4 = G_4(\varphi, X)R + G_{4,X}(\varphi, X) \left[(\Box\varphi)^2 - \varphi_{\mu\nu}\varphi^{\mu\nu} \right] , \tag{2.2.8}$$

$$\mathcal{L}_5 = G_5(\varphi, X)G_{\mu\nu}\varphi^{\mu\nu} - \frac{1}{6}G_{5,X}(\varphi, X) \left[(\Box\varphi)^3 + 2\varphi_\mu{}^\nu\varphi_\nu{}^\alpha\varphi_\alpha{}^\mu - 3\varphi_{\mu\nu}\varphi^{\mu\nu}\Box\varphi \right] , \tag{2.2.9}$$

with K and G_i are functions of the scalar field and its kinetic term $X = -\varphi^\mu\varphi_\mu/2$, and we adopt the notation $\varphi_\mu = \nabla_\mu\varphi$ and $\varphi_{\mu\nu} = \nabla_\nu\nabla_\mu\varphi$.

In principle, the second-order derivatives appearing in $\mathcal{L}_i$ would lead to fourth-order field equations. Thus the theory would not satisfy the Ostrogradski theorem [103], which states that any non-degenerate, higher than second-order derivative equation of motion suffers from ghost-like instabilities. However, the higher-order terms are introduced in such a way in the action that they are cancelled in the field equations, rendering the theory ghost-free. General Relativity is recovered by setting $G_4 = M_{\rm Pl}^2/2$ and $K = G_3 = G_5 = 0$. Horndeski theory contains an entire family of scalar-tensor theories of gravity, such as FJBD theory, k-essence [110, 111], scalar-Gauss-Bonnet gravity [112], and the covariant Galileon [113].

Later it was discovered that if one allows the Lagrangian to be degenerate—meaning the determinant of its Hessian matrix[4] is zero—an even more general action can be written down, leading to higher-than-second-order equations of motion without the propagation of Ostrogradski ghosts. This was first pointed out in the context of massive gravity [114], and later led to the so-called beyond-Horndeski theories [115, 116], and DHOST theories [104, 117, 118]. These theories contain additional higher-derivative terms of the scalar field, while the propagation of a ghost mode is prohibited

[4]The Hessian matrix is obtained by taking the second derivatives of the Lagrangian with respect to velocities.

by invoking certain degeneracy conditions on the coefficients in the theory. We use the same principle in Chapter 5 to generalize khronometric theory (this Lorentz-violating theory is introduced in Section 2.3.2).

2.2.2 Modified Gravity as Dark Energy

Despite the consistency of (most) observational data with a cosmological constant, its introduction is problematic from a theoretical point of view (see Section 1.3.2). Other theories explaining the cosmic acceleration have been introduced throughout the years, and can be roughly divided in dark energy and modified gravity theories. The distinction between these models is often blurred, but for our purposes modified gravity models are the ones in which the scalar field couples non-minimally to the metric, and a fifth force is mediated. A natural consequence of this is that the strong equivalence principle is violated. A large subclass of Horndeski's theory finds application in the construction of the early- and late-time cosmic acceleration, contributing to the theory's popularity. These models originate from theories reproducing the cosmic acceleration without the need of a small but nonzero vacuum energy [119]. Some of these models are expected to be stable under quantum corrections, while others lead to a fine-tuning issue as worrisome as the original cosmological problem. Many of these theories by now have been highly constrained or ruled out by Solar-System precision tests [7], the GW170817 bound on the tensor mode speeds [33, 37], or other constraints based on gravitational-wave propagation [120–122]. We discuss the theory of k-essence (with a conformal coupling to matter) in specific, which we have studied in detail in our work described in Chapter 3 and 4, as it is left unconstrained by these bounds.

The simplest extension of the ΛCDM model is to promote the cosmological constant to a dynamical field. The idea is that the potential energy of the field is dynamically relaxed through some mechanism to a small value. Several models present this feature, and are collectively referred to as *quintessence* models [123]. A common model of quintessence is a scalar field $\varphi(t)$ slowly rolling down a potential $V(\varphi)$ described by the action

$$S_q = \int \mathrm{d}^4x \sqrt{-g} \left[\frac{M_{\rm Pl}^2}{2} R - \frac{1}{2}(\partial\varphi)^2 - V(\varphi) \right] . \tag{2.2.10}$$

This is reminiscent of inflation, with the equation of state $w_\varphi = p/\rho$ behaving as

$$w_\varphi = \frac{\frac{1}{2}\dot{\varphi}^2 - V(\varphi)}{\frac{1}{2}\dot{\varphi}^2 + V(\varphi)} \,. \tag{2.2.11}$$

Thus, the equation of state changes in time, with the present-day acceleration corresponding to $w_\varphi \simeq -1$. In fact, many quintessence models display a tracker behavior, meaning the scalar energy density before matter-radiation equality traces the radiation energy density. At the time of equality, the energy density of the quintessence field freezes at a constant value, acting like a cosmological constant. Due to this feature, these models address the cosmic coincidence problem. However, Weinberg showed in his no-go theorem that quintessence models have to be as finely-tuned as the cosmological constant to explain its small value [89].

A generalization of quintessence models is to consider a non-canonical scalar field, e.g. one with derivative self-couplings. These so-called $K(\varphi, X)$ models[5] were first considered in the context of inflation [111], and applications to the cosmic acceleration go by the name of k-essence [110, 111]. These models may be written as

$$S_k = \int \mathrm{d}^4x \sqrt{-g} \left[\frac{M_{\rm Pl}^2}{2} R - K(\varphi, X) \right] \,, \tag{2.2.12}$$

where for a homogeneous scalar field $\varphi(t)$ the equation of state reads

$$w_\varphi = \frac{K(\varphi, X)}{2XK'(\varphi, X) - K(\varphi, X)} \,, \tag{2.2.13}$$

with $K'(\varphi, X) = \mathrm{d}K/\mathrm{d}X$. By choosing an appropriate $K(\varphi, X)$, it is possible to reproduce the cosmic acceleration. Although these theories generally allow for superluminal propagation, they do not suffer from causal paradoxes [124] (contrary to the claim in [125]).

A different class of k-essence theories is obtained by coupling the scalar field to the matter sector, which can introduce some qualitative differences in the phenomenology of the theory. A subclass of these theories present a screening mechanism, that masks the scalar modifications on astrophysical scales in quasi-static configurations, but still allows for deviations on cosmological distances. Several screening mechanisms are discussed in the next section. In the literature, k-essence theories presenting a screening mechanism are commonly referred to as *k-mouflage* [126].

[5] In the flat case, these are usually referred to as $P(\varphi, X)$ models.

2.2.3 Screening Mechanisms

Gravity is strongly constrained on local scales by Solar-System precision tests, which show good agreement with General Relativity. This limits us in writing down an alternative theory of gravity. In the case of scalar-tensor theories, we can either make the coupling of the scalar field to matter very weak—such that the departure from General Relativity is essentially unobservable—or rely on a mechanism to "hide" the new degree of freedom in local experiments. The first option has the disadvantage that it renders theories highly fine-tuned and close to General Relativity, which is for instance the case for FJBD theory, where the Cassini measurement of the Shapiro delay bounds $\omega_0 > 40000$ at 2σ level [7, 21], limiting its interest for cosmology. Modifications at cosmological distances can only be introduced if they are locally hidden by so-called screening mechanisms that rely on the non-linear behavior of the scalar field in high-density regions, or—more precisely—regions in which the gravitational potential or its derivatives exceed some critical value. These screening mechanisms have been mostly studied in static configurations, and little is known about time-dependent solutions (which is precisely one of the motivations for the work presented in this thesis).

We consider the following schematic representation of the scalar sector in scalar-tensor theories (following the discussion in [127])

$$S = \int \mathrm{d}^4x \sqrt{-g} \left[-\frac{1}{2} Z^{\mu\nu}(\varphi, \partial\varphi, \partial^2\varphi) \partial_\mu\varphi \partial_\nu\varphi - V(\varphi) + \beta(\varphi) T \right] , \tag{2.2.14}$$

where $Z^{\mu\nu}$ represents the derivative self-couplings of the scalar field, $V(\varphi)$ is a potential, $\beta(\varphi)$ is a coupling to matter, and $T = T^{\mu}{}_{\mu}$ is the trace of the energy-momentum tensor. Screening can then be realised in different manners. First, if we choose $\beta(\varphi)$ such that it is small in high-density regions, the scalar field effectively decouples from matter, and the fifth force in those regions is suppressed. However, in low-density regions $\beta(\varphi)$ can be larger, and the gravitational force may be significantly modified. This principle is followed in *symmetron* and *dilaton* models [128–131]. Note that this is different from fine-tuning the coupling to matter to a fixed small value like e.g. in FJBD theory where the absence of non-linearities in the scalar field does not allow for a screening mechanism.

We can also give the scalar field an environmentally-dependent mass such that in high-density regions it has a large effective value. This would make its Compton

wavelength extremely small, suppress the scalar dynamics, and render the fifth force too short-range to be detected. This is how *chameleon* screening is realised. An example of a potential that leads to this effect—the one that was originally introduced in [132, 133]—is

$$V(\varphi) = \frac{\Lambda^{n+4}}{\varphi^n} \,, \tag{2.2.15}$$

where Λ is the characteristic energy scale of the theory. The effective potential receives a contribution from the energy-momentum tensor through the conformal coupling to matter, which leads to an effective mass $m_{eff}^2 = V''_{eff}(\varphi_{\min})$ of the scalar field that depends on the density of the environment.

The other class of screening mechanisms uses derivative self-interactions to hide the fifth force. This can be achieved by choosing $Z^{\mu\nu} = Z^{\mu\nu}(\partial\varphi)$, thus introducing kinetic self-couplings of the scalar field. The *kinetic screening* mechanism—also referred to as k-mouflage [126]—appears when the gradient of the scalar $\partial\varphi$ becomes large. This is the type of screening that appears in $K(\varphi, X)$ theories (and that we study in Chapter 3 and 4 of this thesis), such as k-essence. Many of these theories are shift-symmetric, thus invariant under a transformation $\varphi(x) \longmapsto \varphi(x) + c$, except for a Planck mass suppressed conformal coupling to matter that softly breaks it. A simple example of such theory is given by

$$K(X) = -\frac{1}{2}X - \frac{1}{4\Lambda^4}X^2 \,, \tag{2.2.16}$$

where $X = (\partial\varphi)^2$ and Λ is the strong-coupling scale of the theory. Screening begins when $X/\Lambda^4 \gtrsim 1$, which is when the quadratic kinetic term starts dominating over the canonical one. This seems problematic from an effective field theory approach, as this Lagrangian will generate quantum corrections with higher powers of X that can thus not be ignored in the screened regime. However, by correctly re-summing the loop corrections, it turns out that any form of $K(X)$ is radiatively stable [134, 135]. Scalar fluctuations can also be dynamically suppressed by second derivatives of the scalar field, thus $Z^{\mu\nu} = Z^{\mu\nu}(\partial^2\varphi)$. This is the class of *Vainshtein screening* [136], present in for instance Galileon models (see [137] for a review on this type of screening).

2.3 Lorentz-Violating Theories

Although General Relativity indeed works very well up to the Planck scale, we know it should be treated as an effective field theory that breaks down at some high en-

ergy scale. The theory is non-renormalizable, and therefore only predictive in the low energy limit. Lorentz invariance is usually regarded as a fundamental symmetry in physics, a belief that is strengthened by the absence of Lorentz violations in experimental searches in quantum field theory. However, there are also theoretical suggestions that it might not be an exact symmetry, but rather an accidental symmetry in the low energy limit.

A useful tool in the search for Lorentz violation is the Standard-Model Extension (SME), which is an effective field theory containing the Standard Model and General Relativity, plus all possible Lorentz-violating operators [138]. Using this framework, strong bounds have been set on Lorentz-violating operators in particle physics [139]. Bounds in the much more weakly-coupled gravity sector are not equally as strong [140], which has motivated physicists to explore the Lorentz-violating corner in this discipline. In the next sections, we describe two of these theories, namely Einstein-æther theory and Hořava gravity.

2.3.1 Einstein-Æther Gravity

One way to violate Lorentz symmetry is to introduce a timelike vector u_α with fixed unit norm

$$g^{\alpha\beta}u_\alpha u_\beta = -1 \,, \tag{2.3.1}$$

and couple it to gravity. This is exactly what is done in Einstein-æther, or Æ-theory. In order to preserve general covariance, the vector u_α—which we call the æther—has to be dynamical [141]. We consider a derivative expansion in the metric $g_{\alpha\beta}$ and the æther u_α, and write down the most general covariant action—without a matter coupling—quadratic in derivatives, up to a total divergence:

$$\begin{aligned} S_{Æ} = \frac{1}{16\pi G_{Æ}} \int \mathrm{d}^4x\, \sqrt{-g}\Big[& R - c_1(\nabla_\mu u_\nu)(\nabla^\mu u^\nu) - c_2(\nabla_\mu u^\mu)^2 \\ & - c_3(\nabla_\mu u_\nu)(\nabla^\nu u^\mu) + c_4(u^\alpha\nabla_\alpha u_\mu)(u^\beta\nabla_\beta u^\mu) + \lambda(u^\alpha u_\alpha - 1)\Big] \,, \end{aligned} \tag{2.3.2}$$

where $c_{1,2,3,4}$ are dimensionless constants, and the Lagrange multiplier λ enforces the unit constraint. A term proportional to $R_{\mu\nu}u^\mu u^\nu$ could be included as well, but since it is related to the $(\nabla_\mu u^\mu)^2$ and $(\nabla_\mu u_\nu)(\nabla^\nu u^\mu)$ terms through integration by parts it

has been omitted. The relation between the bare gravitational constant $G_{Æ}$ and G_N can be found by taking the Newtonian limit, and reads

$$G_{Æ} = \left(1 - \frac{c_1 + c_4}{2}\right) G_N \ . \tag{2.3.3}$$

By linearizing over a Minkowski background and constant æther, one finds that there are five massless degrees of freedom in this theory: one spin-2 mode, one spin-1 mode and one spin-0 mode. Their squared speeds are given by a combination of the couplings constants in the theory (see [142] for their form). The lack of Čerenkov radiation in ultra-high-energy cosmic ray observations bounds these speeds to be superluminal (whether or not superluminalities lead to violations of causality is a subtle issue, see e.g. [143, 144]). This, and the theoretical requirements that the modes be stable and their energy positive further constrains the coefficients.

Einstein-æther theory can also be constrained by performing a PPN analysis. The only PPN parameters that are modified with respect to their General Relativity values are α_1 and α_2, which describe preferred frame effects. Their values were found to be [142]:

$$\alpha_1 = -\frac{8(c_3^2 + c_1 c_4)}{2c_1 - c_1^2 + c_3^2} \ , \tag{2.3.4}$$

$$\alpha_2 = \frac{\alpha_1}{2} - \frac{(c_1 + 2c_3 - c_4)(2c_1 + 3c_2 + c_{34})}{c_{123}(2 - c_{14})} \ , \tag{2.3.5}$$

with notation $c_{ij} = c_i + c_j$ and $c_{ijk} = c_i + c_j + c_k$. These PPN parameters can be set to zero by imposing the conditions $c_4 = -c_3^2/c_1$ and $c_2 = (c_3^2 - c_1 c_3 - 2c_1^2)/3c_1$, rendering all PPN parameters in Einstein-æther theory equivalent to their General Relativity counterparts. The preferred frame PPN parameters have been bounded observationally to $|\alpha_1| \lesssim 10^{-4}$ and $|\alpha_2| \lesssim 10^{-7}$ [7].

2.3.2 Hořava Gravity

An approach to render General Relativity renormalizable could be to include higher order curvature terms in the Lagrangian, which, however, generally leads to ghost instabilities induced by the higher order time derivatives. Another approach is to only introduce higher order *spatial* derivatives, making the theory both renormalizable and protected from propagating any ghost degrees of freedom. By treating temporal and spatial derivatives differently, such procedure breaks Lorentz invariance. This

preferred foliation is precisely the principle of Hořava gravity, a theory introduced relatively recently by Hořava in 2009 [145].

First, let us take a look at how Hořava gravity and Einstein-æther theory are related to each other [146]. Suppose we restrict the æther to be hypersurface orthogonal, e.g.

$$u_\alpha = -\frac{\partial_\alpha T}{\sqrt{-\partial_\beta T \partial^\beta T}} \,, \tag{2.3.6}$$

with T a scalar field sometimes called the "khronon". Plugging this into the Einstein-æther action (2.3.2), we obtain a new theory with fewer degrees of freedom (sometimes referred to as "khronometric" theory). One of the coefficients $c_{1,2,3,4}$ becomes redundant, something that is more explicitly shown if one considers a fluid decomposition of the æther as is done in [146]. The equations of motion for Einstein-æther theory turn out to include third-order derivatives, unless one makes the gauge choice

$$u_\alpha = -(g^{TT})^{-1/2}\delta^T_\alpha = -N\delta^T_\alpha \,, \tag{2.3.7}$$

with N the lapse[6]. By fixing the time coordinate with this gauge choice, the theory is not preserved under full diffeomorphisms, but rather under *foliation-preserving diffeomorphisms (FDiffs)*, meaning space-independent time reparametrizations and time-dependent spatial diffeomorphisms:

$$\mathbf{x} \to \tilde{\mathbf{x}}(t, \mathbf{x}) \,, \qquad t \to \tilde{t}(t) \,. \tag{2.3.8}$$

Now, the Einstein-æther action is of the form

$$S_{Æ} = \frac{1}{16\pi G_{Æ}} \int \mathrm{d}t\, \mathrm{d}^3x\, N\sqrt{\gamma} \left[(1-\beta)K_{ij}K^{ij} - (1+\eta)K^2 + {}^{(3)}R + \alpha\, a_i a^i\right] \,, \tag{2.3.9}$$

with K_{ij} the extrinsic curvature, K its trace, ${}^{(3)}R$ the three-dimensional Ricci scalar, $\alpha = c_{14}$, $\beta = c_{13}$ and $\eta = c_2$. This action is exactly what one would get by taking the infrared limit of (non-projectable) Hořava gravity.

The full Hořava action takes the form

$$S_H = \frac{1}{16\pi G_H} \int \mathrm{d}t\, \mathrm{d}^3x\, N\sqrt{\gamma} \left(L_2 + \frac{1}{M_\star^2}L_4 + \frac{1}{M_\star^4}L_6\right) \,, \tag{2.3.10}$$

[6]The lapse, and other ADM quantities, are further defined in Chapter 5 and Appendix A.

where $M_\star$ is a new mass scale, $G_H = G_Æ/(1 - c_{13})$, L_2 is given by (2.3.9), and L_4 and L_6 contain all scalar functions of a_i and h_{ij} up to fourth and sixth order in spatial derivatives, respectively, which respect foliation-preserving diffeomorphism invariance.

Depending on how one deals with the time reparametrization invariance, two versions of the theory can be formulated. First, there is *projectable* Hořava gravity in which the lapse is a function of time only, $N(t)$, and thus can be chosen to be unity by exploiting time reparametrizations as in General Relativity. This version was soon realized to be problematic, as it is strongly-coupled and the scalar mode behaves like a tachyon in the infrared [147]. Despite this, it has been shown to be fully renormalizable (rather than only power-counting renormalizable) in any spacetime dimension [148], and to be ultraviolet complete in $2 + 1$ dimensions [149]. In non-restricted, *non-projectable* Hořava gravity, the lapse depends on the spatial coordinates as well, $N(t, \mathbf{x})$, and the scalar graviton is better behaved [150]. In this version, the number of possible operators is much larger, and showing renormalizability beyond power-counting is complicated by instantaneous modes [147]. Phenomenological studies have mostly been focused on the existence of black holes in the infrared limit of non-projectable gravity (see e.g. [151]), but recently work in the projectable sector has been done as well [152].

3 Screening in the Strong-Field Regime

The accelerated expansion of the Universe is among the biggest mysteries of cosmology. Although the cosmic acceleration is commonly explained by a cosmological constant, this possibility faces long-standing theoretical issues [89] (see also Chapter 1). Gravitational theories differing from General Relativity may explain the accelerated expansion of the Universe without a cosmological constant. However, to pass local gravitational tests, a *screening mechanism* is needed to suppress, on small scales, the fifth force driving the cosmological acceleration (see Chapter 2 for an introduction on screening mechanisms).

We consider a scalar-tensor theory with first-order derivative self-interactions, named k-essence, and explore the workings of its screening mechanism. By studying static and spherically symmetric solutions in this theory, we confirm the presence of *kinetic* screening (k-mouflage [126]) in non-relativistic stars, and extend it to fully relativistic, compact stars. In this chapter, we describe how we obtained those solutions, and present their phenomenology. In Section 3.1, we introduce the theoretical conventions of our work. In Section 3.2, we then present the static solutions we have found in the weak- and strong-field regime.

3.1 Screening in k-essence Theories

As explained in Section 2.2.2, k-essence theories were originally introduced in a cosmological context [110, 111]. They are among the few left unconstrained by bounds from gravitational-wave observations [33,37,120–122], and—as they only involve first-order derivatives of the scalar field—automatically free of Ostrogradski ghosts. More

importantly, the theory exhibits a kinetic screening mechanism that locally produces a General Relativity-like phenomenology, allowing it to pass Solar-System tests.

Kinetic screening in k-essence has been studied in the weak-field limit [126], and is extended to the strong-field regime in this work. To test the viability of a modified gravity theory, it is important to test whether it is able to produce solutions known to exist in nature, with phenomenology corresponding to observational evidence. In this work, we build on previous studies of gravitational collapse in k-essence [153], and study neutron star solutions. Coupling the k-essence scalar to matter is essential to produce screened solutions, which are not present in vacuum due to no-hair theorems in shift-symmetric scalar-tensor theories [154, 155]. Other important tests regarding these objects concern their stability and the initial value problem (Cauchy problem), which will be discussed in Chapter 4. In this section, we introduce the k-essence action and field equations, after which we explain why numerically studying the evolution of stars in k-essence theories of relevance for cosmology is challenging as a result of the hierarchy of scales involved.

3.1.1 Theoretical Set-Up

In the following, we give a detailed description of the theory of k-essence that we will study, and explain the parameter space. The action for k-essence in the Einstein frame is given by

$$S = \int \mathrm{d}^4x\sqrt{-g}\left[\frac{M_{\rm Pl}^2}{2}R + K(X)\right] + S_m\left[\frac{g_{\mu\nu}}{\Phi(\varphi)}, \Psi_m\right] , \tag{3.1.1}$$

where $M_{\rm Pl} = (8\pi G)^{-1/2}$ is the Planck mass, R is the Ricci scalar, $X \equiv g^{\mu\nu}\partial_\mu\varphi\partial_\nu\varphi$ is the kinetic term of the scalar field, and Ψ_m collectively describes the matter degrees of freedom. The Einstein-frame metric $g_{\mu\nu}$ is related to the Jordan-frame metric $\tilde{g}_{\mu\nu}$ through a conformal transformation depending on the scalar field

$$g_{\mu\nu} = \Phi(\varphi)\tilde{g}_{\mu\nu} . \tag{3.1.2}$$

We consider only the lowest order terms in the scalar part of the action

$$K(X) = -\frac{1}{2}X + \frac{\beta}{4\Lambda^4}X^2 - \frac{\gamma}{8\Lambda^8}X^3 + \cdots . \tag{3.1.3}$$

Here, Λ is the strong-coupling scale of the effective field theory, β and γ are dimensionless coefficients of $\mathcal{O}(1)$. Although screening solutions exist in k-essence for

any $\beta < 0$, $\gamma > 0$ in equation (3.1.3), in the following we set $\beta = 0$ and $\gamma = 1$[1], whereas unscreened Fierz-Jordan-Brans-Dicke (FJBD) solutions are obtained by setting $\beta = \gamma = 0$. This ensures that the theory satisfies the condition

$$1 + 2\,X\,K''(X)/K'(X) > 0\,, \tag{3.1.4}$$

for all X [124, 153, 158], and thus evades the so-called Tricomi problem (see Section 4.1.2). This in turn implies that the field equations remain always strongly hyperbolic, and the system well-posed (this is essential to produce stable numerical evolutions, see Chapter 4). The results presented in this work, however, hold (qualitatively) for more general β and γ, provided that condition (3.1.4) is satisfied.

We are mainly interested in learning about the kinetic screening mechanism in this theory, which is why have chosen a shift-symmetric function for $K(X)$[2]. However, we still mildly break this shift symmetry by including a Planck-suppressed conformal coupling to matter. This is necessary to evade no-hair theorems for shift-symmetric scalar-tensor theories that would prohibit these stars from forming any non-trivial scalar profile [154, 155]. The conformal coupling to matter is defined as

$$\Phi \equiv \exp\left(\sqrt{2}\,\alpha\,\frac{\varphi}{M_{\rm Pl}}\right)\,, \qquad \alpha \equiv \frac{1}{\sqrt{3+2\omega}}\,, \tag{3.1.5}$$

with α allowed to be $\sim \mathcal{O}(1)$, because the kinetic screening allows for escaping the Cassini bound [1].

By varying the k-essence action (3.1.1), one obtains the equations of motion for the metric and scalar field

$$G_{\mu\nu} = 8\pi G\Big(T^{\varphi}_{\mu\nu} + T_{\mu\nu}\Big)\,, \tag{3.1.6}$$

$$\nabla_\mu\left(K'(X)\nabla^\mu\varphi\right) = \frac{1}{2}\mathcal{A}T\,, \tag{3.1.7}$$

where $G_{\mu\nu}$ is the Einstein tensor constructed from the Einstein-frame metric, we define $\mathcal{A} \equiv -\Phi'(\varphi)/[2\Phi(\varphi)]$, and the scalar field and matter energy-momentum tensors are

[1] This is also the simplest choice that satisfies recent positivity bounds [156] for a healthy (although unknown) UV completion of the theory. Those bounds dictate that the leading term in $K(X)$ should have odd power and a negative coefficient. See however [157] for a different claim.

[2] More general k-essence theories consider $K(\varphi, X)$.

defined as

$$T^{\varphi}_{\mu\nu} = K(X)g_{\mu\nu} - 2K'(X)\partial_\mu\varphi\partial_\nu\varphi \,, \tag{3.1.8}$$

$$T_{\mu\nu} = \frac{2}{\sqrt{-g}}\frac{\delta S_m}{\delta g_{\mu\nu}} \,, \tag{3.1.9}$$

with $T = T_{\mu\nu}g^{\mu\nu}$. Although the Einstein frame is convenient when solving these equations numerically, we generally convert back to the Jordan frame (e.g. the frame in which matter follows geodesics) to present and interpret our results.

To solve this system of coupled equations, we make a few assumptions. First, we model matter by a perfect fluid in the Jordan frame, with baryonic density $\tilde{\rho}_0$, specific internal energy $\tilde{\epsilon}$, pressure $\tilde{p}$ and four-velocity $\tilde{u}_\mu$. From the definition (3.1.9), the stress-energy tensor in the Einstein frame, $T^{\mu\nu}$, is related to the one in the Jordan frame, $\tilde{T}_{\mu\nu}$, by $T^{\mu\nu} = \tilde{T}^{\mu\nu}\Phi^{-3}$, $T_{\mu\nu} = \tilde{T}_{\mu\nu}\Phi^{-1}$ [159, 160]. We can then write the Einstein-frame stress energy tensor as

$$T_{\mu\nu} = [\rho_0(1+\epsilon) + p]u_\mu u_\nu + p\, g_{\mu\nu} \,, \tag{3.1.10}$$

with ρ_0, p and u_μ related to their Jordan-frame counterparts by $u^\mu = \tilde{u}^\mu\,\Phi^{-1/2}$ (which ensures that the four-velocity has unit norm in both frames), $p = \tilde{p}\,\Phi^{-2}$ and $\rho_0 = \tilde{\rho}_0\,\Phi^{-2}$. These relations imply that if one considers an equation of state relating $\tilde{\rho}_0$, $\tilde{\epsilon}$, $\tilde{p}$ in the Jordan frame, the corresponding equation of state in the Einstein frame will also (in general) involve the scalar field via the conformal factor. We consider a polytropic equation of state in the Jordan frame

$$\tilde{p} = K\tilde{\rho}_0^{\Gamma} \,, \qquad \tilde{p} = (\Gamma - 1)\tilde{\rho}_0\tilde{\epsilon} \,, \tag{3.1.11}$$

where K is a constant of proportionality, and $\Gamma = (n+1)/n$ with n the polytropic index.

Since in the Jordan frame matter is not directly coupled to the scalar field but only to the metric, the usual conservation laws of the matter stress-energy tensor and baryon number apply in that frame. Transforming those conservation laws to the Einstein frame one obtains

$$\nabla_\mu T^{\mu\nu} = \mathcal{A}\nabla^\nu\varphi\, T \,, \tag{3.1.12}$$

$$\nabla_\mu(\rho_0 u^\mu) = \rho_0\mathcal{A}u^\mu\nabla_\mu\varphi \,. \tag{3.1.13}$$

Therefore, unlike in the Jordan frame, the stress-energy tensor and the baryon number are *not* conserved in the Einstein frame.

3.1.2 Hierarchy of Scales

In this chapter, we use units $\hbar = c = 1$, in which the k-essence action is given by equation (3.1.1). When simulating neutron stars numerically, it is convenient to use units adapted to the problem, which are geometric units for which $G = c = M_\odot = 1$.

To see how the k-essence action reads in these units, let us first factor out the Planck mass in the k-essence Lagrangian density:

$$\mathcal{L}_k = \frac{1}{16\pi G}\left(R - \frac{1}{2}\bar{X} + \frac{\beta}{4\bar{\Lambda}^4}\bar{X}^2 - \frac{\gamma}{8\bar{\Lambda}^8}\bar{X}^3 + \dots\right), \tag{3.1.14}$$

where we have introduced $\bar{X} \equiv 2X/M_{\rm Pl}^2$, which is the kinetic energy $\bar{X} \equiv g^{\mu\nu}\partial_\mu\bar{\varphi}\partial_\nu\bar{\varphi}$ for the dimensionless scalar $\bar{\varphi} \equiv \sqrt{2}\varphi/M_{\rm Pl}$, and defined also $\bar{\Lambda} \equiv 2^{1/4}\Lambda/{M_{\rm Pl}}^{1/2}$.

To reinstate $\hbar$, one can then note that in generic units the first two terms (the Ricci curvature and the kinetic energy for the rescaled dimensionless field) have dimensions of a length^{-2}, hence one needs $\bar{\Lambda} = 2^{1/4}\Lambda/(M_{\rm Pl}\hbar)^{1/2}$, which has the correct dimensions of length$^{-1/2}$ (with $c = 1$). For cosmologically relevant Λ, we have $\Lambda_{\rm DE} \sim \sqrt{H_0 M_{\rm Pl}} \sim 2 \times 10^{-3}$ eV (with H_0 the Hubble constant), and thus $\bar{\Lambda} \sim 10^{-13}$ m$^{-1/2}$.

In units $G = c = M_\odot = 1$, lengths are measured in units of the gravitational radius of the Sun, $GM_\odot/c^2 \approx 1.5$ km, and therefore in these units one has $\bar{\Lambda} \sim 4 \times 10^{-12}$. Rewriting then the action (3.1.14) in the same form as equation (3.1.1), but in units $G = c = M_\odot = 1$, one gets

$$\mathcal{L}_k = \frac{1}{16\pi}R - \frac{1}{2}X + \frac{\beta}{4\Lambda^4}X^2 - \frac{\gamma}{8\Lambda^8}X^3 + \dots, \tag{3.1.15}$$

where $X = \bar{X}/(16\pi)$, $\varphi = \bar{\varphi}/\sqrt{16\pi}$ and $\Lambda = \bar{\Lambda}/(16\pi)^{1/4} \approx 10^{-12}$. As will become clear in the next chapter, this very small value is among the reasons why numerical evolutions of the dynamics of stars are challenging for theories with $\Lambda \sim \Lambda_{\rm DE}$. We stress, however, that we could successfully simulate static stars for such theories (thanks to Mathematica's [161] arbitrary machine precision arithmetic).

3.2 Static Configurations

In this section, we present static screened solutions for both weakly- and strongly-gravitating stars in spherical symmetry. To connect to the literature, we first produced solutions for non-relativistic stars using a weak-field approximation. We then improved our methods by solving the full field equations, capturing also the non-linear behavior, and allowing us to study screened relativistic stars. These solutions and some of their characteristics are described in the following.

3.2.1 Weak-Field Approximation

In more detail, [126] suggested that non-relativistic, Sun-like stars in k-essence present a k-mouflage mechanism, whereby General Relativity is recovered within a *screening radius*

$$r_k \sim \Lambda^{-1}\sqrt{M/M_{\rm Pl}}\,, \tag{3.2.1}$$

(with M the star's mass), as a result of the non-linear terms in equation (3.1.3) dominating over the linear one[3]. To check this, we first consider constant-density, non-relativistic stars. Using the same weak-field approximation applied in [162, 163] to study screening in massive (bi-)gravity, we obtain from equations (3.1.6)–(3.1.7) an approximate equation for the scalar-field radial derivatives $y \equiv \varphi'$ and y' (with $' \equiv {\rm d}/{\rm d}r$):

$$\begin{aligned}\frac{r\rho}{M_{\rm Pl}\Lambda^2} = y'\left[\frac{\sqrt{2}\,(3\alpha^2+1)\,r}{\alpha\Lambda^2} + \frac{r^2 y}{M_{\rm Pl}\Lambda^2} + \frac{15\gamma r y^4(2M_{\rm Pl}+\sqrt{2}\alpha r y)}{4\sqrt{2}M_{\rm Pl}\alpha\Lambda^{10}}\right] \\ + \frac{2\sqrt{2}\,(3\alpha^2+1)\,y}{\alpha\Lambda^2} + \frac{4\alpha^2 r y^2}{M_{\rm Pl}\Lambda^2} + \frac{3\gamma y^5}{\sqrt{2}\alpha\Lambda^{10}} + \frac{3\gamma r y^6}{M_{\rm Pl}\Lambda^{10}} + \frac{5\alpha\gamma r^2 y^7}{2\sqrt{2}M_{\rm Pl}^2\Lambda^{10}}\,.\end{aligned} \tag{3.2.2}$$

Approximate analytic solutions to this equation (see Figure 3) can be obtained in the stellar interior: $y_1 \approx [\sqrt{2}\alpha\rho r\Lambda^8/(3\gamma M_{\rm Pl})]^{1/5}$; in the exterior within the screening radius: $y_2 \approx [\alpha M\Lambda^8/(2^{3/2}\pi\gamma M_{\rm Pl} r^2)]^{1/5}$; and outside the screening radius: $y_3 \approx {\rm const}/r^2$. In the FJBD case $\beta = \gamma = 0$, an approximate solution is given by y_3 outside the star, and by $y_0 \approx \alpha\rho r/[2\sqrt{2}M_{\rm Pl}(1+3\alpha^2)]$ inside.

[3] This non-linear regime may seem problematic from an EFT view-point. However, [134] (without gravity) and [135] (with gravity) showed that quantum corrections are under control in the non-linear regime.

These approximate solutions show that in k-essence the scalar derivative (which encodes the additional *fifth force* beyond General Relativity) is suppressed inside r_k. However, the inner solution is not regular at the star's center. Regularity requires $y = \varphi' \propto r$ when $r \to 0$, and a different behavior is not acceptable, as it would cause the appearance of a central conical singularity.

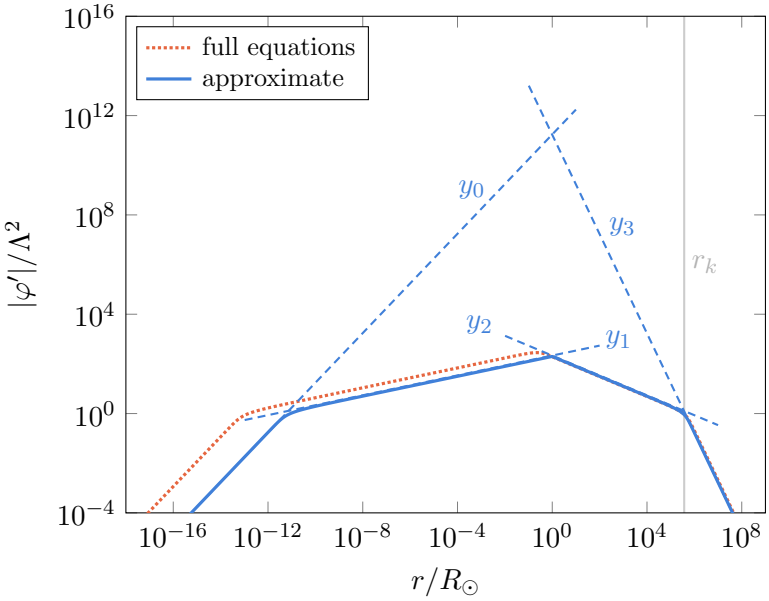

Figure 3: We consider a weakly-gravitating Sun-like star in k-essence, and plot the scalar radial derivative φ' as a function of the radial coordinate r for $\gamma = 1$, $\beta = 0$ and $\alpha \approx 0.35$. We show the numerical solution of equation (3.2.2) (solid blue line), the approximate solutions y_0, y_1, y_2, y_3 (dashed blue lines), and the numerical solution of the full system (3.1.6)–(3.1.7) (dotted orange line). The screening radius r_k is indicated by the gray line.

To amend this behavior, we solve numerically equation (3.2.2), imposing $y \to 0$ when $r \to 0$ as a boundary condition. This completely determines the solution as equation (3.2.2) does not involve y''. Thus, it is not trivial that the regular solution will match the approximates ones (y_1, y_2, y_3) above. In more detail, since equation (3.2.2) is singular at $r = 0$, we must solve it perturbatively at small radii, imposing $y \propto r$ when $r \to 0$. This yields another approximate solution, (which at leading order matches the approximate FJBD inner solution y_0) which we use to "inch away" from

$r = 0$ and provide initial conditions for the numerical integration. This procedure gives the numerical solution (regular at the center) shown by a solid blue line in Figure 3, where we also compare to the approximate solutions y_0, y_1, y_2 and y_3. As can be seen, the regular numerical solution matches the approximate solutions y_1, y_2 and y_3 everywhere but near the center, where we find agreement with y_0 (the FJBD solution) instead.

3.2.2 Strong-Field Solutions

The weak-field results confirm the existence of (regular) k-mouflage solutions in non-relativistic stars, but it is not clear that the same will apply to strongly-gravitating relativistic stars, e.g. neutron stars, or even for weakly-gravitating stars when the full system (3.1.6)–(3.1.7) is solved simultaneously. We therefore write the field equations (3.1.6)–(3.1.7) using a spherically symmetric ansatz for the (Einstein-frame) metric

$$\mathrm{d}s^2 = g_{tt}(r)\mathrm{d}t^2 + g_{rr}(r)\mathrm{d}r^2 + r^2\mathrm{d}\Omega^2 \,, \tag{3.2.3}$$

and for the scalar field, and solve the coupled system by imposing regularity at the center. Since equations (3.1.6)–(3.1.7) depend on φ (and not only on φ' and φ'', unlike equation (3.2.2)), an additional boundary condition is needed for φ. We thus require φ to approach a constant φ_∞ at spatial infinity. If we take $|\varphi_\infty|/\Lambda \lesssim 1$, as expected from cosmological considerations, results are robust against the exact value of φ_∞. We close the system by adopting the polytropic equation of state in (3.1.11). We use $K = 123\ G^3 M_\odot^2/c^6$ and $\Gamma = 2$ for neutron stars, and $K = 5.9 \times 10^{-5}\ G^{1/3} R_\odot^{2/3}/c^{2/3}$ and $\Gamma = 4/3$ for weakly-gravitating, Sun-like stars.

We impose regularity by solving perturbatively the equations near the center, and use this solution to provide initial conditions for the outbound integration at small but non-zero r. These initial conditions depend on the central values of the scalar field and density. We fix the former via a shooting procedure by requiring $\varphi \to \varphi_\infty$ as $r \to \infty$, while the central density is varied on a grid to produce stars of different masses.

The solution for a Sun-like star is shown in Figure 3 (dotted orange line), and presents the same qualitative features as the approximate solution obtained previously. Similarly, the radial profile of φ' for neutron stars in Figure 4 (solid orange line) shows

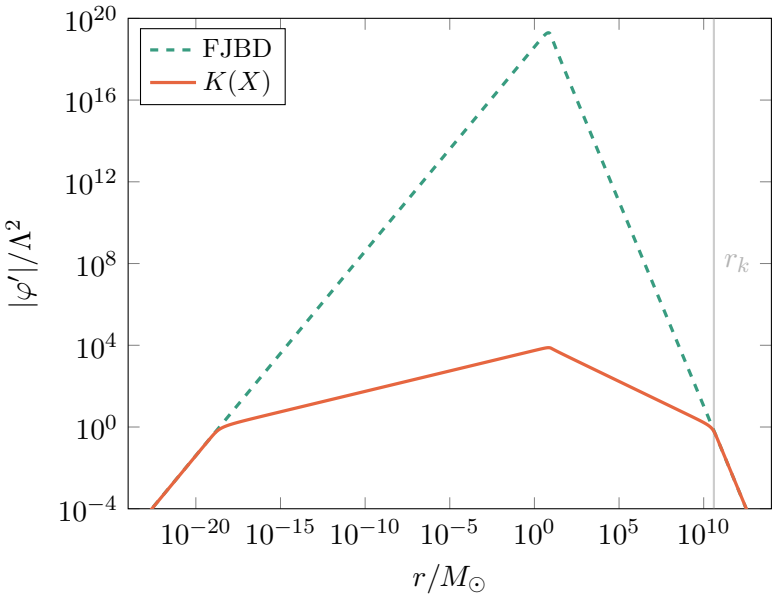

Figure 4: Setting $\alpha \approx 0.35$, we plot the radial profile for φ' for a neutron star in k-essence ($\gamma = 1$ and $\beta = 0$, solid orange line) and FJBD ($\beta = \gamma = 0$, dashed green line). The scalar profile in k-essence is suppressed with respect to the one in FJBD, with a screening radius of about $r_k \sim 1.5 \times 10^{11}$ km (indicated by the gray line which intersects with the outer kink in the orange line).

kinks right outside the center, at the stellar surface, and at the screening radius. We also plot by a dashed green line the solution to equations (3.1.6)–(3.1.7) obtained for $\beta = \gamma = 0$ (i.e. FJBD). The k-mouflage solution matches the FJBD one near the center and outside r_k, but deviates from it (suppressing φ' and thus the scalar force) when non-linearities become important (i.e. when $X/\Lambda^4 \gtrsim 1$). Similar plots and conclusions apply to generic $\beta < 0$ and $\gamma > 0$.

3.2.3 The Fifth Force

In this section, we show explicitly how the screening mechanism in k-essence affects the gravitational force. We evaluate the latter as a function of the Jordan-frame radius, and are especially interested in the regimes $\tilde{r}_\star < \tilde{r} < \tilde{r}_k$ (where screening is at work; $\tilde{r}_\star$ being the radius of the star), and $\tilde{r} > \tilde{r}_k$ (where k-essence starts deviating from General Relativity).

The screening mechanism aims to suppress the scalar fifth force on local scales, and thus tends to make the gravitational force inside the screening radius equal to the one in General Relativity. Since the Newtonian potential $\tilde{U}$ is encoded in the fall-off of the Jordan-frame metric component $\tilde{g}_{tt}$ far from the star, $\tilde{U} \approx -(\tilde{g}_{tt}+1)/2$, we can quantify the difference between the "Newtonian acceleration" $|\mathrm{d}\tilde{U}/\mathrm{d}\tilde{r}|$ in General Relativity and k-essence. In Figures 6 and 7, we show the ratio of these two accelerations for six different solutions: three neutron stars (Figure 6) and three Sun-like stars (Figure 7). To generate these solutions, we have considered three different values for the strong-coupling scale $\Lambda = (4.47 \times 10^4 \text{ eV},\ 4.47 \text{ eV},\ \Lambda_{\rm DE})$, and considered two different values for the conformal coupling constant α. For neutron stars, the central density is fixed to $\rho_c = 9.3 \times 10^{14}$ g/cm^3, whereas for Sun-like stars the central density is fixed to $\rho_c = 77$ g/cm^3. With fixed ρ_c, α, and φ_∞, we expect the central value of the scalar field (which has dimensions of an energy) to go as

$$\varphi_c \propto \Lambda \ , \tag{3.2.4}$$

a relation that is indeed satisfied by our static solutions (at least for sufficiently small Λ giving rise to kinetic screening), as we have explicitly verified and show in Figure 5.

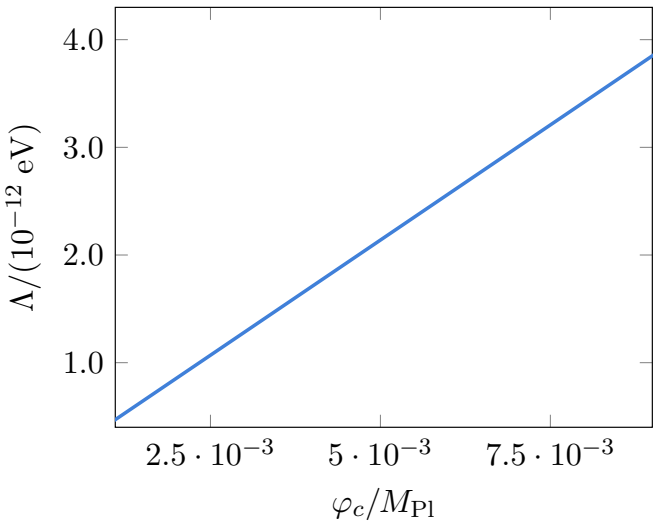

Figure 5: We plot the linear scaling of the central value for the scalar field φ with the strong-coupling scale Λ.

We stress that producing stellar solutions with $\Lambda \approx \Lambda_{\rm DE}$ is far from trivial. In order to resolve the interior of the star, which is crucial to impose regularity at the center (cf. also [1]) one needs to use internal code units adapted to the problem (e.g.

$G = c = M_\odot = 1$ or $G = c = R_\odot = 1$), which yields very small values for $\Lambda_{\rm DE}$ that are difficult to handle. We also stress that this is an issue due to the hierarchy of scales in the problem (which involves both local stellar scales and the cosmological scale $\Lambda_{\rm DE}$, see Section 3.1.2), and which is therefore independent of the choice of units.

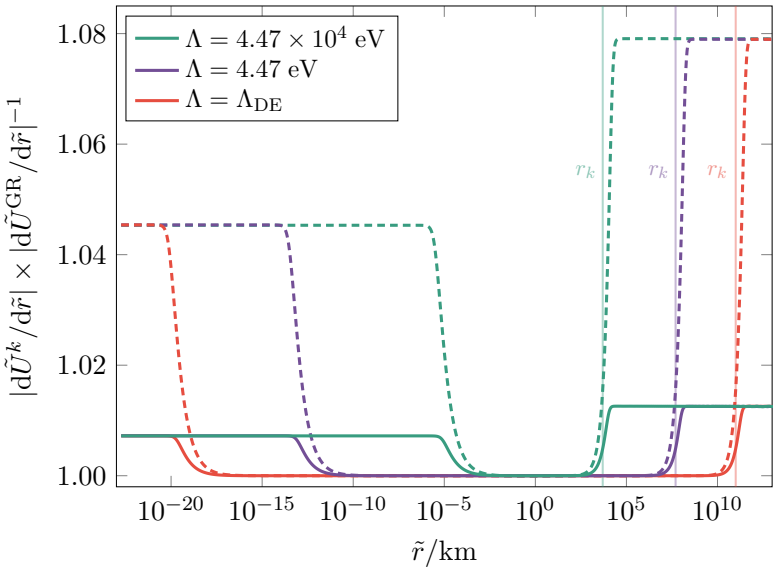

Figure 6: We plot the deviations of the Newtonian acceleration from General Relativity for neutron stars, and for different values of Λ in k-essence, considering both $\alpha \approx 0.14$ (solid lines) and $\alpha \approx 0.35$ (dashed lines). The screening radius r_k for every case is indicated by a straight vertical line.

As can be seen from Figure 6 and 7, the screening works in a similar way in Sun-like and neutron stars. At radii larger than $\tilde{r}_k$, the k-essence Newtonian acceleration deviates from the one in General Relativity, with the magnitude of the deviation depending on the value of α (in Figure 6 and 7 the solid lines correspond to $\alpha \approx 0.14$ and the dashed lines to $\alpha \approx 0.35$). However, when the radius reaches $\tilde{r}_k$, the fifth force starts being suppressed, and $|\mathrm{d}\tilde{U}^k/\mathrm{d}\tilde{r}| \times |\mathrm{d}\tilde{U}^{\rm GR}/\mathrm{d}\tilde{r}|^{-1}$ gets very close to unity. As expected, the smaller the strong-coupling scale Λ, the larger the screening radius $\tilde{r}_k$ within which the fifth force is suppressed. Finally, deep inside the star the fifth force reappears as well. This is expected because at the center of the star the kinetic energy of the scalar field $\tilde{X}$ vanishes because of regularity, and thus k-essence reduces to FJBD theory (cf. also [1]).

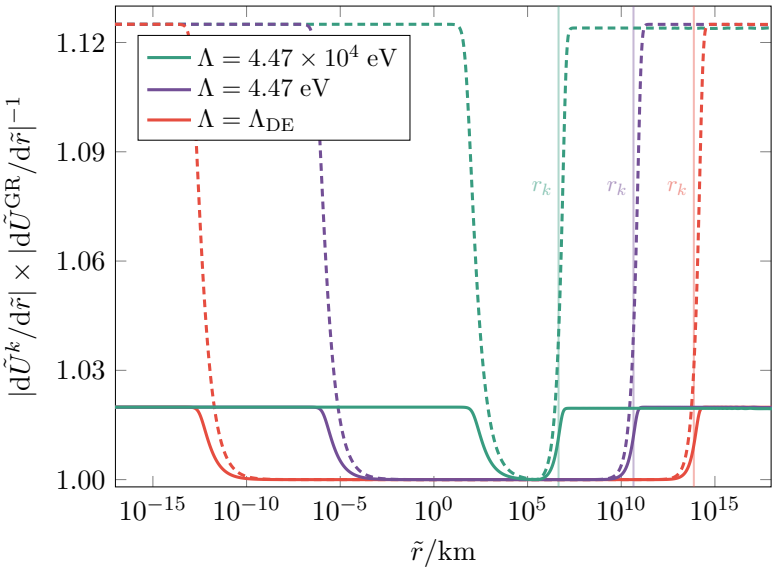

Figure 7: We plot the deviations of the Newtonian acceleration from General Relativity for Sun-like stars, and for different values of Λ in k-essence, considering both $\alpha \approx 0.14$ (solid lines) and $\alpha \approx 0.35$ (dashed lines). The screening radius r_k for every case is indicated by a straight vertical line.

To check whether these results hold also beyond Newtonian order, and more specifically at the first post-Newtonian order (1PN) that is tested in the Solar System, we compare the exterior of our numerical solutions to the parametrized post-Newtonian (PPN) expansion [7,164], and extract the PPN parameters $\beta^{\rm PPN}$ and $\gamma^{\rm PPN}$ (which are unity in General Relativity). The latter are defined in our areal coordinates as [20]

$$\tilde{g}_{tt}(\tilde{r}) = -1 + \frac{2G\tilde{M}}{\tilde{r}} - 2\left(\beta^{\rm PPN} - \gamma^{\rm PPN}\right)\left(\frac{G\tilde{M}}{\tilde{r}}\right)^2 + \mathcal{O}\left(\tilde{r}^{-3}\right) , \tag{3.2.5}$$

$$\tilde{g}_{\tilde{r}\tilde{r}}(\tilde{r}) = 1 + 2\gamma^{\rm PPN}\frac{G\tilde{M}}{\tilde{r}} + \mathcal{O}\left(\tilde{r}^{-2}\right) . \tag{3.2.6}$$

For this analysis, we consider only k-essence theories of cosmological relevance, and thus take $\Lambda = \Lambda_{\rm DE}$ (while fixing $\alpha \approx 0.14$). We extract the PPN parameters from solutions for a Sun-like star in the regime where $\tilde{r}_\star < \tilde{r} < \tilde{r}_k$ and compare their values to the constraints from Solar-System tests. This is justified because Solar-System experiments are performed well within the screening radius of the Sun, but it also poses a practical problem.

Inside the screening radius, the non-linear terms in the action are important, and thus we cannot simply perform a naive perturbative PN expansion of the metric and scalar field [155]. This is evident from the fact that only outside the screening radius the scalar field decays as $1/\tilde{r}$ (in orders of which the PN expansion would be performed). Equivalently, one can observe that a naive PN expansion would lead to the wrong conclusion that at leading (i.e. Newtonian) order k-essence should reduce to FJBD theory (which is not the case inside $\tilde{r}_k$). We therefore use our numerical solutions and simply fit them with the ansatz (3.2.5)–(3.2.6) to extract $\gamma^{\rm PPN}$ and $\beta^{\rm PPN}$, obtaining

$$\gamma^{\rm PPN} - 1 = (-5.54 \pm 1.68) \times 10^{-10} \,, \tag{3.2.7}$$

$$\beta^{\rm PPN} - 1 = (1.27 \pm 0.733) \times 10^{-3} \,, \tag{3.2.8}$$

where the error bars are at 1σ. The PPN parameters are constrained close to unity by Solar-System observations [7,21], with bounds $|\gamma^{\rm PPN} - 1|$, $|\beta^{\rm PPN} - 1| \lesssim 10^{-5}$. As can be seen, our results are compatible with these bounds at 2σ level, but our statistical error on $\beta^{\rm PPN} - 1$ is much larger than the experimental bounds. This arises from the fact that it is challenging to extract $\beta^{\rm PPN}$ from our numerical solutions, since it appears at higher order than $\gamma^{\rm PPN}$ in equations (3.2.5)–(3.2.6). This problem is also exacerbated by the low compactness of the Sun, which limits the range of radii on which we can perform our fit. Repeating indeed the procedure for more compact stars (e.g. for neutron stars), we find the more precise results

$$\gamma^{\rm PPN} - 1 = (-2.98 \pm 1.38) \times 10^{-12} \,, \tag{3.2.9}$$

$$\beta^{\rm PPN} - 1 = (1.10 \pm 0.764) \times 10^{-10} \,, \tag{3.2.10}$$

which is again in perfect agreement with the experimental bounds (see Section 1.1.4 and references therein for a discussion on the experimental bounds of the PPN parameters).

3.2.4 Mass-Radius Curves

We study the characteristics of the screened neutron star solutions we found, and start by determining their mass $\tilde{M}$ and radius $\tilde{r}_\star$. When screening is at play, however, the definition of mass is subtle. Although the gravitational mass is formally defined at spatial infinity, in practice the masses of stars are measured by the observation of orbital motion of bodies/gas well inside the screening radius. Therefore, we can define two different masses, one at spatial infinity ($\tilde{M}_\infty$) and one "felt" by

bodies surrounding the star but located well inside its screening radius ($\tilde{M}_{\rm screened}$). In practice, one can extract the former from the metric component $\tilde{g}_{tt} \approx -1 + 2G\tilde{M}/\tilde{r}$ at spatial infinity, and the latter by fitting it in the range $\tilde{r}/(GM_\odot) \sim 10^5$–$10^7$, which is the typical separation of e.g. binary pulsar systems.

	α	$\tilde{M}_\infty/M_\odot$	$\tilde{r}_\star$/km
GR	absent	1.719	14.47
k-essence	0.14	1.741	14.47
	0.35	1.855	14.47
	0.71	2.262	14.47
FJBD	0.14	1.752	14.42
	0.35	1.929	14.16
	0.71	2.572	13.51

Table 1: We present three neutron star solutions for a central density of $\rho_c = 9.3 \times 10^{14}$ g/cm^3 in General Relativity, k-essence ($\Lambda = \Lambda_{\rm DE}$), and FJBD theory, giving their mass at infinity $\tilde{M}_\infty$ and their radius $\tilde{r}_\star$ for several values of the conformal coupling constant α.

Let us start by considering the mass at spatial infinity. First, we fix the central density to $\rho_c = 9.3 \times 10^{14}\,\mathrm{g/cm^3}$, and consider three different values for the conformal coupling constant α. The corresponding neutron star masses and radii in General Relativity, k-essence, and FJBD are listed in Table 1. Then, we consider a range of central densities to generate different stars in the same three theories, while fixing $\alpha \approx 0.35$ and $\alpha \approx 0.71$, and show the mass-radius curves in Figure 8.

In Table 1, we show that both k-mouflage and FJBD stars become heavier when α increases. Their masses also deviate from the masses of the General Relativity solutions, as expected. Indeed, the gravitational mass is extracted at spatial infinity, where no screening is present and scalar effects can be significant. Conversely, the radius of the star $\tilde{r}_\star$ (defined by $\tilde{p}(\tilde{r}_\star) = 0$) is within the screening radius, and we therefore find that in k-essence it matches the General Relativity stellar radius. As the fifth force is not screened in FJBD theory, stellar radii in the latter do show differences from k-essence and General Relativity. In Figure 8, we show the mass-radius

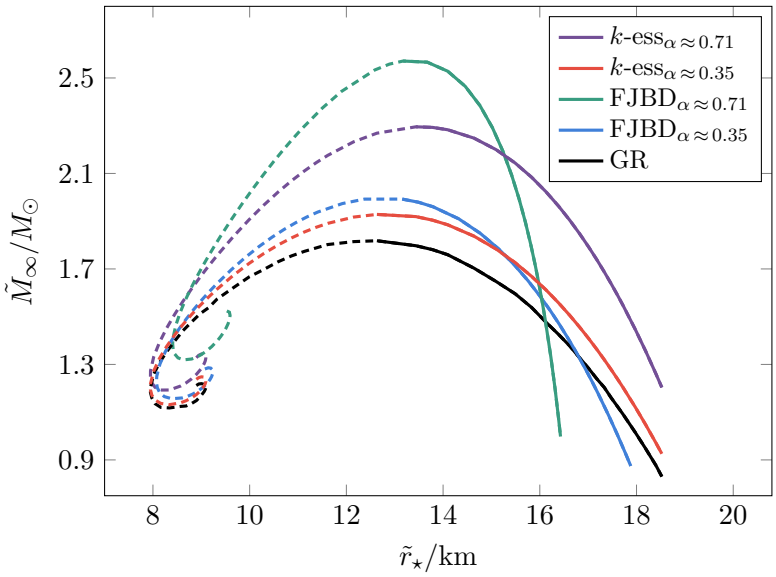

Figure 8: We plot the mass-radius curves for $\tilde{M} = \tilde{M}_\infty$ in k-essence (with $\Lambda = \Lambda_{\rm DE}$), FJBD theory, and General Relativity. We have fixed $\alpha \approx 0.35$ and $\alpha \approx 0.71$, and vary the central density to generate different stars (following the curves from right to left corresponds to increasing ρ_c). We have differentiated between stable (solid lines) and unstable branches (dashed lines).

curves for the three theories, and find that deviations from the General Relativity mass-radius curve are more pronounced for larger α in both k-essence and FJBD theory.

Let us now consider the screened mass $\tilde{M}_{\rm screened}$. The resulting mass-radius curves can be found in Figure 9. One can see that there is a perfect overlap between the General Relativity and k-essence curves. This makes sense since we are fitting the mass within the screening radius $\tilde{r}_k$, where the two theories are equivalent. We do instead find deviations for the FJBD curve, since there is no screening in that theory[4].

[4]None of these mass-radius curves rule out any of the theories, since there is a strong dependence on the equation of state, and different curves could be obtained with a choice different from the polytropic equation of state.

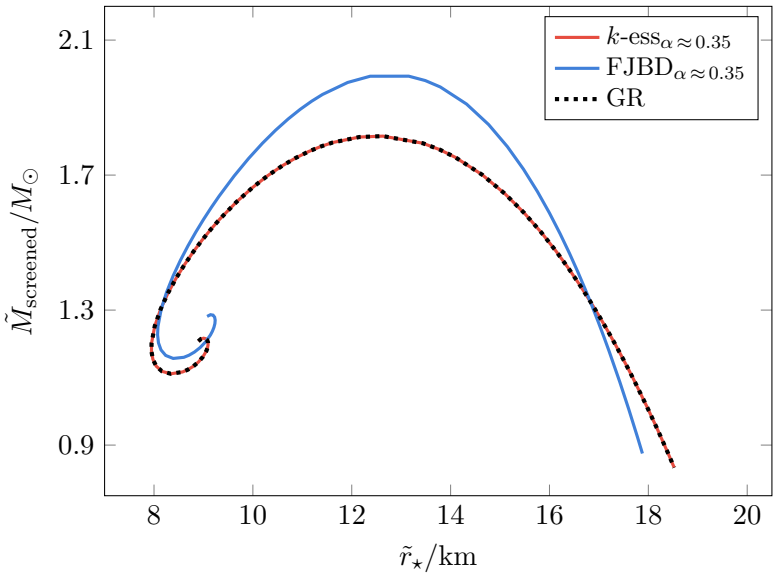

Figure 9: We plot the mass-radius curves for $\tilde{M} = \tilde{M}_{\rm screened}$ in k-essence (with $\Lambda = \Lambda_{\rm DE}$), FJBD theory, and General Relativity. We have fixed $\alpha \approx 0.35$, and vary the central density to generate different stars.

3.2.5 Scalar Charges and Scalar Field Energy

In gravitational theories that modify/extend General Relativity, the universality of free fall (which in General Relativity is satisfied as the theory obeys the equivalence principle) is typically violated, at least for strongly-gravitating objects such as neutron stars [159, 160, 165–174] and black holes [155, 175, 176]. This amounts to a violation of the strong equivalence principle and is ripe of consequences for gravitational-wave generation, as it gives rise to dipole gravitational emission from binary systems (and even monopole emission, for non-circular binaries and collapsing stars), as well as to modifications in the conservative dynamics of binaries [166–168, 171, 173].

Violations of the strong equivalence principle in modified gravitational theories are usually parametrized by *sensitivities* or *charges*, i.e. additional *hair parameters* describing compact objects and their effective coupling to the non-tensor gravitons that are generally present in these theories. These charges vanish in the low-compactness limit if the matter fields couple minimally to the metric, i.e. if the weak equivalence principle is satisfied. However, they can be significant for neutron stars or black holes, especially if non-linear phenomena (e.g. scalarization) are at play [159, 160, 165, 169,

170, 177–179].

In scalar-tensor theories, one can indeed define a dimensionless scalar charge $\bar{\alpha}$ describing the effective coupling between the scalar field and compact objects. From the decay of the scalar field near spatial infinity,

$$\varphi = \varphi_\infty + \frac{\varphi_1}{r} + \mathcal{O}\left(\frac{1}{r^2}\right) , \tag{3.2.11}$$

we can extract the scalar charge as [160, 168]

$$\bar{\alpha} = \sqrt{\frac{4\pi}{G}} \frac{\varphi_1}{M_\infty} , \tag{3.2.12}$$

with M_∞ the gravitational mass in the Einstein frame, extracted from the asymptotic expansion $g_{tt} = -1 + 2GM_\infty/r + ...$ at spatial infinity. As mentioned above, the importance of these scalar charges lies in the modifications that they induce on gravitational-wave generation. Non-zero charges can produce monopole and dipole radiation (the former only in eccentric binaries), as opposed to the quadrupole emission of General Relativity (which also gets modified by the scalar charges) [167, 168, 173]. Scalar charges may also modify the conservative dynamics of binary systems with respect to General Relativity [167, 168, 173]. As a result, non-zero scalar charges can provide a way to test the theory experimentally, a program that was indeed pursued in FJBD-like theories [180].

Results for the scalar charges in k-essence and FJBD theory for two values of the conformal coupling ($\alpha \approx 0.71$ and $\alpha \approx 0.35$) are shown in Figure 10, as functions of the baryon mass in the Jordan frame,

$$\tilde{M}_b = \int \mathrm{d}^3\tilde{x}\sqrt{-\tilde{g}}\ \tilde{\rho}_0 \tilde{u}^0 . \tag{3.2.13}$$

We find that the scalar charge is of the same order of magnitude in k-essence and FJBD, with a larger α corresponding to larger $\bar{\alpha}$ in both theories (for a fixed central density). Another similarity between the theories is that by increasing ρ_c, the scalar charge decreases (i.e., as expected, the scalar charges decreases with compactness).

Differences can be found in both the baryon mass and scalar charge shown in Figure 10. While the baryon mass was expected to behave differently in k-essence and FJBD theory (since it is defined inside the screening radius), the behavior of the

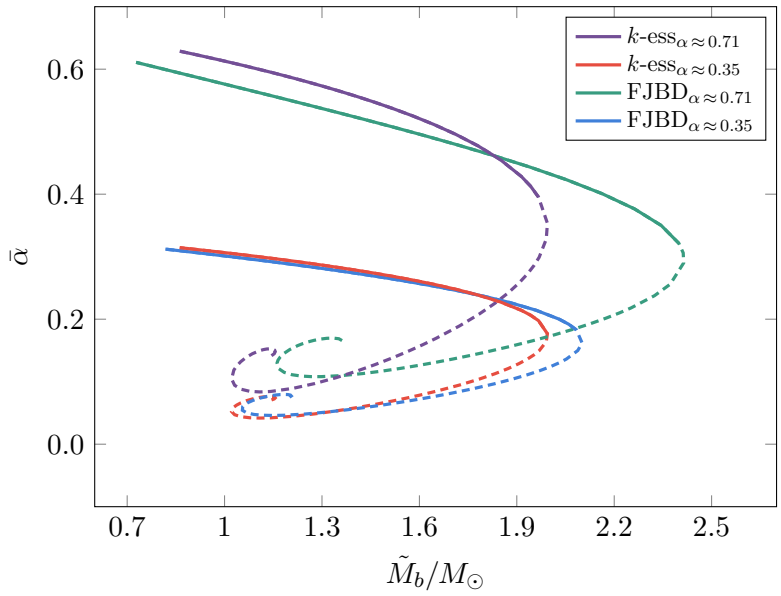

Figure 10: The scalar charge $\bar{\alpha}$ is plotted as a function of the baryon mass $\tilde{M}_b$ for k-essence (with $\Lambda = \Lambda_{\rm DE}$) and FJBD theory for conformal coupling constants $\alpha \approx 0.71$ and $\alpha \approx 0.35$. Again, the stable branches are presented by solid lines, and the unstable branches by dashed lines.

scalar charge is at first sight surprising. Just like the gravitational mass M_∞, the scalar charge $\bar{\alpha}$ is a quantity that is extracted near spatial infinity. In this regime there is no screening, and the linear terms of the scalar action (e.g. the FJBD terms) will dominate over the non-linear (k-essence) ones. Therefore, in the scalar sector, k-essence is equivalent to FJBD theory near spatial infinity, and one would expect the scalar charges to be the same in the two theories. In fact, for fixed central density, the coefficient φ_1 that regulates the decay of the scalar field and which enters the definition (3.2.12) is the same in the two theories, but the Einstein-frame mass (which also enters equation (3.2.12)) is not. As a result, the scalar charges are different.

An important caveat is that the scalar charge, being extracted from the fall-off of the scalar field near spatial infinity, describes the solution in a region where no screening is present and k-essence behaves perturbatively. It should be stressed, however, that the formalism to compute the impact of the scalar charges on gravitational-wave emission and on the conservative dynamics *also* uses PN theory, which is only valid outside the screening radius. As pointed out by [155], this limits the physical

meaningfulness of the scalar charges, which are only relevant for the conservative and dissipative dynamics of binary systems with separations larger than the sum of their screening radii. Since for $\Lambda \approx \Lambda_{\rm DE}$ a neutron star's screening radius is $\sim 10^{11}$ km, this excludes known binary pulsars, whose separation is typically $\lesssim 10^6$ km.

Therefore, testing k-essence with binary pulsar timing data would require solving for the non-linear dynamics inside the screening radius, and cannot rely on PN theory. While some work in this direction has been done by using a Wentzel-Kramers-Brillouin approximation [181–183], results are still inconclusive because full-fledged non-linear simulations (including a dynamical spacetime) of the dynamics of k-essence within the screening radius are still missing. In the next chapter, our work that contributes to solving this problem will be presented. It should also be noted that the Square Kilometre Array is expected to discover several new millisecond pulsars, especially near the Galactic center [69]. Based on the distribution of semi-major axes of known S-stars (which are $\gtrsim 1000$ au $\approx 10^{11}$ km [184]), it is not to be excluded that the conservative dynamics of millisecond pulsars around Sgr A* may be used, in the near future, to test k-essence in the perturbative regime where scalar charges are relevant.

To understand the impact of the scalar, we calculate the contribution of the scalar field to the energy of the star. The energy of the scalar field can be defined as the spatial integral of the time component of the current $\tilde{J}^\mu = \tilde{T}^{\mu\nu}_\varphi n_\nu$, where $n^\mu = \delta^\mu_t/\sqrt{-\tilde{g}_{tt}}$ is the unit norm vector orthogonal to the foliation. The scalar field energy (in the Jordan frame) within a radius $\tilde{r}$ is then

$$\begin{aligned}\tilde{E}_\varphi(\tilde{r}) &= -\int_{|\boldsymbol{x}|<\tilde{r}} \mathrm{d}^3\tilde{x}\sqrt{-\tilde{g}}\ \tilde{J}^t \\ &= 4\pi\int_0^{\tilde{r}} \mathrm{d}\tilde{r}\ [-\tilde{r}^2\sqrt{\tilde{g}_{\tilde{r}\tilde{r}}}\Phi^2 K(X)]\ , \end{aligned} \tag{3.2.14}$$

where the minus sign ensures that $\tilde{E}_\varphi > 0$.

In Table 2, we present seven different solutions for varying Λ and report their total scalar field energy $\tilde{E}^\varphi_\infty$. Besides the value of $\tilde{E}^\varphi_\infty$, normalized by both $\Lambda_{\rm DE}$ and $M_{\rm GR}$ (equal to 1.719 $M_\odot$, see Table 1), we also show the gravitational mass $\tilde{M}_\infty$, the baryon mass $\tilde{M}_b$, the radius of the star $\tilde{r}_\star$, and the screening radius $\tilde{r}_k$ of the solutions. All these quantities are evaluated in the Jordan frame. Note that $\Lambda = \infty$ corresponds to FJBD theory. In Figures 11 and 12, we plot $\tilde{E}_\varphi(\tilde{r})$ for the solutions presented

Λ/eV	$\tilde{M}_\infty/M_\odot$	$\tilde{M}_b/M_\odot$	$\tilde{r}_\star$/km	$\tilde{r}_k$/km	$\tilde{E}^\varphi_\infty/\Lambda_{\rm DE}$	$\tilde{E}^\varphi_\infty/M_{\rm GR}$
∞	1.752	1.889	14.42	absent	1.592×10^{9}	1.619×10^{-3}
4.47×10^{6}	1.745	1.877	14.47	67.73	1.982×10^{8}	2.016×10^{-4}
4.47×10^{4}	1.741	1.872	14.47	6.639×10^{3}	1.966×10^{6}	2.000×10^{-6}
4.47×10^{2}	1.741	1.872	14.47	6.637×10^{5}	1.965×10^{4}	1.999×10^{-8}
4.47	1.741	1.872	14.47	6.637×10^{7}	1.965×10^{2}	1.999×10^{-12}
4.47×10^{-2}	1.741	1.872	14.47	6.637×10^{9}	1.965	1.999×10^{-12}
$\Lambda_{\rm DE}$	1.741	1.872	14.47	1.327×10^{11}	9.825×10^{-2}	9.994×10^{-14}

Table 2: In this table, we are showing the mass at spatial infinity $\tilde{M}_\infty$, the baryon mass $\tilde{M}_b$, the stellar radius $\tilde{r}_*$, and the screening radius $\tilde{r}_k$ of seven different solutions for varying Λ. We also show the scalar field energy at spatial infinity normalized by either $\Lambda_{\rm DE}$ or $M_{\rm GR}$, in the Jordan frame ($\tilde{E}^\varphi_\infty$). The central density of the stars is fixed to $\rho_c = 9.3 \times 10^{14}$ g/cm^3, and the conformal coupling constant to $\alpha \approx 0.14$.

in Table 2.

There are a few things to notice in Table 2. First, as expected, we see that the gravitational mass of the stars decreases with decreasing Λ (and thus more suppression of the scalar field in the screened regime). At the same time, the radius of the stars increases, resulting in less compact stars for smaller Λ. We also confirm again that the screening radius increases for decreasing Λ. The scalar field energy at infinity is always small compared to the gravitational mass in General Relativity (i.e. $\tilde{E}^\varphi_\infty/M_{\rm GR} \lesssim 10^{-3}$), and for $\Lambda \sim 10^{-1}$ eV it starts being $\tilde{E}^\varphi_\infty/\Lambda_{\rm DE} \lesssim \mathcal{O}(1)$. In Figures 11 and 12, we can see the scalar energy as a function of $\tilde{r}$. It starts being suppressed when screening kicks in (deep within the star, not included in the figure), and even more so once we go outside the surface of the star (indicated with a light gray line in the Figure 12). When $\tilde{r} \sim \tilde{r}_k$, the profile flattens and the scalar field energy asymptotes to its value at infinity.

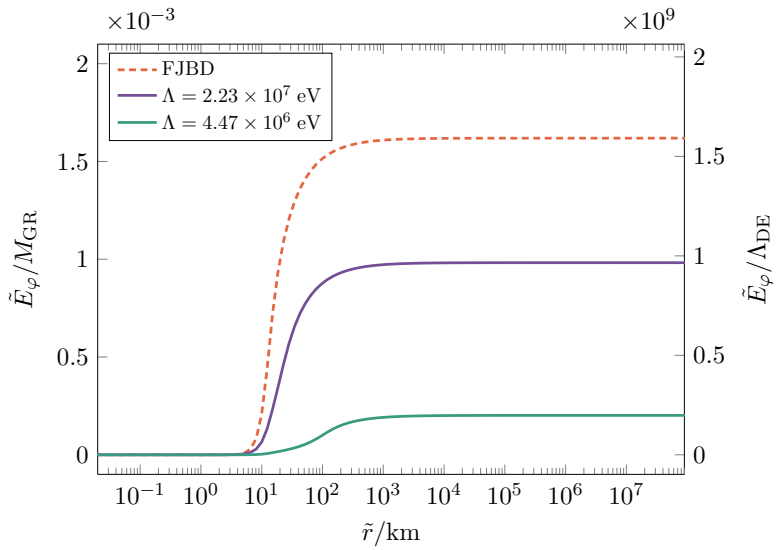

Figure 11: This is the scalar energy as a function of the Jordan-frame radius for a neutron star in FJBD theory, and in two k-essence theories (with two distinct strong-coupling scales Λ).

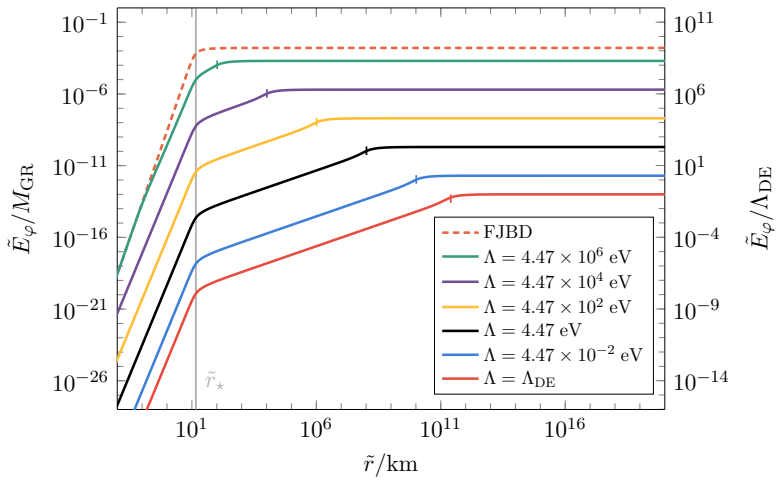

Figure 12: We plot the scalar energy of the solutions presented in Table 2. The radius of the star $\tilde{r}_\star$ is indicated by a light gray line, and the screening radii $\tilde{r}_k$ by small vertical lines on top of the solutions.

3.3 Summary

In this chapter, we studied kinetic screening in k-essence (k-mouflage) in the strong-field regime. First, we looked at weakly-gravitating stars such as the Sun, and found screened solutions by means of a weak-field approximation (reproducing results from the literature [126]), and solving the full non-linear equations numerically. In both cases, we improved on previous results by correctly accounting for the physically important requirement of regularity at the star's center. Then, we showed that kinetic screening of scalar effects also occurs in isolated stars that are highly compact/relativistic in k-essence.

We then computed the Newtonian acceleration in k-essence, and showed that the fifth force only appears deep inside the star and outside a screening radius $r_k \propto \Lambda^{-1}$. By comparing our numerical solutions to the PPN expansion, we confirmed the validity of this result at 1PN order within 2σ. We explained the definition of mass in theories with screening is subtle, and derived the mass of k-mouflage stars both near spatial infinity and within the screening radius. This led to different mass-radius curves for the stars. The scalar charge is a quantity extracted outside of the screening radius, and thus it was found to be of the same order for k-mouflage and FJBD stars. Lastly, we computed the contribution of the scalar field to the total energy of the star, once again confirming its suppression within the screening radius.

4 Dynamics of Screening in Modified Gravity

Screening has mostly been tested in static or quasi-static configurations, and its validity has often been taken for granted in dynamical settings. In this chapter, we will verify this assumption. We have shown in the previous chapter that kinetic screening (k-mouflage) of scalar effects occurs in isolated stars in k-essence, even when the stars are highly compact or relativistic and the physically important requirement of regularity at the star's center is accounted for. Now, we numerically evolve the static solutions in time, and see whether the screening mechanism survives.

In Section 4.1, we adopt a spherically symmetric ansatz, and introduce our evolution formalism and numerical methods for the first time. We presents results from evolving the static solutions, perturbed and unperturbed, and extract the monopole signal. Then, in Section 4.2, we perform numerical simulations in $3+1$ dimensions, allowing us to study screening in binaries, and to extract the full gravitational-wave signal.

4.1 Non-Linear Evolution in Spherical Symmetry

In this section, we describe the formalism that we employ to perform fully non-linear numerical evolutions in our formulation of k-essence. We use as initial data the static solutions presented in Chapter 3, subject to suitable initial perturbations that trigger stellar oscillations or spherical collapse. We present results for the evolution and show that gravitational collapse generically leads to diverging characteristic velocities, which can be avoided by adding a *fixing equation* in the spirit of the approach of [185, 186]. We then present the monopole radiation that can be extracted from these evolutions.

4.1.1 Evolution Formalism

The covariant field equations (3.1.6)–(3.1.7) and (3.1.12)–(3.1.13) can be written as an evolution system by splitting explicitly the spacetime into a foliation of space-like hypersurfaces with a normal time-like vector. Assuming spherical symmetry, we can adopt the line element

$$\mathrm{d}s^2 = -N^2(t,r)\mathrm{d}t^2 + g_{rr}(t,r)\mathrm{d}r^2 + r^2 g_{\theta\theta}(t,r)\mathrm{d}\Omega^2\,, \tag{4.1.1}$$

where $N(t,r)$ is the lapse function, while $g_{rr}(t,r)$ and $g_{\theta\theta}(t,r)$ are positive metric functions. These quantities are defined on each spatial slice with normal $n_\mu = (-N, 0)$ and extrinsic curvature $K_{ij} \equiv -\frac{1}{2}\mathcal{L}_n \gamma_{ij}$, where $\mathcal{L}_n$ is the Lie derivative along n^μ and γ_{ij} is the metric induced on each spatial slice.

The Einstein equations (3.1.6) can be written as a hyperbolic evolution system (which allows for a well-posed initial value problem, see Section 2.1.2) by using the Z3 formulation [187], in which the momentum constraint is included in the evolution system by considering an additional vector Z_i as an evolution field [188–191]. Equation (3.1.6) can be expressed as a first order system by introducing the following first derivatives of the fields as independent variables,

$$\begin{aligned} A_r = \frac{1}{N}\partial_r N\,, \qquad D_{rr}{}^r = \frac{g^{rr}}{2}\partial_r g_{rr}\,, \quad D_{r\theta}{}^\theta = \frac{g^{\theta\theta}}{2}\partial_r g_{\theta\theta}\,, \\ \chi \;=\; \partial_r\varphi\,, \qquad \Pi = -\frac{1}{N}\partial_t\varphi\,. \end{aligned} \tag{4.1.2}$$

A coordinate system for the lapse (i.e. slicing condition) is required to close the evolution system. Numerical simulations crash when a collapse singularity arises due to a non-invertible space metric [192]. By choosing an appropriate slicing condition, the simulation can be slowed down in regions close to the physical singularity, but continued in regions far away from it, rendering the simulations healthy. We use the singularity-avoiding $1+\log$ slicing condition[1]

$$\partial_t \ln N = -2\,\mathrm{tr}K\,, \tag{4.1.3}$$

[1]Other singularity-avoiding slicing conditions are the maximal slicing condition, $\mathrm{tr}K = 0$, or harmonic slicing, $\partial_t \ln N = -N\,\mathrm{tr}K$. The maximal slicing condition involves solving an elliptic equation, which generally is more computationally expensive. The harmonic and $1+\log$ slicing condition can be generalized in what is called the Bona-Massó gauge: $\partial_t N = -N^2 f(N)\,\mathrm{tr}K$, with an arbitrary function $f(N) \geq 0$ [193]. The $1+\log$ slicing condition has better singularity-avoiding properties than the harmonic slicing, and has been shown to mimic maximal slicing near the singularity.

where $\mathrm{tr}K = K^r_r + 2K^\theta{}_\theta$ [193]. The final set of evolution fields for the Z3 formulation in spherical symmetry can be found in [191].

In order to deal with shocks appearing in k-mouflage stars [1], the scalar field equation needs to be written as a conservation law (cf. equation (3.1.7)). With the definitions in (4.1.2) it reads

$$\partial_t \varphi = -N\Pi\,, \tag{4.1.4}$$

$$\partial_t \chi = -\partial_r\left(N\Pi\right)\,, \tag{4.1.5}$$

$$\partial_t \Psi = -\partial_r F^r_\Psi - \frac{2}{r}F^r_\Psi + \frac{1}{2}N\zeta\mathcal{A}T\,, \tag{4.1.6}$$

where $\zeta = \sqrt{g_{rr}}g_{\theta\theta}$ and

$$\Psi = \zeta K'\Pi\,, \tag{4.1.7}$$

$$F_\Psi = N\zeta K' g^{rr}\chi\,. \tag{4.1.8}$$

Note that we have introduced a new conserved field Ψ, depending implicitly on the primitive fields $\{\Pi, \chi\}$ through the non-linear equation (4.1.7). In fact, during the evolution, this equation has to be solved numerically at each time-step to recover Π (for further discussion see [153]).

Finally, the conservation of the stress-energy tensor and of the baryon number, equations (3.1.12)–(3.1.13), can be written as a (first-order) evolution system by splitting the four-velocity vector into its components parallel and orthogonal to the vector n^μ, namely $u^\mu = W(n^\mu + v^\mu)$, being $W = -n_\mu u^\mu$ the Lorentz factor and v^μ the spatial velocity measured by Eulerian observers (e.g. observers that are at rest on a spatial slice and follow the congruence given by n^μ). Assuming again spherical symmetry, the conservation equations (3.1.12)–(3.1.13) become

$$\partial_t(\zeta D) = -\partial_r(\zeta D N v^r) + N\mathcal{A}\zeta D(-\Pi + v^r\chi) - \frac{2}{r}\zeta D N v^r\,, \tag{4.1.9}$$

$$\begin{aligned}\partial_t(\zeta U) = &-\partial_r(\zeta N S^r) + N\zeta\mathcal{A}\Pi T \\ &+ \zeta N\left[S^r{}_r K^r{}_r + 2S^\theta{}_\theta K^\theta{}_\theta - S^r\left(A_r + \frac{2}{r}\right)\right]\,,\end{aligned} \tag{4.1.10}$$

$$\begin{aligned}\partial_t(\zeta S_r) = &-\partial_r(\zeta N S^r{}_r) + N\zeta\mathcal{A}\chi T \\ &+ \zeta N\left[S^r{}_r\left(D_{rr}{}^r - \frac{2}{r}\right) + 2S^\theta{}_\theta\left(D_{r\theta}{}^\theta + \frac{1}{r}\right) - UA_r\right]\,.\end{aligned} \tag{4.1.11}$$

The evolved conserved quantities $\{\zeta D, \zeta U, \zeta S_r\}$ are respectively proportional to the rest-mass density measured by Eulerian observers (D), the energy density (U) and the momentum density (S_r). These quantities, together with the non-trivial spatial components of the stress-energy tensor, can be written in terms of the physical (or primitive) fluid fields $\{\rho_0, \epsilon, p, v^r\}$ as

$$D = \rho_0 W\,, \qquad S_r = hW^2 v_r\,, \qquad U = hW^2 - p\,,$$
$$S_r{}^r = hW^2 v_r v^r + p\,, \qquad S_\theta{}^\theta = p\,, \tag{4.1.12}$$

where $h \equiv \rho_0(1+\epsilon)+p$ is the enthalpy, v^r is the radial velocity and the Lorentz factor is simply $W^2 = 1/(1 - v_r v^r)$.

Note that, during the evolution, one needs to recover the primitive fields $\{\rho_0, \epsilon, p, v^r\}$ in order to calculate the right-hand-side of the evolution equations for the conserved fields $\{D, U, S_r\}$. This can only be achieved by including a closure relation between the pressure and the other thermodynamic fields. Here, we close the system by employing (both in the Jordan and the Einstein frame) the ideal fluid equation of state $p = (\Gamma - 1)\rho_0\epsilon$, where Γ is the same adiabatic index used for generating the initial data (this is equal to (3.1.11) used to compute the static solutions). Furthermore, as in the case of the scalar field, the transformation from conserved to primitive fields requires to solve non-linear equations, which we do numerically at each time-step. For further discussion about the algorithm to convert from conserved to primitive fields, see [191].

Finally, the complete evolution system is written in flux-conservative form

$$\partial_t \mathbf{u} + \partial_r F(\mathbf{u}) = \mathcal{S}(\mathbf{u})\,, \tag{4.1.13}$$

where $\mathbf{u} = \{N\,, g_{rr}\,, g_{\theta\theta}\,, K_r{}^r\,, K_\theta{}^\theta\,, A_r\,, D_{rr}{}^r\,, D_{r\theta}{}^\theta\,, Z_r, \varphi\,, \Pi\,, \Psi\,, D\,, U\,, S_r\}$ is a vector containing the full set of evolution fields, and neither the radial fluxes $F(\mathbf{u})$ nor the source terms $\mathcal{S}(\mathbf{u})$ contain terms with derivatives of the evolution fields.

4.1.2 Tricomi and Keldysh Problem

In order for the Cauchy problem to be well-posed in k-essence, we would like the evolution system to be strongly hyperbolic (as explained in Section 2.1.2). We will therefore now analyse the character of the evolution equations in spherical symmetry. This analysis can be restricted to the scalar evolution equation, since the evolution

equations for the metric take the same form as in General Relativity (which are strongly hyperbolic [194]), and the source terms only involve derivatives of lower order than the derivatives in the principal part. This means that the character of the evolution equations is the same as in vacuum [153, 195]. The scalar equation of motion can be written in first-order form as

$$\partial_t \mathbf{U} + \mathbb{V}\partial_r \mathbf{U} = S(\mathbf{U}) \,, \tag{4.1.14}$$

where $\mathbf{U} = (\partial_t\varphi, \partial_r\varphi)$, $S(\mathbf{U})$ is a source term, and $\mathbb{V}$ is the characteristic matrix. We rewrite the scalar equation of motion as $\gamma^{\mu\nu}\nabla_\mu\nabla_\nu\varphi = \frac{1}{2}\mathcal{A}T/K'(X)$, with an effective metric

$$\gamma^{\mu\nu} \equiv g^{\mu\nu} + \frac{2K''(X)}{K'(X)}\nabla^\mu\varphi\nabla^\nu\varphi \,. \tag{4.1.15}$$

Then, the system is strongly hyperbolic if the principal part of this equation has real eigenvalues and a complete set of eigenvectors [99–102]. The characteristic matrix for the scalar evolution system reads

$$\mathbb{V} = \begin{pmatrix} 0 & \frac{N}{\sqrt{g_{rr}}} \\ -\frac{\sqrt{g_{rr}}}{N}\frac{\gamma^{rr}}{\gamma^{tt}} & -\frac{\gamma^{tr}}{\gamma^{tt}} \end{pmatrix} \,. \tag{4.1.16}$$

Its eigenvalues, which can be physically interpreted as the characteristic speeds of the scalar field, are

$$V_\pm = -\frac{\gamma^{tr}}{\gamma^{tt}} \pm \sqrt{\frac{-\det(\gamma^{\mu\nu})}{(\gamma^{tt})^2}} \,, \tag{4.1.17}$$

where for future purposes we write out the components of $\gamma^{\mu\nu}$ more explicitly:

$$\gamma^{tr} = \frac{2K''\Pi\chi}{N g_{rr} K'} \,, \tag{4.1.18}$$

$$\gamma^{tt} = -\frac{1}{N^2}\left(1 - \frac{2K''}{K'}\Pi^2\right) \,, \tag{4.1.19}$$

$$\gamma^{rr} = \frac{1}{g_{rr}}\left(1 + \frac{2K''}{K'}\frac{\chi^2}{g_{rr}}\right) \,. \tag{4.1.20}$$

As shown in [153], at leading order (on Minkowski space and in standard Cartesian coordinates) these velocities reduce to the usual expression for the speed of the scalar mode in k-essence, $c_s = \pm\sqrt{1 + 2XK''/K'}$ (see e.g. [124]), of which they constitute the non-linear generalization. With these definitions, we can see that the eigenvalues $V_\pm$ are real and distinct when $\det(\gamma^{\mu\nu}) < 0$. This condition is definitely not true for all $t \geq 0$, since the determinant of $\gamma^{\mu\nu}$ might cross zero during the evolution,

in which case the strong hyperbolicity of the system would be lost: when $\det(\gamma^{\mu\nu})$ becomes zero (positive), the system becomes parabolic (elliptic). This is what we call the *Tricomi problem* [196, 197] in analogy to the behavior of the Tricomi equation $\partial_t^2\varphi(t,r) + t\,\partial_r^2\varphi(t,r) = 0$. Let us take a closer look at the determinant of $\gamma^{\mu\nu}$ to understand when this happens. We find that

$$\det(\gamma^{\mu\nu}) = -\frac{1}{N^2 g_{rr}}\left(1 + \frac{2K''}{K'}X\right) . \tag{4.1.21}$$

From here it follows that we avoid the Tricomi problem if our theory satisfies [124]

$$1 + 2XK''/K' > 0 , \tag{4.1.22}$$

for all values of X. By plugging in the function $K(X)$ we are studying, e.g. equation (3.1.3), we find that

$$1 + 2XK''/K' = \frac{15\gamma X^2 - 12\beta X\Lambda^4 + 4\Lambda^8}{3\gamma X^2 - 4\beta X\Lambda^4 + 4\Lambda^8} . \tag{4.1.23}$$

Thus, condition (4.1.22) is satisfied for $\beta = 0$ and $\gamma > 0$ (which is a branch of k-essence that presents screened solutions), and the Tricomi breakdown can be avoided by limiting ourselves to this part of the parameter space[2].

Although we have established a Tricomi type behavior will never appear in our specific form of k-essence theory, there is still another problem that might (and in fact does) appear during evolving this system. To understand why, we take another look at the eigenvalues $V_\pm$ and realize that they might diverge for

$$\gamma^{tt} \to 0 . \tag{4.1.24}$$

In this case the hyperbolicity of the system is preserved, but the evolution breaks down nevertheless, a type of breakdown we refer to as the *Keldysh problem* [196, 197] (see Section 4.1.5 for more details). This happens also in vacuum close to critical collapse [153] and is at the very least a practical problem, as it makes the theory unpredictive (because simulations cannot be evolved past this divergence as a result of the Courant–Friedrichs–Lewy (CFL) condition). As we stressed in [153], diverging characteristic speeds are not necessarily pathological and may occur because of

[2]Note that even for some $\beta \neq 0$ the Tricomi condition can be satisfied initially, but this might change when X evolves to different values.

gauge choices (see e.g. a wave equation on flat space in Eddington-Finkelstein coordinates, $\mathrm{d}s^2 = -\mathrm{d}v^2 + 2\mathrm{d}v\mathrm{d}r + r^2\mathrm{d}\Omega^2$). Like in vacuum [153], the characteristic speeds may be kept finite during the evolution if a non-vanishing shift in the metric is allowed (although in spherical symmetry one has to adopt another approach). The Keldysh breakdown might also constitute a conceptual pathology, since the characteristic speeds generalize the background scalar speed to non-linear orders, albeit in a gauge-dependent way.

In this work, we build on the framework of [1,153] and show that this divergence of the characteristic speeds can be resolved by slightly modifying the dynamics by adding a "fixing equation" in the spirit of the proposal by Cayuso, Ortiz and Lehner [185] (see also [186, 198]), which was in turn inspired by the work of Israel and Stewart on relativistic dissipative hydrodynamics [199]. The addition of this equation modifies the dynamics of the theory, but the true evolution of k-essence is recovered in the limit when a free timescale τ, appearing in the fixing equation, vanishes. We show here that by taking a small $\tau \neq 0$, the evolution of collapsing neutron stars (in spherical symmetry) matches the results of pure k-essence before the divergence of the characteristic speeds, but also proceeds unobstructed past it. We then use this framework to confirm the validity of kinetic screening in these dynamical settings and to study gravitational collapse in k-essence (in addition to non-linear stellar oscillations, for which a fixing equation is not needed).

4.1.3 Numerical Methods

The numerical code employed in this work is an extension of the one presented in [153], which was used to study the dynamics of k-essence in vacuum spacetimes, with the model given by equation (3.1.3). The code has been fully tested also in General Relativity, by studying the dynamics of black holes [188], boson stars [190, 200], fermion-boson stars [191] and anisotropic compact objects [201], and in the context of scalar-tensor theories [195, 202].

We use a high-resolution shock-capturing (HRSC) scheme, based on finite-differences, to discretize both the Einstein equations and the relativistic hydrodynamics equations [188]. This method can be interpreted as a fourth-order finite difference scheme plus a third-order adaptive dissipation. The dissipation coefficient is given by the maximum propagation speed at each grid point. For the scalar field we use a more

robust HRSC second-order method, by combining the Lax-Friedrichs flux formula with a monotonic-centered limiter [203, 204].

The time evolution is performed through the method of lines using a third-order accurate strong stability preserving Runge-Kutta integration scheme. We set a CFL factor $\Delta t/\Delta r = 0.125$, in units $G = c = M_\odot = 1$, so that the CFL condition imposed by the principal part of the evolution system is always satisfied. Most of the simulations presented in this work have been performed with a spatial resolution of $\Delta r = 0.008\ M_\odot$, in a domain with outer boundary located at $r = 480\ M_\odot$. We use maximally dissipative boundary conditions for the spacetime variables, and outgoing boundary conditions for the scalar field and matter. We have verified that the results do not vary significantly when the position of the outer boundary is changed. We have also performed evolutions with different resolutions, which indicate that the results presented here are consistent and within the convergent regime.

Unlike in General Relativity, monopole gravitational radiation (in the form of scalar field waves) is permitted in scalar-tensor theories (as explained in Section 1.2.1), and is produced by gravitational collapse in Fierz-Jordan-Brans-Dicke (FJBD) theories [205–207]. In the following we will see that a non-vanishing monopole flux is also emitted by stellar oscillations and by gravitational collapse (in spherical symmetry) in k-essence. Tensor[3] and scalar gravitaional waves are encoded respectively in the Jordan-frame Newman-Penrose invariants $\tilde{\psi}_4 = -\tilde{R}_{l\bar{m}l\bar{m}} = \Phi\,\psi_4$ and in $\tilde{\phi}_{22} = -\tilde{R}_{lml\bar{m}} = \varphi\ (\phi_{22} - l^\nu l^\mu \nabla_\nu \nabla_\mu \log\Phi/2 + ...)$, with a tilde denoting quantities in the Jordan frame (we perform our simulations in the Einstein frame) and the dots denoting terms subleading in the distance r. The tensor strain is defined by integrating $\tilde{\psi}_4$ twice in time, i.e. $\tilde{\psi}_4 = \partial_t^2 h/2$. Far away from the source, we find

$$\tilde{\phi}_{22} \simeq -\alpha\sqrt{16\pi\, G}\partial_t^2\varphi + O\left(\frac{1}{r^2}\right) . \tag{4.1.25}$$

In deriving this expression, [159] assumed a decay $\propto 1/r$ for the scalar field, which, as stressed already in Chapter 3, is only a good approximation outside the screening radius in k-essence. For this reason, and because the distance of the interferometer from the source is typically much larger than the screening radius (even for $\Lambda \sim \Lambda_{\rm DE}$), we only compute $\tilde{\phi}_{22}$ at extraction radii $r_{\rm ext} > r_k$. From $\tilde{\phi}_{22}$ one can then obtain

[3]For future convenience, we discuss already here tensor gravitational waves, although they do not play a role in spherically symmetric configurations.

the scalar strain h_s via $\tilde{\phi}_{22} \propto \partial_t^2 h_s$ (which, by virtue of equation (4.1.25), yields $h_s(r_{\rm ext}) \propto \varphi(r_{\rm ext})$, up to terms constant and linear in time). The scalar strain can in turn be used to compute the signal-to-noise ratio (SNR) for a given detector [205,206].

4.1.4 Stellar Oscillations

The non-linear stability of k-mouflage stars in equilibrium configurations, like those constructed in Chapter 3, can be tested by perturbing them and following their evolution numerically using the formalism described above. Here, we consider k-essence theories with conformal coupling $\alpha \approx 0.14$, but differing for the value of Λ, which we fix to either $\Lambda = 71.8$ MeV or $\Lambda = 4.04$ MeV. The former gives rise to stars that are very similar to solutions of FJBD theory (with the same conformal coupling), while the latter produces a rather significant screening effect on the scalar field. Notice that we cannot consider Λ as small as $\Lambda_{\rm DE}$, because, even though we can simulate static stars for this value of the strong-coupling scale, the corresponding dynamical evolutions become intractable because of large round-off errors[4]. Moreover, as shown in [1], simulations of stars with significant screening are also challenging as they require significant spatial resolution near the origin, where the solutions pass from the non-linear regime applicable to the outer layers of the star to a FJBD-like behavior. Because of this, $\Lambda = 4.04$ MeV is the smallest value for Λ we can consider.

We consider equilibrium configurations with a central energy density of $\rho_c = 9.3 \times 10^{14}$ g/cm^3, and excite oscillations by increasing the internal energy of the stars by 4% ("small oscillations") or 14% ("large oscillations"). Notice that although this initial perturbation introduces small constraint violations, these are comparable to the solution's truncation error. Therefore, it is not necessary to solve the energy constraint on the initial slice. Results for the two values of Λ are presented in Figure 13, which displays the central values for the rest-mass density and for the scalar field as a function of time. The purple lines show the dynamics of unperturbed stars (i.e., stars only perturbed by numerical truncation errors), which confirms the stability of these systems. For small perturbations (red lines) and large perturbations (green lines), the stars begin to oscillate. Indeed, since we increase the internal energy of the stars to trigger the oscillations, the stellar compactness initially decreases, and so does the

[4]Since, as already mentioned and detailed in Section 3.1.2, the hierarchy of scales between the screening and stellar radii requires one to use code units $G = c = M_\odot = 1$, in which $\Lambda_{\rm DE} \sim 10^{-12}$.

scalar field magnitude. The latter oscillates with the same frequency as the density, but with a small time shift. Notice that the oscillations do not grow in amplitude, confirming that these stars are stable.

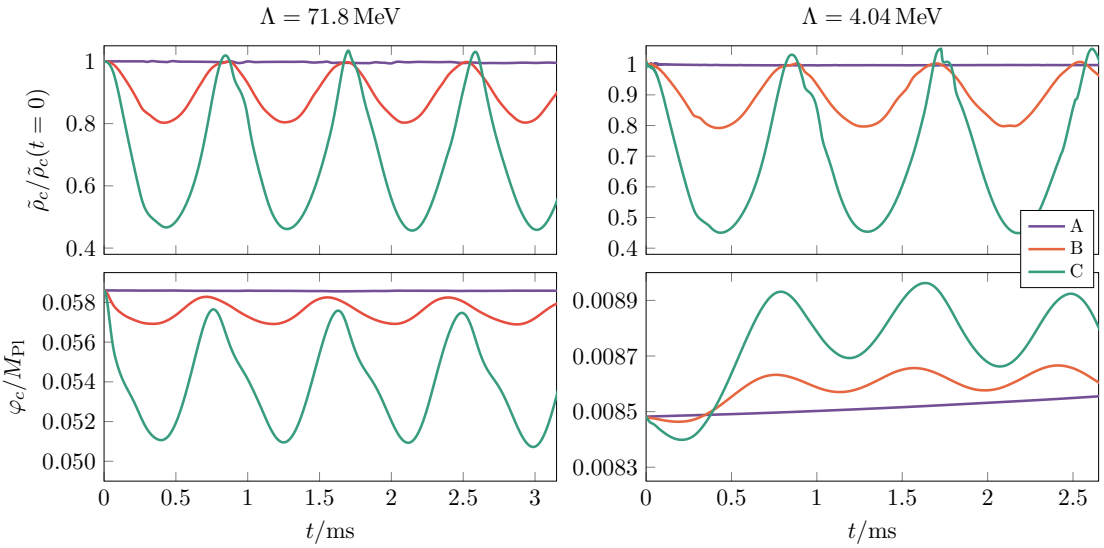

Figure 13: Evolution of the rest-mass density and the scalar field in the Jordan frame as a function of time for $\Lambda = 71.8\,\text{MeV}$ (left panel) and $\Lambda = 4.04\,\text{MeV}$ (right panel), and conformal coupling $\alpha \approx 0.14$. We consider static initial conditions (A), as well as small (i.e. 4%) and large (i.e. 14%) initial perturbations in the internal energy density (B and C, respectively). Note that no secular growth is present, i.e. k-mouflage stars are non-linearly stable.

As can be seen from Figure 13 (right panel), the amplitude of the central scalar field oscillations decreases with Λ, just like the central scalar field of the static solutions (cf. equation (3.2.4) and Figure 5). This seems to confirm the validity of kinetic screening even in this dynamical case. To strengthen this conclusion, we have also extracted the scalar monopole signal ϕ_{22} for oscillating stars initially subjected to the same large ($\sim 14\%$) perturbations of the internal density, for $\Lambda = (71.8, 12.8, 7.18, 4.04, 2.27)$ MeV. The results are presented in Figure 14 for an extraction radius $r_{\rm ext} = 150\ GM_\odot > r_k$, as a function of retarded time, defined as $t_{\rm ret} = t - r_{\rm ext}$. As can be seen, the amplitude of the signal is an increasing function of Λ.

In order to see the effect of screening more clearly, we have plotted in Figure 15

(left panel) the amplitude of the same signals, which we compute as the root mean square of the time series. Notice that with the exception of $\Lambda = 71.8$ MeV, for which there is no screening (even in the static case), the monopole amplitude scales as Λ, as expected from the scaling of the central scalar field of the static stellar solutions (cf. equation (3.2.4) and Figure 5). By integrating ϕ_{22} in time twice to get the monopole strain h_s, we can compute its SNR for Advanced LIGO (at design sensitivity[5]) for an optimally oriented source at 8 kpc (corresponding to the distance between the Earth and the center of the Galaxy). The results are displayed in Figure 15 (right panel) and show again a scaling roughly linear with Λ. Extrapolating to values of $\Lambda \sim \Lambda_{\rm DE}$ relevant for dark energy, one would get a tiny unobservable SNR $\sim 10^{-6}$ at 8 kpc.

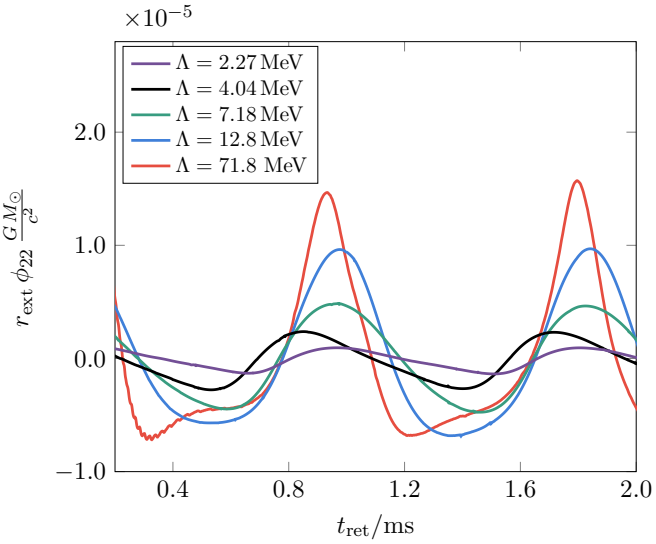

Figure 14: The Jordan-frame Newman-Penrose invariant ϕ_{22} (which describes monopole scalar radiation) for oscillating stars (with large 14% initial perturbations in the internal energy density), as function of the retarded time $t_{\rm ret} = t - r_{\rm ext}$, with $r_{\rm ext} = 150\ GM_\odot > r_k$ the extraction radius. The conformal coupling is set to $\alpha \approx 0.14$.

4.1.5 Gravitational Collapse

As discussed before, the characteristic propagation speeds of the scalar field equations (3.1.7) diverge when k-mouflage stars collapse ("Keldysh problem"). During the

[5]For the sensitivity, we used the zero detuning, high power configuration of https://dcc.ligo.org/LIGO-T0900288/public.

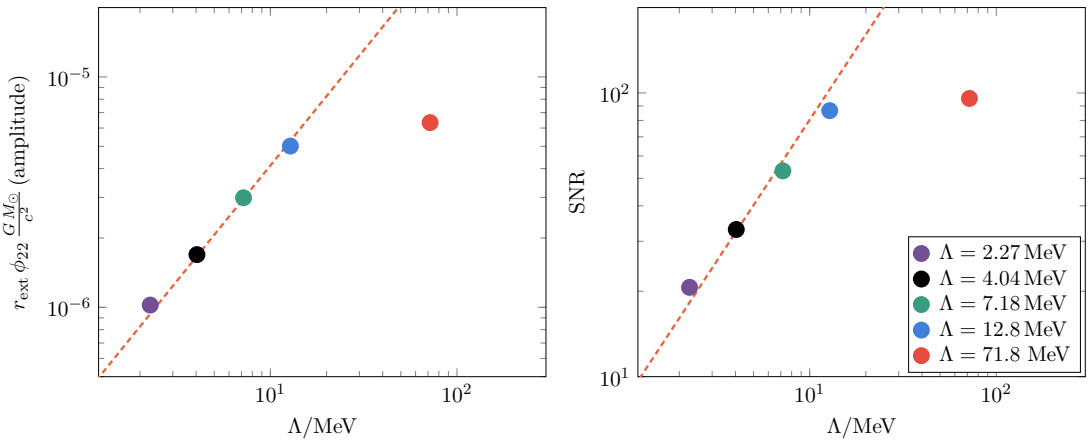

Figure 15: The amplitude of $r_{\rm ext}\,\phi_{22}$ as plotted in Figure 14 (left panel) and the corresponding SNR at 8 kpc for Advanced LIGO at design sensitivity (right panel) as a function Λ. The orange dashed lines show a linear scaling in Λ (cf. equation (3.2.4)).

gravitational collapse of a k-mouflage star (which can be triggered e.g. by decreasing its internal energy), these velocities diverge because γ^{tt} goes to zero. This problem also appears during the collapse of scalar field pulses in vacuum [153, 197, 208], and resembles the behavior of the Keldysh equation

$$t\,\partial_t^2\varphi(t,r) + \partial_r^2\varphi(t,r) = 0\,. \tag{4.1.26}$$

This equation is hyperbolic with characteristic speeds $\pm(-t)^{-1/2}$ for $t<0$, leading to a divergence at $t=0$. Diverging characteristic speeds constitute at the very least a practical obstacle that prevents one from evolving the dynamics past this divergence by using explicit time integrators, since the CFL bound forces the time step to vanish when the Keldysh behavior appears. As stressed in [153], this divergence may in principle be avoided by allowing for a non-vanishing shift. However, neither [153] nor [1] managed to find a suitable coordinate condition in spherical symmetry that would maintain the characteristic speeds finite while still ensuring stable numerical evolutions. This leaves open the possibility that the Keldysh problem that we find might have a physical relevance, besides a practical one.

Here, however, we assume that the Keldysh problem is not fundamental, and we attempt to amend it by using an approach inspired by [185, 186], which put forward a method to ameliorate the stability of Cauchy evolutions in theories with higher

derivatives (see also [198] for an application of this approach to a specific higher derivative extension of General Relativity). The method consists of modifying the theory's dynamics by adding extra fields and "fixing equations" for them. This fixing technique works like a driver which is chosen such that on sufficiently long timescales the evolution dynamics approximately matches that of the theory under consideration (k-essence in our case). We stress that this modification of the field equations does not correspond to a standard ultraviolet completion of k-essence, which is not known for theories giving screening [209].

To apply the method of [185, 186], let us first recall that in [1] we found that the scalar field equation needs to be written as a conservation law in order to deal with shocks in k-mouflage stars. The "fixing equation" that we introduce must therefore share this property. Let us then introduce the new field Σ and the modified evolution system

$$\partial_t \left(\sqrt{-g}\Sigma\nabla^t\varphi\right) + \partial_i \left(\sqrt{-g}\Sigma\nabla^i\varphi\right) = \frac{1}{2}\sqrt{-g}\mathcal{A}T\,, \tag{4.1.27}$$

$$\partial_t\Sigma = -\frac{1}{\tau}(\Sigma - K'(X))\,. \tag{4.1.28}$$

The second equation is a driver that will force Σ to $K'(X)$ on a timescale $\tau > 0$. As can be seen, the principal part of this system takes indeed the form of a conservation law. Restricting then to the spherical symmetric case and using the line element (4.1.1), equations (4.1.27)–(4.1.28) can be written as

$$\partial_t\varphi = -N\Pi\,, \tag{4.1.29}$$

$$\partial_t\chi = -\partial_r\left[N\Pi\right]\,, \tag{4.1.30}$$

$$\partial_t\Psi = -\partial_r F^r_\Psi - \frac{2}{r}F^r_\Psi + \frac{1}{2}N\zeta\mathcal{A}T\,, \tag{4.1.31}$$

$$\partial_t\Sigma = -\frac{1}{\tau}\left(\Sigma - K'(X)\right)\,, \tag{4.1.32}$$

where $\Psi = \zeta\,\Sigma\,\Pi$ and $F^r_\Psi = N\,\zeta\,\Sigma\,g^{rr}\,\chi$. As in the original k-essence equations in balance law form [153], there is a set of conserved evolved fields $\{\chi, \Psi, \Sigma\}$ and a set of primitive fields $\{\chi, \Pi, \Sigma\}$ required to calculate the right-hand side of the equations. In this case, the only unknown primitive field (Π) can be found by solving the linear equation $\Pi = \Psi/(\zeta\,\Sigma)$ at each time-step. Finally, notice that the evolution equations (4.1.29)–(4.1.32) lead to a strongly hyperbolic system, thus ensuring that the Cauchy problem is well-posed. We stress that this approach works trivially for

FJBD theories, since for the latter $K'(X) = -1/2$ is constant, and the driver in equation (4.1.32) relaxes Σ to $K'(X)$ exponentially on the timescale τ. Moreover, we have tested it against the oscillating stars presented in the previous section obtaining very good agreement.

Results for gravitational collapse in a theory with $\Lambda = 4.04$ MeV are shown in Figure 16, for the minimum of the lapse (top panel) and the central rest-mast density (bottom panel). The black circles represent results obtained by solving the field equations (3.1.6)–(3.1.7). In this case, the characteristic speeds of the scalar field diverge (at the time marked by a black cross) and the simulation stops long before formation of a horizon because of the CFL condition. The solid red line shows instead the results obtained by adding the fixing equation, which allows for the simulation to successfully complete, leading to the formation of a hairless Schwarzschild black hole. The results are obtained for values of τ down to $30\,GM_\odot$, and are extrapolated to $\tau = 0$.

Figure 17 shows instead the time evolution of the scalar field far from the source (at an extraction radius $r_{\rm ext} = 200\,GM_\odot > r_k$) as a function of time, for three values of Λ giving screening in the static case ($\Lambda = 12.8$, 7.18, 4.04 MeV). The results are again obtained for finite values of τ (as small as 10 or 30 $GM_\odot$ according to the value of Λ) and then extrapolated to $\tau = 0$. As indicated, the scalar field is multiplied by the extraction radius so that the value displayed is independent of the exact extraction position, i.e. we show $\varphi\, r_{\rm ext}$, with $r_{\rm ext} = 200\,GM_\odot$. As can be seen, $\varphi\, r_{\rm ext}$ goes from a constant non-vanishing value at the beginning of the simulation to zero at late times, for all values of Λ. This behavior is readily explained. The initial value is set by the coefficient φ_1 of equation (3.2.11), which is proportional to the scalar charge (cf. equation (3.2.12)) and which is largely independent of Λ, since scalar effects are not screened for $r > r_k$. The final value is zero because a black hole forms, and in k-essence black holes have no hair (i.e. no scalar charge) because the theory is shift symmetric [210, 211]. Therefore, we can interpret the difference between the initial and final values of $\varphi r_{\rm ext}$ as due to the collapsing star shedding its scalar hair.

Moreover, smaller values of Λ seem to lead to longer characteristic timescales (i.e. lower frequencies) in the simulations of Figure 17. In fact, if one plots the scalar field's evolution as function of a rescaled time $t' = (t - t_0)\sqrt{\Lambda} G^{1/4}$ (with t_0 a suitable

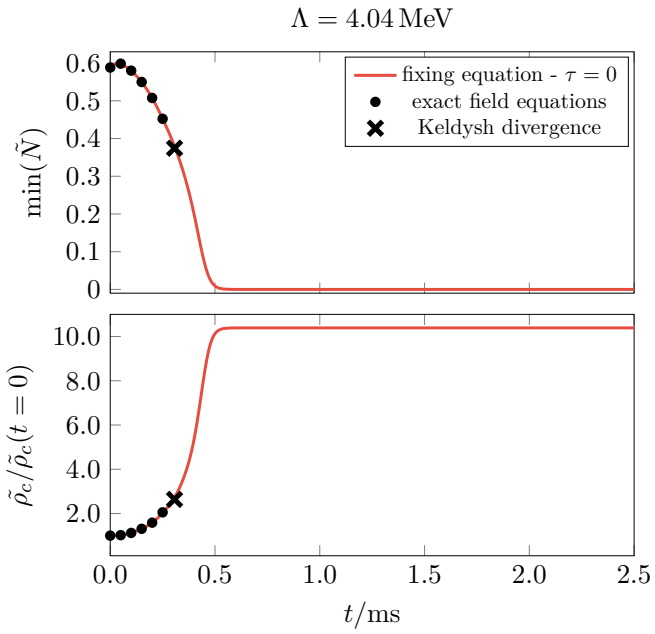

Figure 16: Evolution of the minimum of the lapse across the radial grid (top panel) and the central rest-mast density (bottom panel) in the Jordan frame, for the gravitational collapse of a neutron star in a theory with $\Lambda = 4.04$ MeV and $\alpha \approx 0.14$. The red lines represent the evolution obtained with the fixing equation (extrapolated to $\tau = 0$), and the black circles represent results obtained by solving the field equations (3.1.6)–(3.1.7). Note that the latter evolution presents diverging characteristic speeds for the scalar field at $t = 0.37\,\mathrm{ms}$ ("Keldysh behavior", black cross), which effectively halts the simulation.

offset), the results are very similar, as shown in the inset of Figure 17. From this "self-similarity", we can conclude that the frequencies contained in the signal should scale as $f \propto \sqrt{\Lambda}$. By combining this with the observation that the initial and final values of φ are independent of Λ, we can infer that ϕ_{22} should scale with Λ as $\phi_{22} \propto (2\pi f)^2\varphi \propto \Lambda$. We have verified this scaling by computing ϕ_{22} explicitly (Figure 18, left panel), extracting its amplitude as the root mean square of its time series, and verifying that the amplitude scales roughly linearly with Λ (Figure 18, right panel).

As for the SNR of the results shown in Figure 17, we have computed it (assuming optimal source orientation) for Advanced LIGO at design sensitivity, and obtained values of ~ 200 at 8 kpc, with no appreciable dependence on the value of Λ. This roughly constant (and detectable) SNR comes about because the difference between

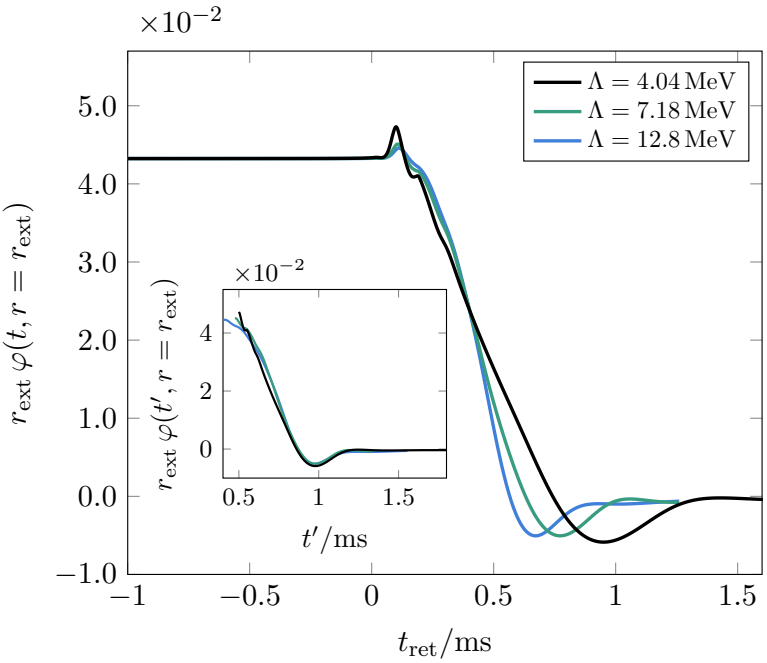

Figure 17: Evolution of the scalar field far from the source as a function of the retarded time $t_{\rm ret}$ in the Jordan frame for different values of Λ and $\alpha \approx 0.14$. These results have been obtained by extrapolating to $\tau = 0$. In the inset we display the scalar field as a function of the rescaled time t', to show the self-similarity of these solutions during the gravitational collapse.

the initial and final value of φ (and thus the scalar strain h_s) are largely independent of Λ, since the star has to shed all of its hair before forming a back hole. Because of the scaling of the frequency with $\sqrt{\Lambda}$, however, we expect that for $\Lambda \to \Lambda_{\rm DE}$ the signal will eventually fall out of the frequency band of terrestrial detectors. The latter are insensitive to frequencies lower than 1-10 Hz because of seismic noise (even for third generation detectors such as the Einstein Telescope [212] or Cosmic Explorer [59]). In fact, when going from $\Lambda \sim 10$ MeV for the results in Figure 17 (whose frequencies are $\sim$ kHz) to $\Lambda \sim 10$ eV, we expect the frequency to drop by a factor ~ 1000 to ~ 1 Hz. Scalar monopole signals in theories with $\Lambda \lesssim 10$ eV are therefore likely unobservable from Earth, but would fall in principle in the band of space-borne detectors such as LISA. By using the self-similarity of our solutions to compute the SNR for LISA in the case of $\Lambda \approx \Lambda_{\rm DE} \approx 2\,{\rm meV}$, we obtain SNR $\sim$ 30–40 (according to whether we use the LISA sensitivity curve from the proposal to ESA [213] or from the Science Requirements Document [214]) for optimally oriented sources at 8 kpc distance. For

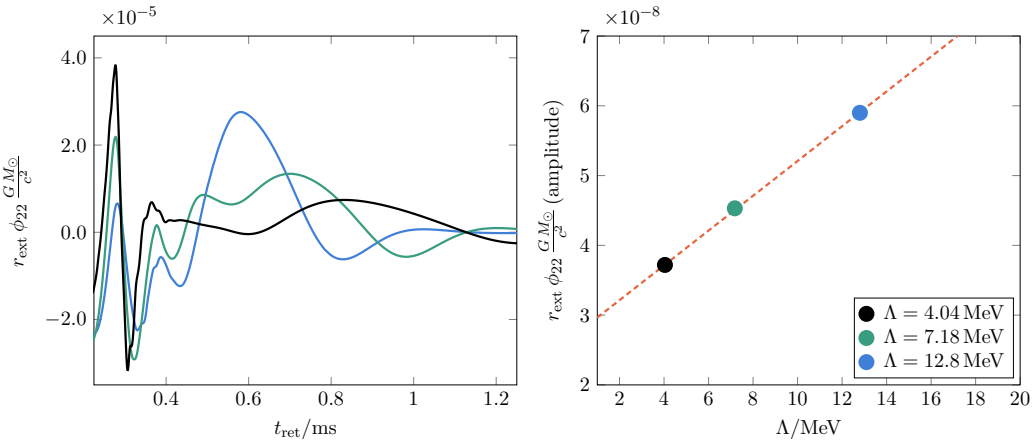

Figure 18: In the left panel, we show the Jordan-frame Newman-Penrose invariant ϕ_{22} for collapsing stars, as function of the retarded time $t_{\rm ret}$, with $r_{\rm ext} = 200\,GM_\odot > r_k$ and conformal coupling $\alpha \approx 0.14$. On the right, we show the amplitude of ϕ_{22} as a function of Λ, together with a linear fit in Λ (orange dashed line).

$\Lambda \approx 10$ meV, we get instead SNR $\sim$ 7–10. We should stress again, however, that these results involve an extrapolation over nine orders of magnitude in Λ, based on the self-similarity of our simulations.

4.2 Screening in Binaries

In spherical symmetry, we managed to evolve gravitational collapse past the scalar-speed divergence by slightly modifying the dynamics, with the addition of an extra driver field. This technique, while *ad hoc* and approximate, suggests that the divergence is not of physical origin, but rather linked to the gauge choice, as conjectured in [153]. In this part of the work, we use indeed a gauge choice (including a non-vanishing shift) that maintains the characteristic speeds finite during both gravitational collapse and binary evolutions in $3+1$ dimensions. The latter constitute the first fully dynamical simulations of the gravitational-wave generation by binary systems in theories with screening.

4.2.1 Evolution Formalism: Updated

The covariant equations of motion we study in this section are the same as in the spherically symmetric case, e.g. equations (3.1.6)–(3.1.7) and (3.1.12)–(3.1.13). We do, however, update our evolution formalism, and choose a non-zero shift in the metric ansatz. In the following, the precise updates with respect to the spherically symmetric evolutions in the evolution set-up are outlined.

The Einstein equations (3.1.6) are written as an evolution system by using the covariant conformal Z4 (CCZ4) formulation [204, 215, 216], which extends the Einstein equations by introducing a four-vector Z_μ as follows

$$R_{\mu\nu} + \nabla_\mu Z_\nu + \nabla_\nu Z_\mu = 8\pi \left[\left(T^{\varphi}_{\mu\nu} + T_{\mu\nu}\right) - \frac{1}{2} g_{\mu\nu} \left(T^{\varphi} + T\right) \right] + \kappa_z \left(n_\mu Z_\nu + n_\nu Z_\mu - g_{\mu\nu} n^\sigma Z_\sigma\right) , \tag{4.2.1}$$

where $\kappa_z > 0$ is a damping term enforcing the dynamical decay of the constraint violations associated with Z_μ [217].

As customary, we split the spacetime tensors and equations into their space and time components by using a $3+1$ decomposition. The line element is then given by

$$\mathrm{d}s^2 = -N^2\,\mathrm{d}t^2 + \gamma_{ij}\Big(\mathrm{d}x^i + \beta^i \mathrm{d}t\Big)\Big(\mathrm{d}x^j + \beta^j \mathrm{d}t\Big), \tag{4.2.2}$$

where N and γ_{ij} are defined as before, and β^i is the shift vector. By introducing a (spatial) conformal decomposition and some definitions, namely

$$\begin{aligned} \bar{\gamma}_{ij} &= \chi\,\gamma_{ij} \quad , \quad \bar{A}_{ij} = \chi\left(K_{ij} - \frac{1}{3}\gamma_{ij}\mathrm{tr}K\right), \\ \mathrm{tr}\hat{K} &= \mathrm{tr}K - 2\,\Theta \quad , \quad \hat{\Gamma}^i = \bar{\Gamma}^i + 2Z^i/\chi, \end{aligned} \tag{4.2.3}$$

where $\bar{\Gamma}^i = -\partial_j \bar{\gamma}^{ji}$, $\mathrm{tr}K = \gamma^{ij}K_{ij}$ and $\Theta \equiv -n_\mu Z^\mu$, one can obtain the final equations for the evolution fields $\{\chi, \bar{\gamma}_{ij}, \mathrm{tr}\hat{K}, \bar{A}_{ij}, \hat{\Gamma}^i, \Theta\}$. The explicit form of these equations is lengthy and can be found in [216]. Note that the definitions above lead to new conformal constraints,

$$\bar{\gamma} = \det(\bar{\gamma}_{ij}) = 1\,, \qquad \mathrm{tr}\bar{A} = \bar{\gamma}^{ij}\bar{A}_{ij} = 0, \tag{4.2.4}$$

which can also be enforced dynamically by including additional damping terms proportional to $\kappa_c > 0$ in the evolution equations. Finally, we supplement these equations

with gauge conditions for the lapse and shift. We use the 1+log slicing condition [193] (for non-zero shift) and the Gamma-driver shift condition [218], namely

$$\partial_t N = \beta^k \partial_k N - N^2 f(N) \mathrm{tr}\hat{K} \,, \tag{4.2.5}$$

$$\partial_t \beta^i = \beta^k \partial_k \beta^i + \eta \beta^i - N^2 g(N) \hat{\Gamma}^i \,, \tag{4.2.6}$$

being $f(N)$ and $g(N)$ arbitrary functions depending on the lapse, and η a constant parameter. In our case, a successful choice is $f(N) = 2/N$, $g(N) = 3/(4N^2)$ and $\eta = 2$.

Concerning the scalar equation, we follow the same procedure as before, and write it in balance law form. By defining the following new evolved fields

$$\varphi_i \equiv \partial_i \varphi \,, \tag{4.2.7}$$

$$\Pi \equiv -n_\mu \partial^\mu \varphi = -\frac{1}{N}(\partial_t \varphi - \beta^i \varphi_i) \,, \tag{4.2.8}$$

the evolution equations for the scalar field in terms of the $3+1$ quantities can be written as

$$\partial_t \varphi = \beta^k \varphi_k - N\Pi \,, \tag{4.2.9}$$

$$\partial_t \varphi_i = -\partial_i(-\beta^k \varphi_k + N\Pi) \,, \tag{4.2.10}$$

$$\partial_t(\sqrt{\gamma}\Psi) = -\partial_k[\sqrt{\gamma}(-\beta^k \Psi + N K'(X) \gamma^{kj} \varphi_j)] + \frac{1}{2} N \sqrt{\gamma} \mathcal{A} T \,, \tag{4.2.11}$$

where $\gamma = \det(\gamma_{ij})$ and $\Psi = K'(X)\Pi$. Therefore, our conservative evolved fields are $\{\varphi, \varphi_i, \Psi\}$, while the primitive physical variables required to compute the fluxes and sources are given by $\{\varphi, \varphi_i, \Pi\}$. In order to calculate Π from Ψ, the following non-linear equation

$$K'(X)\Pi - \Psi = 0 \tag{4.2.12}$$

must be resolved numerically (for instance with a Newton-Raphson method) at each time-step.

The general relativistic hydrodynamics equations are written in flux-conservative form

as well, i.e.

$$\partial_t(\sqrt{\gamma}D) + \partial_k[\sqrt{\gamma}D(Nv^k - \beta^k)] = N\mathcal{A}\sqrt{\gamma}D(-\Pi + v^k\varphi_k)\,, \tag{4.2.13}$$

$$\partial_t(\sqrt{\gamma}\tau) + \partial_k[\sqrt{\gamma}(-\beta^k\tau + N[S^k - Dv^k])] = N\sqrt{\gamma}\mathcal{A}\left[\Pi T + \Pi D - v^k\varphi_k D\right] + \sqrt{\gamma}\left[NS^{ij}K_{ij} - S^i\partial_i N\right]\,, \tag{4.2.14}$$

$$\partial_t(\sqrt{\gamma}S_i) + \partial_k[\sqrt{\gamma}(-\beta^k S_i + NS_i^k)] = N\sqrt{\gamma}\mathcal{A}\left[\varphi_i T\right] + \sqrt{\gamma}\left[N\Gamma^j_{ik}S^k_j + S_j\partial_i\beta^j - (\tau + D)\partial_i N\right]\,, \tag{4.2.15}$$

where v^i is the fluid velocity measured by an Eulerian observer

$$v^i = \frac{u^i}{W} + \frac{\beta^i}{N}, \tag{4.2.16}$$

with $W \equiv 1/\sqrt{1 - \gamma^{ij}v_iv_j}$ the Lorentz factor. The evolved conserved variables in this case are the rest-mass density measured by an Eulerian observer (D), the energy density (with the exclusion of the mass density) (τ) and the momentum density (S_i), which are defined in terms of the primitive field as follows:

$$D = \rho_0 W\,, \tag{4.2.17}$$

$$\tau = hW^2 - p - D\,, \tag{4.2.18}$$

$$S_i = hW^2 v_i\,, \tag{4.2.19}$$

$$S_{ij} = \frac{1}{2}\left(v_iS_j + v_jS_i\right) + \gamma_{ij}p\,, \tag{4.2.20}$$

being $h = \rho_0(1 + \epsilon) + p$ the enthalpy as before (notice that the other definitions are trivial generalizations of the spherically symmetric definitions). Again, the relation between the evolved and the primitive fields is non-linear and it needs to be solved numerically by using a Newton-Raphson method in order to calculate the fluxes and sources.

4.2.2 Numerical Set-Up

In order to perform fully relativistic numerical simulations of binary mergers in k-essence theory, we consider the Einstein frame and evolve the CCZ4 formulation of the Einstein equations coupled to a perfect fluid (adopting an ideal-gas equation of state with $\Gamma = 2$) [219] and a scalar field [220]. Without loss of generality, we again fix $\beta = 0$ and $\gamma = 1$ [1, 2, 153]. Furthermore, we set the conformal coupling to $\alpha \approx 0.14$. As discussed in [2], $\Lambda \sim \Lambda_{\rm DE}$ is intractable numerically due to the hierarchy between

binary and cosmological scales (which leads to $\Lambda_{\rm DE} \sim 10^{-12}$ in units adapted to the binary system). Like in [1, 2], we study $\Lambda \gtrsim 1\,\text{MeV}$ (for which screening is already present).

The computational code, generated by using the platform *Simflowny* [221–223], runs under the SAMRAI infrastructure [224–226], which provides parallelization and the adaptive mesh refinement (AMR) required to solve the different scales in the problem. We use fourth-order finite difference operators to discretize our equations [204]. For the fluid and the scalar, we use High-Resolution Shock-Capturing (HRSC) methods to deal with shocks, as discussed in [1,2,153]. A similar General Relativity code, using the same methods, has been recently used to simulate binary neutron stars [219,227]. Our computational domain ranges from $[-1500, 1500]^3\,\text{km}$ and contains 6 refinement levels. Each level has twice the resolution of the previous one, achieving a resolution of $\Delta x_6 = 300\,\text{m}$ on the finest grid. We use a CFL factor $\lambda_c \equiv \Delta t_l/\Delta x_l = 0.4$ on each refinement level l to ensure stability of the numerical scheme.

4.2.3 Binary Evolutions

We construct initial data for neutron star systems in k-essence theory by relaxation [159, 160], i.e. we generate General Relativity solutions using LORENE [228] and evolve them in k-essence until that they relax to stationary solutions. These solutions agree with the non-rotating solutions for k-mouflage stars found in [1, 2], thus validating our relaxation technique (Figure 19, left panel). Similarly, we have also considered rotating solutions in k-essence, finding for the first time that *(i)* they behave qualitatively like the non-spinning ones, and *(ii)* the screening mechanism also survives in axisymmetry (Figure 19, left panel). We also reproduced the dynamics of stellar oscillations in k-essence found in [1, 2], and managed to follow the (spherical) black-hole collapse of a neutron star (Figure 19, right panel). These simulations were inaccessible, due to the diverging characteristic speeds, within the framework of [1], without the addition of an extra driver field and a "fixing equation" [185, 186] for it [2]. Here, using the gauge conditions mentioned above (and typically employed in numerical-relativity simulations of compact objects in $3+1$ dimensions), we found no divergence of the characteristic speeds in our class of k-essence theories. The collapse obtained with this gauge matches exactly the results obtained in [2], as shown in the right panel of Figure 19, corroborating the (approximate) "fixing equation" technique employed there. We will therefore use the aforementioned gauge conditions also for

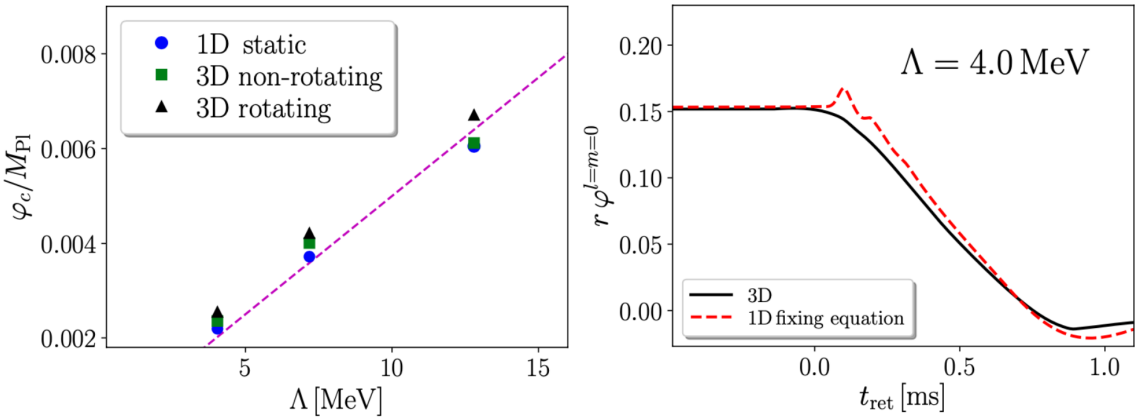

Figure 19: *Left*: Central scalar field for rotating/non-rotating stars produced with our three-dimensional code and non-rotating ones produced with the static one-dimensional code of [1]. Stellar masses are $M \approx 1.74\,M_\odot$. Also shown is the expected linear scaling with Λ [2]. *Right*: Scalar field at the extraction radius for gravitational collapse (with mass $M \approx 1.74\,M_\odot$), obtained with the one-dimensional code of [2] (using an approximate fixing-equation approach) and our three-dimensional code.

binary evolutions.

Like in the isolated case, initial data for binary systems are constructed by relaxation. The relaxation process occurs approximately in the initial 4 ms of our simulations, and does not impact significantly the subsequent binary evolution. We consider binary neutron stars in quasi-circular orbits with a total gravitational mass $2.8-2.9\,M_\odot$ and mass ratio $q = M_2/M_1 = \{0.72, 1\}$. Time snapshots of a binary with mass ratio $q = 0.9$ in a theory with $\Lambda \approx 4$ MeV are shown in Figure 20, displaying both the star's density and the scalar field. The screening radii of the stars in isolation are ~ 120 km and thus larger than the initial system separation. This is the physically relevant situation, as for $\Lambda \sim \Lambda_{\rm DE}$ the screening radii are $\sim 10^{11}$ km. Also observe the formation of a scalar wake trailing each star (for the most part), with the two wakes merging in the last stages of the inspiral.

We place our extraction radius for the gravitational wave signal outside the screening radius of the individual neutron stars, at distances of 300 km from the center of mass. This is justified because the distance to the detector is typically $\gg 10^{11}$ km, which is the screening radius for $\Lambda \sim \Lambda_{\rm DE}$, even for Galactic sources. We decompose h and

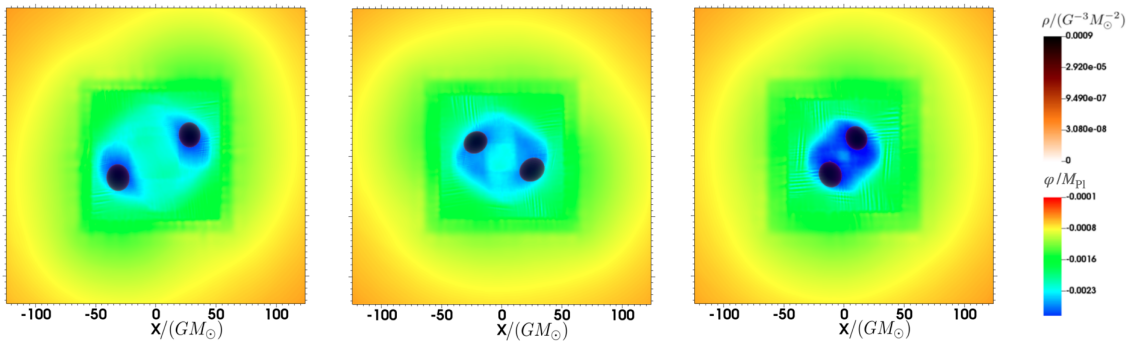

Figure 20: Unequal-mass ($q = 0.91$) neutron star binary with $\Lambda = 4.0\,\mathrm{MeV}$, shown at successive times. The color code represents the scalar field, which is initially centered on each star and then develops into a common "envelope", while the dark orange represents the fluid density.

h_s (or φ) into spin-weighted spherical harmonics. As expected, the dominant contribution comes from the $l = m = 2$ mode for the tensor strain. For the scalar emission the monopole $l = m = 0$ is suppressed, and the main contribution comes from the dipole ($l = m = 1$) mode and (mostly) the quadrupole ($l = m = 2$) mode. The results for four simulations—for $\Lambda \approx 4$, 5 and 7 MeV and for FJBD (corresponding to $\Lambda \to \infty$), with $\alpha \approx 0.14$—are shown in Figure 21. Notice that we do not show the General Relativity tensor strain as it is practically indistinguishable from the FJBD one on this timescale [159]. The three values of Λ predict screening radii larger than the initial separation between the stars.

As can be seen, the tensor strains are very similar, even after the merger (corresponding to the peak amplitude). As for the scalar, the suppression of the $l = m = 0$ mode is expected, since monopole emission vanishes in FJBD theory for quasi-circular binaries [167, 168]. The $l = m = 1$ dipole mode is instead small but non-vanishing, as expected for unequal-mass binaries in FJBD, with signs of screening suppression as Λ decreases. However, the (dominant) $l = m = 2$ scalar quadrupole mode is always *larger* than in FJBD theory, suggesting that the screening is not effective at suppressing the quadrupole scalar emission in the late inspiral/merger. The amplitude also seems to increase when going to low frequencies/early times, in the simulations with $\Lambda \approx 4$ and 5 MeV. Note that one does not expect a continuous limit to FJBD ($\Lambda \to \infty$) when Λ increases. In FJBD theory there is no screening and the binary is always in the perturbative regime, while in k-essence the separation is always smaller

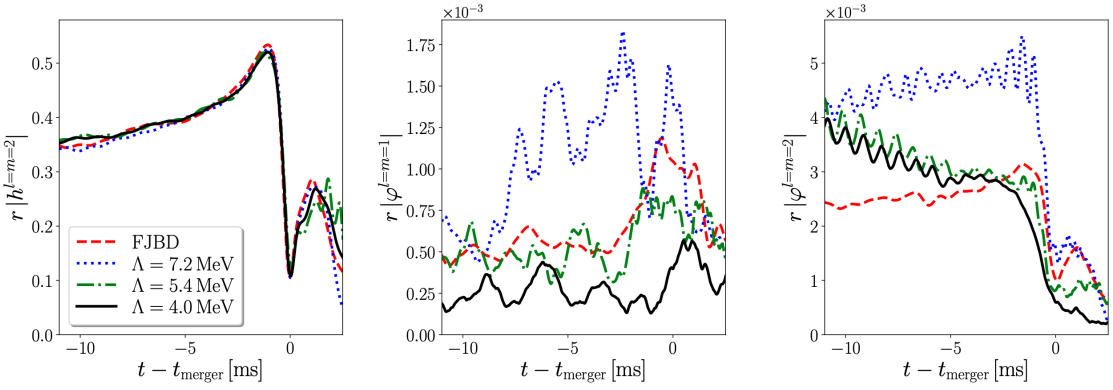

Figure 21: Tensor ($l = m = 2$) and scalar ($l = m = 1$ and $l = m = 2$) strain for a NS merger with $q = 0.91$, in k-essence and FJBD.

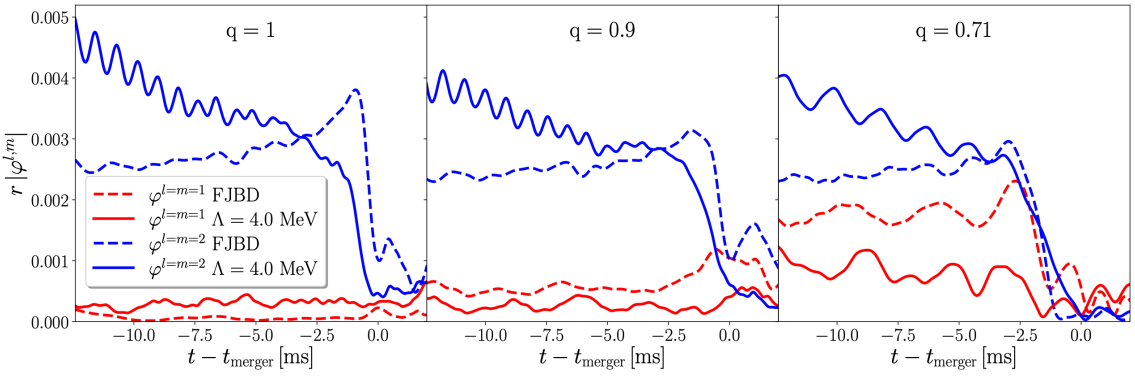

Figure 22: Dipole ($l = m = 1$) and quadrupole ($l = m = 2$) scalar strain for merging neutron star binaries of varying mass ratio, in k-essence and FJBD.

than the screening radii. This is true even for observed binary pulsars, which have separations $\lesssim 10^5$ km vs screening radii of $\sim 10^{11}$ km for $\Lambda \sim \Lambda_{\rm DE}$.

The dependence on the mass ratio of the binary (which we set to $q = 1$, 0.9 and 0.71) is shown in Figure 22, for the FJBD and $\Lambda \approx 4$ MeV cases. As can be observed, quadrupole fluxes are largely unaffected by q in both theories, with the k-essence ones consistently larger, especially at early times. The dipole fluxes in k-essence show again signs of suppression relative to FJBD, at least for $q \neq 1$, but in both theories they grow as q decreases. This is expected, since PN calculations in FJBD [167,168] predict that the dipole amplitude should scale as the difference of the stellar scalar charges, which grows as q decreases. For $q = 1$, instead, the dipole flux in FJBD is compatible with zero (as predicted by PN theory [167,168]), while it does *not* vanish in k-essence.

4.3 Summary

In this chapter, we studied the evolution of k-mouflage stars in spherical symmetry and $3+1$ dimensions. We first explored the stability of the screened neutron star solutions in spherical symmetry by perturbing their internal energy and evolving them numerically in time. In our first attempt, we showed that k-mouflage solutions are stable to small perturbations, and also to large ones as long as they do not cause gravitational collapse. We extracted the resulting monopole scalar radiation outside the screening radius for theories with Λ as small as a few MeV, and by extrapolating to $\Lambda \sim$ meV, we have concluded that no observable monopole emission is to be expected from stellar oscillations in these theories.

However, when large perturbations with the right sign to trigger collapse were applied to k-mouflage solutions, the evolution led to diverging characteristic speeds for the scalar, well before the formation of apparent black-hole/sound horizons. This divergence might not be pathological in itself, but prevents dynamical evolutions of the collapse of k-mouflage stars. By modifying the theory's equations in a UV-agnostic way inspired by dissipative hydrodynamics [186], we managed to dynamically evolve the spherically symmetric gravitational collapse of a k-mouflage star as well. This method has allowed us to simulate gravitational collapse without incurring in any divergent characteristic speed, for strong-coupling scales as low as a few MeV. We have found that, unlike in the case of stellar oscillations, kinetic screening does not

suppress the monopole scalar radiation (extracted outside the screening radius) from the collapse. This happens because the collapsing star must shed away all of its scalar hair in scalar waves before forming a (hairless) black hole. This scalar signal would not be detectable by terrestrial gravitational wave detectors because its very low frequency (at least for values of $\Lambda \sim$ meV relevant for dark energy), but we conjecture that it might be observable with space-based detectors such as LISA, if a supernova explodes in the Galaxy.

Finally, we performed fully $3+1$ relativistic simulations of binary neutron stars in k-essence, adopting a gauge with non-zero shift that prevents the divergences of the characteristic speeds (this confirmed that these pathologies were in fact a gauge issue). In the late inspiral and merger of binary neutron stars, the (subdominant) dipole scalar emission is screened (at least for unequal masses), but the (dominant) quadrupole scalar flux is not. In fact, our results seem to hint at quadrupole scalar emission being as important (or even larger, especially at low frequencies) in k-essence than in FJBD theories with the same conformal coupling α, as long as the strong-coupling scale is in the MeV range that we can simulate. If this feature survives for $\Lambda \sim \Lambda_{\rm DE}$, k-essence theories may become as fine-tuned as FJBD theory (which will wash out any effect on large-scale structure observations). Considering for instance the relativistic double-pulsar system $J0737-3039$ [229–231], in FJBD the absence of scalar quadrupole radiation constrains $|\alpha| \lesssim 4.4 \times 10^{-2}$.

5 Degenerate Hořava Gravity

As we saw in Chapter 2, an alternative approach to go beyond General Relativity is by giving up Lorentz invariance. Hořava gravity breaks Lorentz symmetry by introducing a dynamical timelike scalar field (the khronon), which can be used as a preferred time coordinate (thus selecting a preferred space-time foliation). Adopting the khronon as the time coordinate, the theory is invariant only under time reparametrizations and spatial diffeomorphisms.

In the infrared limit, this theory is sometimes referred to as khronometric theory. Here, we explicitly construct a generalization of khronometric theory, which avoids the propagation of Ostrogradski modes as a result of a suitable degeneracy condition (although stability of the latter under radiative corrections remains an open question). While this new theory does not have a general-relativistic limit and does not yield a Friedmann-Robertson-Walker-like cosmology on large scales, it still passes, for suitable choices of its coupling constants, local tests on Earth and in the Solar System, as well as gravitational-wave tests. We also comment on the possible usefulness of this theory as a toy model of quantum gravity, as it could be completed in the ultraviolet into a "degenerate Hořava gravity" theory that could be perturbatively renormalizable without imposing any projectability condition.

5.1 Motivation

Hořava gravity [145] is a gravitational theory that is power-counting renormalizable in the ultraviolet (UV), at the expense of giving up Lorentz symmetry. The theory, written in terms of $3+1$ Arnowitt-Deser-Misner (ADM) variables [232], is indeed invariant only under foliation-preserving diffeomorphisms (FDiffs), i.e. (monotonic) time reparametrizations and spatial diffeomorphisms, and *not* under full-fledged four-

dimensional diffeomorphisms. The action of the theory involves up to six spatial derivatives of the ADM fields, but is only quadratic in the time derivatives (which only appear via the extrinsic curvature, i.e. via the time derivative of the spatial metric). It is this anisotropic scaling between space and time derivatives that ensures power-counting renormalizability.

Performing a Stuckelberg transformation, Hořava gravity can be recast as a Lorentz-violating scalar-tensor theory [146]. The scalar field, sometimes referred to as the khronon, is constrained by a Lagrange multiplier to be timelike (i.e. its gradient must be timelike), and it thus plays the role of a preferred time by selecting a preferred manifold slicing. Using this covariant formulation, as opposed to the original $3+1$ one (i.e. the unitary gauge where the khronon is adopted as time coordinate), it becomes more clear why the $3+1$ action is built without any time derivatives of the lapse. In fact, to avoid Ostrogradski instabilities [103] (or "ghosts"), one may naively require that the covariant action be quadratic in the unit-norm "æther" vector field proportional to the khronon's gradient. This vector field turns out to be $\boldsymbol{u} = -N dt$ in the unitary gauge, with N the lapse, and one may naively try to obtain time derivatives of N by introducing the acceleration $a^\nu = u^\mu \nabla_\mu u^\nu$. The latter, however, only includes spatial derivatives of N because of the unit norm condition (which implies $a^\mu u_\mu = 0$).

The absence of time derivatives of the lapse poses a hurdle to proving perturbative renormalizability (beyond power counting). Calculations of the latter are technically involved and have so far only been performed in the unitary gauge [148, 233], where the lapse satisfies an elliptic equation as a result of the absence of its time derivatives in the action [147]. This leads to the "instantaneous" propagator $1/(k_i k^i)$. To overcome this problem, [148] proved perturbative renormalizability in Hořava gravity under the "projectability condition", i.e. the assumption that the lapse is a function of time only. The resulting theory, while considered in the first paper by Hořava [145], is disjoint from general (i.e non-projectable) Hořava gravity [147], and is strongly coupled on flat space [147, 234, 235].

It should be noticed, however, that including derivatives of the lapse (i.e. second time derivatives of the khronon scalar field) does not lead automatically to Ostrogradski ghosts, if the Lagrangian is *degenerate*. This fact is very well known in the context of Lorentz-symmetric scalar tensor theories, where it led first to beyond-Horndeski

theories [115,116] and then to Degenerate Higher-Order Scalar-Tensor (DHOST) theories [104, 117, 118]. These theories have field equations that are higher than second order in time, but still propagate no ghosts.

In the following, we will apply this degeneracy program to the infrared (IR) limit of non-projectable (i.e. general) Hořava gravity. In that limit, the theory is sometimes referred to as khronometric theory, and while it still violates Lorentz symmetry (being only invariant under FDiffs in the unitary gauge), it is quadratic in both time and space derivatives (of the spatial metric and khronon) [146, 147]. We will show that khronometric theory can be modified to include second time derivatives of the khronon (i.e. time derivatives of the lapse), while still propagating no Ostrogradski ghost. Although similar constructions were already obtained in [236–238], here we additionally show that the resulting theory is invariant under spatial diffeomorphisms and a special set of (monotonic) time reparametrizations (which will turn out to be given by "hyperbolic" time compactifications). While invariance under this special group of transformations is sufficient to determine the form of the kinetic term for the lapse, it does not fix its coefficient unambiguously. Therefore, the radiative stability of the fine-tuning of the coupling constants needed to eliminate the ghost remains an open issue. We will comment on promising ways forward on this issue in the following.

As a result of this construction, the novel "degenerate Hořava gravity" theory that we find does not have a limit to General Relativity (GR). However, somewhat surprisingly, this does not prevent the theory from having the correct Newtonian limit, nor from reproducing (at least for specific values of the coupling constants) the dynamics of GR at the first post-Newtonian (1PN) order and thus passing Solar-System tests. However, the behavior on cosmological scales is wildly different from GR, at least at the background level (i.e. assuming isotropy and homogeneity). We will discuss this issue, its implications, and possible solutions below.

This chapter is organized as follows. In Section 5.2 we review Hořava gravity both in the unitary gauge and in the covariant (Stuckelberg) formalism. In Section 5.3 we then consider theories invariant under a smaller gauge group, i.e. restricted foliation-preserving diffeomorphisms (RFDiffs), as an intermediate step toward Section 5.4, where we introduce our degenerate generalization of Hořava gravity. We study its phenomenology in Section 5.5, and we discuss our conclusions in Section 5.6. We

utilize units in which $c = 1$, except in Appendix B, where we discuss the PN expansion of degenerate Hořava gravity and we thus reintroduce c as a book-keeping parameter.

5.2 Hořava Gravity

In this section, we review the construction of Hořava gravity and the subgroup of the four-dimensional diffeomorphisms under which the theory is invariant. The distinction between space and time introduces a preferred frame, and thus a preferred time coordinate, which corresponds to endowing the space-time manifold with a preferred foliation by space-like surfaces. This means that the arbitrary reparameterization of time $t \to \tilde{t}(t, \mathbf{x})$ is not a symmetry of the theory anymore.

The basic ingredients to describe the spacetime geometry are the spatial metric γ_{ij}, the shift N^i and the lapse function N entering the $3+1$ decomposition of the four-dimensional metric [232]

$$\mathrm{d}s^2 = -N^2 \mathrm{d}t^2 + \gamma_{ij}(\mathrm{d}x^i + N^i \mathrm{d}t)(\mathrm{d}x^j + N^j \mathrm{d}t)\,. \tag{5.2.1}$$

The Hořava action is built from quantities invariant under the following unbroken symmetry, which is commonly referred to as FDiffs:

$$\mathbf{x} \to \tilde{\mathbf{x}}(t, \mathbf{x})\,, \qquad t \to \tilde{t}(t)\,, \tag{5.2.2}$$

where $\tilde{t}(t)$ is a monotonic function of t. Notice that this is the largest possible unbroken gauge group that one can have, once a preferred foliation is introduced. Under this symmetry the fields in (5.2.1) transform as

$$N \to \tilde{N} = N \frac{\mathrm{d}t}{\mathrm{d}\tilde{t}}\,, \quad N^i \to \tilde{N}^i = \left(N^j \frac{\partial \tilde{x}^i}{\partial x^j} - \frac{\partial \tilde{x}^i}{\partial t} \right) \frac{\mathrm{d}t}{\mathrm{d}\tilde{t}}\,, \quad \gamma_{ij} \to \tilde{\gamma}_{ij} = \gamma_{kl} \frac{\partial x^k}{\partial \tilde{x}^i} \frac{\partial x^l}{\partial \tilde{x}^j}\,. \tag{5.2.3}$$

Up to dimension six, the action takes the form [145]

$$S = \frac{1}{16\pi G} \int \mathrm{d}^3x\, \mathrm{d}t\, N \sqrt{\gamma} \Big[(1-\beta) K_{ij} K^{ij} - (1+\lambda) K^2 + \alpha\, a_i\, a^i + {}^{(3)}\!R - \mathcal{V} \Big]\,, \tag{5.2.4}$$

where K_{ij} is the extrinsic curvature of the surfaces of constant time[1]

$$K_{ij} = \frac{1}{2N} \left(\dot{\gamma}_{ij} - D_i N_j - D_j N_i \right) \tag{5.2.5}$$

[1]Note that our definition of K_{ij} differs by an overall sign from the definition used in some textbooks (e.g. [239, 240]), although it agrees e.g. with [150, 241, 242].

with D_i three-dimensional covariant derivatives compatible with the spatial metric γ_{ij} and with an overdot denoting partial time derivatives, $K \equiv K_{ij}\gamma^{ij}$ is the trace of the extrinsic curvature, ${}^{(3)}R$ is the three-dimensional Ricci scalar and

$$a_i \equiv N^{-1}\partial_i N \tag{5.2.6}$$

is the acceleration vector. Besides the bare gravitational constant G, there are three free dimensionless constants: α, β and λ. The "potential" $\mathcal{V}$ depends on the three-dimensional Ricci tensor ${}^{(3)}R_{ij}$ and the acceleration a_i, with all possible operators of dimension four and six. This potential therefore involves only a finite number of these operators, which were fully classified e.g. in [243] and [150]. While crucial for renormalizability, for our purposes the potential is completely irrelevant. Therefore, we omit to write explicitly its form here, and we focus on the IR limit of the theory (obtained by neglecting $\mathcal{V}$) in the rest of this chapter.

Also notice that the kinetic part of the action (i.e. the part where time derivatives appear) is fully contained in the first two terms of equation (5.2.4). In addition to the helicity-2 modes of the graviton, there is also a propagating scalar field, usually referred to as the "khronon" [147]. This extra mode appears because the two first-class constraints (primary and secondary) associated with time diffeomorphisms in GR become here second-class constraints, because of the breaking of time diffeomorphisms. The theory therefore possesses six first-class constraints (associated with spatial diffeomorphisms) and 2 second-class constraints, leaving $[20-(6\cdot 2)-2]/2 = 3$ dynamical degrees of freedom.

5.2.1 Stuckelberg Formalism

This formalism allows one to single out explicitly the extra degree of freedom that appears because of the breaking of diffeomorphism invariance. It amounts to rewriting the action in a generally covariant form, at the expense of introducing a compensator field that transforms non-homogeneously under the broken part of the four-dimensional diffeomorphisms.

In more detail, one encodes the foliation structure of the spacetime in a scalar field φ, such that the foliation surfaces are identified with those of constant φ. The action (5.2.4) then corresponds to the frame where the coordinate time coincides with φ

(i.e. $\varphi = t$). This choice of coordinates is often referred to as "unitary gauge". The action in a generic frame is then obtained by performing the Stuckelberg transformation and reads

$$S = \frac{1}{16\pi G}\int \mathrm{d}^4x\,\sqrt{-g}\left[R - \beta\,\nabla_\mu u^\nu \nabla_\nu u^\mu - \lambda\,(\nabla_\mu u^\mu)^2 + \alpha\,a_\mu a^\mu\right]\,, \tag{5.2.7}$$

where

$$u_\mu = \frac{\partial_\mu\varphi}{\sqrt{-X}}\,, \qquad X \equiv \partial_\mu\varphi\partial^\mu\varphi\,, \qquad a^\mu \equiv u^\nu\nabla_\nu u^\mu\,, \tag{5.2.8}$$

and R is the four-dimensional Ricci scalar. Notice that this is the action of Einstein-æther theory when the æther vector field is hypersurface orthogonal [244]. For later purposes, it is convenient to write the action (5.2.7) explicitly in terms of the khronon field

$$\begin{aligned} S = \frac{1}{16\pi G}\int \mathrm{d}^4x\,\sqrt{-g}\Bigg[R + \beta\,\frac{\varphi_{\mu\nu}\varphi^{\mu\nu}}{X} + \lambda\,\frac{(\Box\varphi)^2}{X} - 2\lambda\,\frac{(\Box\varphi)\varphi^\mu\varphi_{\mu\nu}\varphi^\nu}{X^2} \\ +(\alpha-2\beta)\frac{\varphi^\mu\varphi_{\mu\rho}\varphi^{\rho\nu}\varphi_\nu}{X^2} + (\beta+\lambda-\alpha)\frac{(\varphi^\mu\varphi_{\mu\nu}\varphi^\nu)^2}{X^3}\Bigg]\,, \end{aligned} \tag{5.2.9}$$

where to avoid clutter we have introduced the notation $\varphi_\mu \equiv \partial_\mu\varphi$ and $\varphi_{\mu\nu} \equiv \nabla_\nu\partial_\mu\varphi$. Notice that the action above is invariant under reparameterizations of φ,

$$\varphi \to \tilde{\varphi} = f(\varphi)\,, \tag{5.2.10}$$

where f is a (monotonic) arbitrary function. This reflects the invariance (in the unitary gauge) under the FDiffs (5.2.2).

Naively, the higher-order derivatives in the action (5.2.9) would suggest the presence of an Ostrogradski ghost in the theory. However, the counting of the degrees of freedom cannot be straightforwardly performed from the covariant action (5.2.9), because of the absence of a standard kinetic term for the khronon and the non-local $1/X$ dependence. However, one can easily perform the counting in the preferred frame, where φ cannot be constant and has a non-vanishing time profile $\varphi = t$. In this frame, as can be seen in the unitary gauge action (5.2.4), the ghost mode is absent.

From the point of view of the covariant action (5.2.9), the absence of the Ostrogradski mode is guaranteed by the highly non-trivial tuning among the coefficients of the five operators in the action, which translates in the absence of $\dot{N}$ terms in the unitary gauge action (5.2.4). Remarkably, this tuning is protected against radiative

corrections by the reparameterization invariance (5.2.10). A detuning of the action coefficients would necessary break the symmetry (5.2.10), generate $\dot{N}$ terms in the unitary gauge action, and generically reintroduce the ghost mode.

Finally, notice that the action (5.2.9) does not belong to any of the DHOST classes identified in [118, 245]. This is because when the full diffeomorphism invariance is broken, the degeneracy of the Hessian matrix of the velocities can be achieved in a less restrictive way. The full diffeomorphism invariant analog of action (5.2.9) is the Horndeski Lagrangian [109], which in the unitary gauge does not present $\dot{N}$ terms.

5.3 RFDiff Gravity

Noticeably, there exists also a smaller unbroken gauge group according to which we can construct our Lagrangian, namely the group of RFDiffs

$$\mathbf{x} \to \tilde{\mathbf{x}}(t, \mathbf{x}) \,, \qquad t \to \tilde{t} = t + \text{const} \,, \tag{5.3.1}$$

which differs from FDiffs because the invariance under general time reparametrizations is replaced by the invariance under time translations. In the Stuckelberg formulation, this symmetry of the khronon action reduces to the shift symmetry

$$\varphi \to \tilde{\varphi} = \varphi + \text{const} \,, \tag{5.3.2}$$

which allows for a general dependence of the action on the derivatives of φ.

Restricting the symmetry from FDiffs to RFDiffs therefore allows one to include in the action a kinetic term for the lapse N. Moreover, all dimensionless couplings in the Lagrangian may now acquire an arbitrary dependence on N, and we can thus include in the potential $\mathcal{V}$ a generic function of N. The kinetic term for N is fixed by the invariance under RFDiffs to be of the form

$$\left(\dot{N} - N^i \partial_i N\right)^2 \,. \tag{5.3.3}$$

However, a general dependence of the action on this term inevitably leads to the propagation of an additional ghost scalar degree of freedom [147]. In the Stuckelberg formulation, this is the Ostrogradski mode associated with the higher derivatives of the khronon, which re-appears because of the detuning of the coefficients of the action (5.2.9).

5.3.1 Degenerate RFDiff Gravity and its Downsides

It is well established that if the kinetic term (5.3.3) and the trace of the extrinsic curvature appear in the Lagrangian in such a way as to enforce the existence of a primary constraint (which in turn generates a secondary constraint), then the ghost mode can be safely removed [117,118,246,247]. The constraints structure – and so the number of degrees of freedom – becomes indeed the same as in Horava gravity, with the only difference that the second-class primary constraint given by the vanishing of the momentum conjugate to N (i.e. $\partial L/\partial \dot{N} \approx 0$) is replaced by a linear combination of the momenta conjugate to N and γ.

Therefore, it is possible to realize healthy theories within RFDiff gravity, provided that suitable degeneracy conditions are imposed. These models have been fully classified in [236–238], but they may not be very attractive for two reasons. First, the presence of arbitrary functions of N in the Lagrangian results in an infinite number of coupling constants. Second, the degeneracy conditions are not protected by the RFDiff symmetry, so that radiative corrections will generically induce a detuning of the action and hence reintroduce the ghost. This is very different from Hořava gravity, where the tuning of the action (5.2.9) is required by the FDiff symmetry and hence is protected by it.

5.4 Degenerate Hořava Gravity

In this section, we present a new class of gravity theories invariant under a symmetry intermediate between FDiffs and RFDiffs. In more detail, the transformation of time is restricted to take the form of a specific hyperbolic function $\tilde{t}(t)$, and the symmetry is realized up to a total derivative. Our starting point is a generalization of the Hořava action (5.2.4), which includes the time derivative of the lapse in the RFDiff invariant way (5.3.3). By introducing the definition

$$V \equiv -\frac{1}{N^2}\left(\dot{N} - N^i \partial_i N\right) , \tag{5.4.1}$$

we write the action as

$$S = \frac{1}{16\pi G}\int \mathrm{d}^3x\,\mathrm{d}t\, N\sqrt{\gamma}\Big[\omega\, V^2 + 2\,\sigma\, K\, V + (1-\beta) K_{ij}\, K^{ij} - (1+\lambda) K^2 + \alpha\, a_i\, a^i + {}^{(3)}\!R\Big] , \tag{5.4.2}$$

where ω and σ are two additional dimensionless constants. Clearly, the first two terms in (5.4.2) break FDiff invariance, although they are RFDiff invariant. At this stage, two scalar degrees of freedom propagate, one of which is a ghost [147].

We can then impose the existence of a primary constraint by requiring that the determinant of the kinetic matrix of the two scalar modes in (5.4.2) vanishes [248–250]:

$$\det \begin{pmatrix} \omega & \sigma \\ \sigma & -\lambda - \frac{\beta+2}{3} \end{pmatrix} = 0 \,. \tag{5.4.3}$$

In Hořava gravity, this condition is trivially realized since $\omega = \sigma = 0$, but a non-trivial solution is also possible and is given by

$$\omega = -\frac{3\,\sigma^2}{3\,\lambda + \beta + 2} \,. \tag{5.4.4}$$

To completely remove one degree of freedom, the primary constraint, enforced by the condition (5.4.4), must generate a secondary constraint. The conditions for this to happen were derived in complete generality for field theories in [250], and in the case at hand they are automatically satisfied because of the absence of the following couplings in the action:

$$V\partial_i N \,, \qquad K\partial_i N \,, \qquad {}^{(3)}\!R \cdot V \,, \qquad {}^{(3)}\!R \cdot K \,. \tag{5.4.5}$$

Therefore, condition (5.4.4) is all that is needed to completely eliminate the ghost mode and remain with a single scalar field, the khronon.

Thus far, we have not made any progress with respect to degenerate RFDiff theories, of which the action (5.4.2)—with the condition (5.4.4) enforced—is a particular case. In fact, nothing prevents the couplings in the Lagrangian from being functions of N and, more dangerously, quantum corrections from spoiling the condition (5.4.4). Ideally, our aim is to determine whether there exists a gauge group, smaller than the FDiffs one but larger than the RFDiffs one, that could protect the condition (5.4.4).

For this purpose, after imposing the condition (5.4.4), we transform the action (5.4.2) under the FDiffs (5.2.2) and obtain a new action, which now differs from the original one, because V is not invariant. Indeed, using equation (5.2.3), we find that

$$V \to \tilde{V} = V - \frac{1}{N}\frac{\mathrm{d}^2 t}{\mathrm{d}\tilde{t}^2}\left(\frac{\mathrm{d}t}{\mathrm{d}\tilde{t}}\right)^{-2} \,. \tag{5.4.6}$$

By requiring that the new terms generated by equation (5.4.6) in the action are a total derivative, one imposes that the equations of motion are invariant. In this way, we obtain a third-order differential equation for $\tilde{t}(t)$, which has a non-trivial solution only if the following condition is imposed on the coefficients of the Lagrangian

$$\sigma = -\lambda - \frac{\beta + 2}{3} \,. \tag{5.4.7}$$

In this case, there exists a unique family of solutions for $\tilde{t}(t)$ given by

$$\tilde{t}(t) = \frac{c_2}{c_1 + t} + c_3 \,, \tag{5.4.8}$$

where $c_{1,2,3}$ are free integration constants. Being (5.4.8) a hyperbolic function, we refer to this family of time reparametrizations (together with spatial diffeomorphisms) as "hyperbolic-foliation-preserving Diffs" (HFDiffs). Notice that equation (5.4.8) is a monotonic function on intervals not including its pole, which prevents violations of causality.

By inspection of the resulting Lagrangian, it is easy to realize that the conditions (5.4.4) and (5.4.7) force the kinetic term to be

$$(V + K)^2 \,, \tag{5.4.9}$$

which is indeed invariant under HFDiffs up to a total derivative since

$$N\sqrt{\gamma}\,(V+K)^2 \to N\sqrt{\gamma}\,(V+K)^2 - 4\left[\partial_t\left(\frac{\sqrt{\gamma}}{N(c_1+t)}\right) - \partial_i\left(\frac{\sqrt{\gamma}N^i}{(c_1+t)N}\right)\right] . \tag{5.4.10}$$

However, being $N\sqrt{\gamma}K^2$ FDiff invariant, if one starts from the generic Lagrangian (5.4.2), invariance under HFDiffs (up to a total derivative) only requires the kinetic term to be of the form $V^2 + 2KV$, with an arbitrary coefficient in front. Therefore, this implies that radiative corrections may induce a running of the coefficients of the Lagrangian. This can potentially detune the degeneracy condition (5.4.4) and thus reintroduce the ghost.

A way out of this unappealing situation would be to enlarge the group of HFDiffs to a custodial symmetry sufficient to ensure stability of the degeneracy condition under quantum corrections. Such a gauge group must necessarily lie in between HFDiffs and full-fledged four-dimensional diffeomorphisms (since the latter would

simply require the theory to be GR). Therefore, one might consider a specific class of time reparametrizations that are explicit functions of the spatial coordinate, e.g. $\tilde{t}(t,\mathbf{x}) = c_2/(c_1+t) + c_3 + f(\mathbf{x})$, although we have been unable to identify a suitable function $f(\mathbf{x})$ of the spatial coordinates.

To summarize, we have found a new unbroken gauge group that: *(i)* allows for a kinetic term for the lapse; *(ii)* avoids the presence of arbitrary functions of the lapse in the action; although *(iii)* it does not yet prevent the propagation of a ghost mode. These are the HFDiffs

$$\mathbf{x} \to \tilde{\mathbf{x}}(t,\mathbf{x})\,, \qquad t \to \tilde{t} = \frac{c_2}{c_1+t} + c_3\,, \tag{5.4.11}$$

and the corresponding action is given by

$$S = \frac{1}{16\pi G}\int \mathrm{d}^3x\,\mathrm{d}t\,N\sqrt{\gamma}\left[-\left(\lambda+\frac{\beta+2}{3}\right)\left(V^2+2\,K\,V\right)\right.$$
$$\left. +(1-\beta)K_{ij}\,K^{ij} - (1+\lambda)K^2 + \alpha\,a_i\,a^i + {}^{(3)}\!R\right]. \tag{5.4.12}$$

Comparing with the Hořava action (5.2.4) we notice that, although there are two new operators, the number of coupling constants is the same. In the this new action, however, even when all couplings are set to zero, we do not recover the GR limit.

5.4.1 Stuckelberg Formalism

It is now instructive to look at the new action (5.4.12) in the Stuckelberg formalism. As in Section 5.2.1, we perform the Stuckelberg transformation and obtain

$$S = \frac{1}{16\pi G}\int \mathrm{d}^4x\,\sqrt{-g}\left[R + \beta\,\frac{\varphi_{\mu\nu}\varphi^{\mu\nu}}{X} + \lambda\,\frac{(\Box\varphi)^2}{X} + \frac{2(\beta+2)}{3}\,\frac{(\Box\varphi)\varphi^\mu\varphi_{\mu\nu}\varphi^\nu}{X^2}\right.$$
$$\left. +(\alpha-2\beta)\frac{\varphi^\mu\varphi_{\mu\rho}\varphi^{\rho\nu}\varphi_\nu}{X^2} + \frac{(2\beta-3\alpha-2)}{3}\,\frac{(\varphi^\mu\varphi_{\mu\nu}\varphi^\nu)^2}{X^3}\right]. \tag{5.4.13}$$

Comparing with the khronon action for Hořava gravity, equation (5.2.9), we see that the coefficients of the third and fifth operators have changed. This new highly non-trivial tuning guarantees the absence of the Ostrogradski ghost at least at tree level. Moreover, the Lagrangian (5.4.13) is invariant under the transformation

$$\varphi \to \tilde{\varphi} = \frac{c_2}{c_1+\varphi} + c_3\,, \tag{5.4.14}$$

up to the total derivative

$$-4\left(\lambda+\frac{\beta+2}{3}\right)\nabla_\mu\left(\frac{1}{c_1+\varphi}\partial^\mu\varphi\right)\,. \tag{5.4.15}$$

This reflects the invariance, up to a total derivative and in the unitary gauge, under the HFDiffs (5.4.11).

Finally, notice that also in this case, action (5.4.13) does not belong to any of the DHOST classes [118, 245]. Although the end result is the same as in the DHOST and beyond Horndeski constructions (i.e. higher order equations of motion without Ostrogradski ghost), there is no connection between those theories and ours. In fact, our theory is Lorentz-violating and the absence of ghosts is guaranteed precisely by the existence of a preferred foliation, where kinetic terms take their standard form and the non-local $1/X$ terms present in the Stuckelberg action disappear.

5.4.2 Conformal and Disformal Transformation

Looking at the form of the kinetic terms, equation (5.4.9), a natural question is whether the new theory is related to Hořava gravity by a conformal and/or disformal transformation. To check this, it is convenient to work in the Stuckelberg formalism, where these transformations read [251]

$$\bar{g}_{\mu\nu}=\Omega(X)g_{\mu\nu}+\Gamma(X)\partial_\mu\varphi\,\partial_\nu\varphi\,, \tag{5.4.16}$$

with Ω and Γ free functions of X only. (Notice that a φ dependence would break even the shift symmetry and therefore it is not allowed).

It is well known that Hořava gravity is invariant under the transformation given by [252]

$$\Omega=1\,,\qquad \Gamma=\frac{\varsigma}{X}\,, \tag{5.4.17}$$

where ς is a constant, provided the following rescaling of the coefficients

$$\bar{\lambda}=\lambda+\varsigma\,(\lambda+1)\,,\qquad \bar{\beta}=\beta+\varsigma\,(\beta-1)\,. \tag{5.4.18}$$

A feature of the new theory is that it also enjoys this invariance for the very same choice of functions [equation (5.4.17)] and for the same rescaling of the coefficients [equation (5.4.18)]. Moreover, any choice different from equation (5.4.17) would

change the power of X appearing in each of the operators of the Lagrangian, and therefore cannot connect the two theories.

As a consequence, a generic transformation of the form (5.4.16) cannot map Hořava gravity into its degenerate HFDiff generalization, and both theories are stable under the same transformation (5.4.17). Once again, the non-local form of Γ in (5.4.17) is signaling that the two theories make sense only for $X \neq 0$, i.e. the khronon must always be timelike.

5.5 Phenomenology

To study the phenomenology of "degenerate" HFDiff Hořava gravity, we first derive the field equations by varying the action (5.4.12) with respect to the spatial metric γ_{ij}, the shift N_i and the lapse N. We denote by D_i the covariant derivative defined with respect to γ_{ij}, and $D_t \equiv \partial_t - N_k D^k$. We also define the following quantities in terms of the variation of the matter action [241, 242]

$$\mathcal{E} = -\frac{1}{\sqrt{\gamma}}\frac{\delta S_{\rm m}}{\delta N} = N^2 T^{00} \,, \tag{5.5.1}$$

$$\mathcal{J}^i = \frac{1}{\sqrt{\gamma}}\frac{\delta S_{\rm m}}{\delta N_i} = N\left(T^{0i} + N^i T^{00}\right) \,, \tag{5.5.2}$$

$$\mathcal{T}^{ij} = \frac{2}{N\sqrt{\gamma}}\frac{\delta S_{\rm m}}{\delta \gamma_{ij}} = T^{ij} - N^i N^j T^{00} \,, \tag{5.5.3}$$

where $T^{\mu\nu}$ is the four-dimensional matter energy-momentum tensor.

The variation with respect to N leads to

$$\begin{aligned}\frac{{}^{(3)}R}{1-\beta} + \frac{\lambda+1}{1-\beta}K^2 - K_{ij}K^{ij} + \frac{\alpha(D_i N)(D^i N)}{(1-\beta)N^2} - \frac{2\alpha D^i D_i N}{(1-\beta)N} \\ + \frac{2(2+\beta+3\lambda)}{3(1-\beta)}\left[KV + V^2 - K^2 - D_t\left(\frac{K+V}{N}\right)\right] = \frac{16\pi G\mathcal{E}}{(1-\beta)c^4} \,,\end{aligned} \tag{5.5.4}$$

which unlike in GR is not a constraint, but rather an evolution equation for N (c.f. the presence of both second-order space and time derivatives of N). Notice that in (non-degenerate) Hořava gravity[2], this equation is instead an elliptic equation for N, to be solved on each slice [241, 242]. In the covariant formalism, this equation becomes

[2]We often refer to the original Hořava gravity [equation (5.2.4)] as "non-degenerate", in order

indeed (in both non-degenerate and degenerate Hořava gravity) the khronon evolution equation.
Varying with respect to N_i one obtains the momentum constraint equation

$$D_j\left[\left(K^{ij}-\frac{\lambda+1}{1-\beta}\gamma^{ij}K\right)-\frac{(2+\beta+3\lambda)\gamma^{ij}V}{3(1-\beta)}\right] - \frac{(2+\beta+3\lambda)}{3(1-\beta)}\left(D^iN\right)\left(\frac{K+V}{N}\right)=-\frac{8\pi G\mathcal{J}^i}{(1-\beta)c^4}\,, \tag{5.5.5}$$

while variation with respect to γ_{ij} yields the evolution equation

$$\begin{aligned}
&\frac{1}{1-\beta}\left[{}^{(3)}R^{ij}-\frac{1}{2}\,{}^{(3)}R\gamma^{ij}\right]+\frac{1}{N}D_t\left(K^{ij}-\frac{\lambda+1}{1-\beta}K\gamma^{ij}-\frac{(2+\beta+3\lambda)}{3(1-\beta)}V\gamma^{ij}\right)\\
&+\frac{2}{N}D_k\left(N^{(i}[K^{j)k}-\frac{\lambda+1}{1-\beta}K\gamma^{j)k}-\frac{(2+\beta+3\lambda)}{3(1-\beta)}V\gamma^{j)k}]\right)-\frac{2\lambda+1+\beta}{1-\beta}KK^{ij}\\
&+2K^{ik}K^j_k-\frac{1}{2}\gamma^{ij}\left(K_{kl}K^{kl}+\frac{\lambda+1}{1-\beta}K^2\right)-\frac{1}{(1-\beta)N}\left[(D^iD^jN)-(D_kD^kN)\gamma^{ij}\right]\\
&+\frac{\alpha}{N^2(1-\beta)}\left[(D^iN)(D^jN)-\frac{1}{2}(D_kN)(D^kN)\gamma^{ij}\right]\\
&+\frac{2(2+\beta+3\lambda)}{3(1-\beta)}\left[\frac{1}{4}V^2\gamma^{ij}-K^{ij}V-\frac{K+V}{N^2}N^{(i}(D^{j)}N)\right]=\frac{8\pi G}{(1-\beta)c^4}\mathcal{T}^{ij}\,.
\end{aligned} \tag{5.5.6}$$

5.5.1 Solar-System Tests and Gravitational-Wave Propagation

To check the experimental viability of the theory on Earth and in the Solar System, we perform a post-Newtonian expansion over flat space and compare to the parametrized PN metric (PPN) [7, 164]. This will allow us to extract the values of the PPN parameters in degenerate Hořava gravity and compare them to their experimental bounds. The details of the calculation follow [242], which performs the same analysis for (non-degenerate) Hořava gravity, and are presented in Appendix B. Here, we will simply summarize the main results.

to distinguish it from its degenerate extension [equation (5.4.12)]. However, it should be by now well understood that even non-degenerate Hořava gravity is a degenerate theory that satisfies (although trivially) the degeneracy condition (5.4.3). This is even more evident from the tuning of the parameters in its khronometric formulation (5.2.9).

We find that the only PPN parameters differing from GR are the preferred-frame parameters α_1 and α_2, which take the form

$$\alpha_1 = \frac{4(\alpha - 2\beta)}{\beta - 1} \,, \tag{5.5.7}$$

$$\alpha_2 = -\frac{(\alpha - 4\beta + 2)(3\alpha - 4\beta - 2)}{3(\alpha - 2)(\beta + \lambda)} + \frac{2(\alpha - 2)}{\beta - 1} + \frac{-27\alpha + 28\beta + 12\lambda + 38}{3(\alpha - 2)} \,. \tag{5.5.8}$$

Experimental bounds on these parameters are $|\alpha_1| \lesssim 10^{-4}$ and $|\alpha_2| \lesssim 10^{-7}$ [7]. Comparing to their expressions in (non-degenerate) Hořava gravity [242,253], we see that while α_1 is unchanged, α_2 gets modified. In (non-degenerate) Hořava gravity, α_1 and α_2 are both proportional to $\alpha - 2\beta$, i.e. they are both small for $\alpha \approx 2\beta$.

At this point, let us notice that constraints on the propagation speed of gravitational waves from GW170817 require $|\beta| \lesssim 10^{-15}$ in (non-degenerate) Hořava gravity [37,254], as well as in the degenerate version of the theory that we are considering here. Indeed, the kinetic term of the tensor modes is given by $K_{ij}\,K^{ij}$ and the spatial gradient is contained in ${}^{(3)}R$, which gives [c.f. equations (5.2.4) and (5.4.12)] a gravitational-wave propagation speed $c_{\rm GW} = (1-\beta)^{-1/2}$, which matches the speed of light only for $\beta = 0$.

The Solar System bound on α_1 then gives $\alpha \approx \beta \approx 0$ in both non-degenerate [255,256] and degenerate Hořava gravity. For $\alpha \approx \beta \approx 0$, equation (5.5.8) then yields

$$\alpha_2 \approx -\frac{(1+2\lambda)(2+3\lambda)}{3\lambda} \,. \tag{5.5.9}$$

The experimental constraint $|\alpha_2| \lesssim 10^{-7}$ then selects $\lambda \approx -1/2$ or $\lambda \approx -2/3$. For the latter, the coefficient in front of $V^2 + 2KV$ in the action disappears, i.e. one is left with the non-degenerate version of the theory. Therefore, there exists only one non-trivial set of parameters, namely $\alpha \approx \beta \approx 0$ and $\lambda \approx -1/2$, for which degenerate Hořava gravity can satisfy Solar-System tests and the bound on the propagation speed of gravitational waves. For these values the action reads

$$S = \frac{1}{16\pi G}\int \mathrm{d}^4x\,\sqrt{-g}\left[R - \frac{1}{2}\frac{(\Box\varphi)^2}{X} + \frac{4}{3}\frac{(\Box\varphi)\varphi^\mu\varphi_{\mu\nu}\varphi^\nu}{X^2} - \frac{2}{3}\frac{(\varphi^\mu\varphi_{\mu\nu}\varphi^\nu)^2}{X^3}\right] \tag{5.5.10}$$

or, in the unitary gauge,

$$S = \frac{1}{16\pi G}\int \mathrm{d}^3x\,\mathrm{d}t\,N\sqrt{\gamma}\left[-\frac{1}{6}\left(V^2 + 2\,K\,V\right) + K_{ij}\,K^{ij} - \frac{1}{2}K^2 + {}^{(3)}R\right] \,. \tag{5.5.11}$$

5.5.2 Cosmology

To test the behavior of the theory on cosmological scales, we assume a standard homogeneous and isotropic Robertson-Walker metric

$$\mathrm{d}s^2 = -\mathrm{d}t^2 + a^2(t)\delta_{ij}\mathrm{d}x^i\mathrm{d}x^j \,, \tag{5.5.12}$$

where $a(t)$ is the scale factor, and $\gamma_{ij} = a^2(t)\delta_{ij}$. Notice that we have assumed flat spatial slices, but our conclusions are unchanged if we allow for curvature.

Replacing this ansatz in the field equations, the only non-trivial equations are provided by the khronon equation (5.5.4) and by the trace of the evolution equation (5.5.6), which give the system

$$(2+\beta+3\lambda)(3H^2+2\dot{H}) = -16\pi G\rho \,, \tag{5.5.13}$$

$$(2+\beta+3\lambda)(3H^2+2\dot{H}) = -16\pi G p \,, \tag{5.5.14}$$

with $H = \dot{a}/a$ the Hubble rate, while ρ and p are the energy density and pressure of the cosmic matter.

As can be seen, this system is completely different from the Friedmann-Robertson-Walker equations of GR. This is no surprise since the theory does not reduce to GR for any values of the coupling constants. More worrisome is the fact that by taking the difference of the two equations, one obtains that the cosmic matter must necessarily have $\rho = p$ (stiff fluid). In other words, the theory does not allow for the usual radiation and matter eras, nor for an early- or late-time accelerated expansion (even in the presence of a cosmological constant). As a curiosity, however, it is worth mentioning that if we set $\rho = p$ in equations (5.5.13)–(5.5.14) and solve for H, we find $H(t) = 2/[3(t+C)]$, with C an integration constant. For $C = 0$ this reduces to the Hubble rate of the standard matter-dominated era, and is reminescent of the appearance of Dark Matter as an integration constant in projectable Hořava gravity [257].

5.6 Summary

In this work, we have shown that it is possible to construct a novel khronometric theory with a dynamical lapse, which (via a degenerate Lagrangian) propagates only

a graviton and a khronon. This theory is invariant under a special subgroup of the FDiff symmetry, equation (5.4.11), which we have referred to as hyperbolic-foliation-preserving Diffs (HFDiffs). This new unbroken gauge group selects a specific kinetic term for the lapse (although it does not fix its overall coefficient), and it avoids an arbitrary dependence of the action on the lapse. HFDiffs are not sufficient by themselves to ensure stability of the degeneracy condition under radiative corrections, thus potentially letting the ghost re-appear beyond tree level. However, an enlarged gauge group lying between HFDiffs and four-dimensional diffeomorphisms may protect the fine-tuning of the degeneracy condition.

Our construction has a two-fold interest for both phenomenology and theory. On the phenomenological side, it is a remarkable example of a theory which, despite being Lorentz breaking and not admitting a GR limit, does pass Earth-based, Solar-System and gravitational-wave tests, at least for a suitable choice of its coupling constants. Unfortunately, the theory fails to reproduce the standard Friedmann-Robertson-Walker cosmology and can provide an (effective) matter-dominated era only if the universe contains stiff matter alone ($\rho = p$).

However, while clearly the cosmology of the theory does not seem to work out of the box, a couple possibilities are worth mentioning. First, equations (5.5.13)–(5.5.14) assume a minimal coupling to matter. If matter is instead conformally coupled to gravity, it may be possible to obtain a matter-dominated era and a late-time accelerated expansion, although it would still be impossible to accommodate a radiation era and it might be tricky to pass Solar-System tests (at least in the absence of a screening mechanism protecting local scales from the conformal coupling). Second, and perhaps more importantly, since dark matter seems to arise naturally as an integration constant in our new theory, it may be worth trying to explain the observed late-time acceleration of the universe in the context of non-standard cosmologies that violate the homogeneity/isotropy assumptions of the Robertson-Walker ansatz (see e.g. [258] for a review, and references therein).

On the theoretical side, if a custodial symmetry protecting the degeneracy condition is identified, this theory may provide a version of Hořava gravity that does not require the absence of time derivatives of the lapse to avoid ghosts, and hence may not present the same technical hurdles [148,233] in proving perturbative renormalizability (beyond

power counting) that one encounters in FDiff (i.e. non-degenerate) Hořava gravity (at least in its general non-projectable form).

Concluding Remarks

In the field of modified gravity, we challenge General Relativity by comparing it to alternative theories of gravity. There are numerous possibilities to go beyond General Relativity, two of which we considered in this work, e.g. adding a scalar degree of freedom to the gravitational sector and breaking Lorentz invariance. In this concluding section, we summarize our most important results.

In Chapter 3 and 4, we studied a scalar-tensor theory with first-order derivative self-interactions named k-essence. Interestingly, due to its non-linear kinetic terms, the theory exhibits a screening mechanism (k-mouflage) that hides the scalar fluctuations on scales smaller than a certain screening radius. This allows the theory to pass Solar-System tests, while still being able to deviate on cosmological scales. After confirming previously known results in the weak-field regime, we investigated whether the screening mechanism survives in the strong-field regime, e.g. for isolated neutron stars. With a spherically symmetric ansatz, we found that these highly compact/relativistic k-mouflage stars indeed do exist, and that they are stable upon small perturbations of their internal energy.

To simulate gravitational collapse induced by large perturbations of screened stars in spherical symmetry, we needed to introduce a driver field in the evolution equations to render the scalar characteristic speeds finite (note that later we managed to perform the simulations in a $3+1$ code in spherical symmetry without including a driver field). We were able to extract the monopole scalar radiation for theories with a strong-coupling scale Λ as small as a few MeV, and concluded that for a cosmologically relevant Λ the monopole emission from stellar oscillations is expected to be negligible. This is not true for gravitational collapse, where—as a result of the star shedding away all of its scalar hair—the monopole signal could potentially be observable with space-based detectors such as LISA.

Then, we performed fully $3+1$ relativistic simulations of binary neutron stars in k-essence with $\Lambda \sim$ a few MeV. We did not have to include a driver field, as an appropriate gauge choice with non-zero shift prevented the characteristic speeds from diverging. We found that in the late inspiral and merger of binary neutron stars the (subdominant) dipole scalar emission is effectively screened, but the (dominant) quadrupole scalar radiation is not. It would be interesting to check whether these results remain true for $\Lambda = \Lambda_{\rm DE}$, as in this case k-essence would be constrained to be as fine-tuned as Fierz-Jordan-Brans-Dicke (FJBD) theories with the same conformal coupling α. With our current numerical precision it is not possible to consider such small values of Λ, and thus a different strategy would have to be taken. Additionally, it would be ideal to find a formulation of k-essence which at the same time exhibits a screening mechanism, and is ultraviolet complete[3]. No such description has been found yet, but if it is exists, its dynamical behaviour and gravitational-wave signatures could be analysed by the techniques explained in these chapters.

In Chapter 5, we considered Lorentz-violating theories of gravity and constructed a generalization of khronometric theory. This new theory is invariant under hyperbolic-foliation-preserving Diffs (HFDiffs), and avoids Ostrogradski instabilities as a result of a suitable degeneracy condition (reminiscent of techniques applied in DHOST theories). However, to protect the fine-tuning of the degeneracy condition and ensure radiative stability, an enlarged gauge group lying between HFDiffs and four-dimensional Diffs is necessary. If such a symmetry can be identified, it might be easier to prove perturbative renormalizability for this novel khronometric theory than for FDiff (non-projectable) Hořava gravity, which would be an exciting future prospective. Phenomenologically, the theory does not have a General Relativity limit, nor is it able to produce a Friedmann-Robertson-Walker-like cosmology on large scales. It does, however, pass Earth-based, Solar-System and gravitational-wave tests for suitable choices of its coupling constants.

In conclusion, this research work has touched upon several aspects of gravity beyond General Relativity, and has allowed us to test our current understanding of gravitation. Now that we have the experimental tools to perform precision tests of

[3]This would introduce a violation of one of the assumptions of the positivity bounds, e.g. locality and Lorentz invariance, as described in [209].

gravitational phenomena, it is more important than ever to ask ourselves whether there could be an alternative to General Relativity. Many questions and challenges still lie ahead, but the importance of this new era of precision gravitational-wave astronomy can hardly be overstated.

A ADM Formalism

A.1 The ADM Decomposition

The ADM decomposition[1] was introduced by Richard Arnowitt, Stanley Deser and Charles Misner as a Hamiltonian formulation of General Relativity [259,260]. The decomposition foliates spacetime in three-dimensional spacelike hypersurfaces parametrized by a time function t (see Figure 23). We define n^a to be the unit normal vector to the spatial hypersurfaces Σ_t. The spatial metric γ_{ab} is then related to the spacetime metric g_{ab} by

$$\gamma_{ab} = g_{ab} + n_a n_b \, . \tag{A.1.1}$$

Next, we define a vector t^a on the spacetime manifold, which may interpreted as the "flow of time" throughout the spacetime, and decompose it in a part normal and a part tangential to the spatial hypersurfaces: $t^a = Nn^a + N^a$. This gives us the definition of the lapse function N and the shift vector N^a

$$N = -g_{ab} t^a n^b \, , \tag{A.1.2}$$

$$N^a = \gamma^a{}_b t^b \, . \tag{A.1.3}$$

With these definitions, we can write an expression for the spacetime metric in ADM quantities that looks like

$$\mathrm{d}s^2 = -N^2 \mathrm{d}t^2 + \gamma_{ij}(\mathrm{d}x^i + N^i \mathrm{d}t)(\mathrm{d}x^j + N^j \mathrm{d}t) \, , \tag{A.1.4}$$

or

$$g_{\mu\nu} = \begin{pmatrix} -N^2 + N_i N^i & N_i \\ N_i & \gamma_{ij} \end{pmatrix} \, , \qquad g^{\mu\nu} = \begin{pmatrix} -N^{-2} & N^{-2} N^i \\ N^{-2} N^i & \gamma^{ij} - N^{-2} N^i N^j \end{pmatrix} \, . \tag{A.1.5}$$

[1] Also referred to as the Cauchy or $3+1$ decomposition.

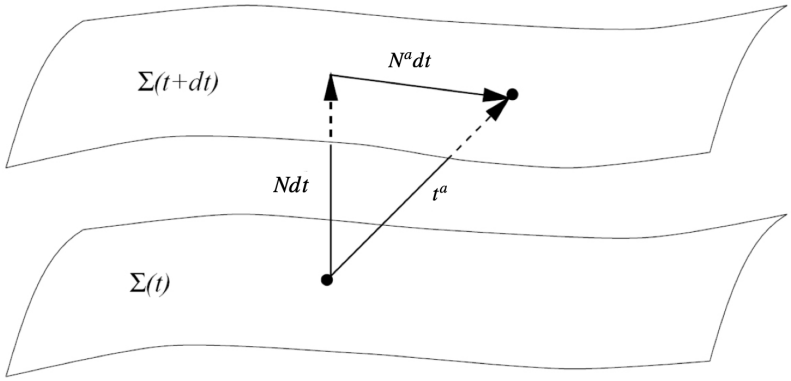

Figure 23: The ADM decomposition of spacetime in time-ordered spatial hypersurfaces $\Sigma(t) = \Sigma_t$. The ADM quantities are the lapse (N), the shift (N^a), and the timelike vector t^a is given by $t^a = Nn^a + N^a$.

The extrinsic geometry of Σ_t is characterized by the extrinsic curvature K_{ab}. The extrinsic curvature is defined as $K_{ab} = \nabla_a \xi_b$, where ξ_b is a unit tangent to the congruence of timelike geodesics orthogonal to Σ_t. Since n^a is also a unit timelike vector which is normal to Σ_t, its derivative along a direction tangential to Σ_t must agree with ξ_b. We therefore have

$$K_{ab} = \gamma_a^c \nabla_c n_b = \frac{1}{2} \pounds_n \gamma_{ab} \ , \tag{A.1.6}$$

which can also be written as

$$K_{ab} = \frac{1}{2N} \left(\dot{\gamma}_{ab} - D_a N_b - D_b N_a \right) \ , \tag{A.1.7}$$

with D_i three-dimensional covariant derivatives compatible with the spatial metric. The four-dimensional Ricci scalar is decomposed as (up to total derivatives)

$$^{(4)}R = K_{ab} K^{ab} - K^2 + \ ^{(3)}R \ , \tag{A.1.8}$$

where K is the trace of the extrinsic curvature, and $^{(3)}R$ the three-dimensional Ricci scalar on the hypersurfaces Σ_t. With $\sqrt{-g} = N\sqrt{\gamma}$ the Einstein-Hilbert action in ADM quantities looks like

$$S_{EH} = \int \mathrm{d}^4 x N \sqrt{\gamma} \left(K_{ab} K^{ab} - K^2 + \ ^{(3)}R \right) \ . \tag{A.1.9}$$

From here, we can derive

$$\partial_t \gamma_{ij} = 2NK_{ij} + D_i N_j + D_j N_i \ , \tag{A.1.10}$$

$$\begin{aligned} \partial_t K_{ij} = N\ {}^{(3)}R + NKK_{ij} - 2NK_{ik}K^k{}_j - D_i D_j N \\ + K_{kj} D_i N^k + N_{ik} D_j N^k + N^k D_k K_{ij} \ , \end{aligned} \tag{A.1.11}$$

and

$$\mathcal{H} := {}^{(3)}R + K^2 - K_{ij}K^{ij} = 0 \ , \tag{A.1.12}$$

$$\mathcal{M}_i := D_j K^j{}_i - D_i K = 0 \ , \tag{A.1.13}$$

where the first two are evolution equations for K_{ij} and γ_{ij}, and the latter two are the Hamiltonian and momentum constraint equations (in vacuum). Thus, K_{ij} and γ_{ij} are the dynamical variables in this formalism, whereas N and N_a are not (they just tell you how to move the coordinates forward in time), and can be chosen freely.

B Parametrized Post-Newtonian Expansion

B.1 PPN Formalism

We follow the discussion in [7] in this section. In the Post-Newtonian limit, almost every theory of gravity predicts the same structure for the metric $g_{\mu\nu}$. It can be expanded around the Minkowski metric in terms of a set of scalar, vector and tensor potentials built up from matter variables. These variables are the baryonic density (ρ_0), pressure (p), internal energy (ϵ), the coordinate velocity of matter (v_i), and the coordinate velocity of the PPN coordinate system relative to the mean rest-frame of the Universe (w_i). The corresponding metric potentials are then:

$$\phi_N = -G_N \int \mathrm{d}^3x' \, \frac{\rho(\mathbf{x}', t)}{|\mathbf{x} - \mathbf{x}'|} \,, \tag{B.1.1}$$

$$\Phi_{ij} = -G_N \int \mathrm{d}^3x' \, \frac{\rho(\mathbf{x}', t)(x - x')_i (x - x')_j}{|\mathbf{x} - \mathbf{x}'|^3} \,, \tag{B.1.2}$$

$$\Phi_W = \int \mathrm{d}^3x' \, \mathrm{d}^3x'' \, \frac{\rho_0(\mathbf{x}', t)\rho_0(\mathbf{x}'', t)(\mathbf{x} - \mathbf{x}')}{|\mathbf{x} - \mathbf{x}'|^3} \left(\frac{\mathbf{x}' - \mathbf{x}''}{|\mathbf{x} - \mathbf{x}''|} - \frac{\mathbf{x} - \mathbf{x}''}{|\mathbf{x}' - \mathbf{x}''|} \right) \,, \tag{B.1.3}$$

$$\mathcal{A} = \int \mathrm{d}^3x' \, \frac{\rho_0(\mathbf{x}', t)[\mathbf{v}(\mathbf{x}', t) \cdot (\mathbf{x} - \mathbf{x}')]^2}{|\mathbf{x} - \mathbf{x}'|^3} \,, \tag{B.1.4}$$

$$\Phi_1 = G_N \int \mathrm{d}^3x' \, \frac{\rho_0(\mathbf{x}', t)[v(\mathbf{x}', t)]^2}{|\mathbf{x} - \mathbf{x}'|} \,, \tag{B.1.5}$$

$$\Phi_2 = -G_N \int \mathrm{d}^3x' \, \frac{\rho_0(\mathbf{x}', t)\phi_N}{|\mathbf{x} - \mathbf{x}'|} \,, \tag{B.1.6}$$

$$\Phi_3 = G_N \int \mathrm{d}^3x' \, \frac{\rho_0(\mathbf{x}', t)\epsilon(\mathbf{x}', t)}{|\mathbf{x} - \mathbf{x}'|} \,, \tag{B.1.7}$$

$$\Phi_4 = G_N \int \mathrm{d}^3x' \, \frac{p(\mathbf{x}', t)}{|\mathbf{x} - \mathbf{x}'|} \, , \tag{B.1.8}$$

$$V_i = G_N \int \mathrm{d}^3x' \, \frac{\rho_0(\mathbf{x}', t) v_i(\mathbf{x}', t)}{|\mathbf{x} - \mathbf{x}'|} \, , \tag{B.1.9}$$

$$W_i = G_N \int \mathrm{d}^3x' \, \frac{\rho_0(\mathbf{x}', t) \left[\mathbf{v}(\mathbf{x}', t) \cdot (\mathbf{x} - \mathbf{x}')\right] (x - x')_i}{|\mathbf{x} - \mathbf{x}'|^3} \, . \tag{B.1.10}$$

The potentials satisfy some relations that will useful in Section B.2:

$$\nabla^2 V_i = -4\pi G_N \rho_0 v_i \, , \quad \nabla^2 \Phi_1 = -4\pi G_N \rho_0 v^2 \, , \quad \nabla^2 \Phi_2 = 4\pi G_N \rho_0 \phi_N \, , \tag{B.1.11}$$
$$\nabla^2 \Phi_4 = -4\pi G_N p \, , \quad \partial_i V^i = \partial_t \phi_N \, , \quad \partial_i V^i = -\partial_i W^i \, .$$

The metric depends on the potentials and a set of ten parameters, which have been chosen in such a way that they indicate some physical property of the theory. The metric looks like:

$$\begin{aligned} g_{00} = -1 &- 2\frac{\phi_N}{c^2} - 2\beta \frac{\phi_N^2}{c^4} - 2\xi \frac{\Phi_W}{c^4} + (2\gamma + 2 + \alpha_3 + \zeta_1 - 2\xi) \frac{\Phi_1}{c^4} \\ &+ 2(3\gamma - 2\beta + 1 + \zeta_2 + \xi) \frac{\Phi_2}{c^4} + 2(1 + \zeta_3) \frac{\Phi_3}{c^4} \\ &+ 2(3\gamma + 3\zeta_4 - 2\xi) \frac{\Phi_4}{c^4} - (\zeta_1 - 2\xi) \frac{\mathcal{A}}{c^4} + (\alpha_1 - \alpha_2 - \alpha_3) \frac{w^2 \phi_N}{c^4} \\ &+ \alpha_2 \frac{w^i w^j \Phi_{ij}}{c^4} + (2\alpha_3 - \alpha_1) \frac{w^i V_i}{c^4} + \mathcal{O}\left(\frac{1}{c^6}\right) \, , \end{aligned} \tag{B.1.12}$$

$$\begin{aligned} g_{0i} = &-\frac{1}{2}(4\gamma + 3 + \alpha_1 - \alpha_2 + \zeta_1 - 2\xi) \frac{V_i}{c^3} - \frac{1}{2}(1 + \alpha_2 - \zeta_1 + 2\xi) \frac{W_i}{c^3} \\ &+ \frac{1}{2}(\alpha_1 - 2\alpha_2) \frac{w^i \phi_N}{c^3} + \alpha_2 \frac{w^j \Phi_{ij}}{c^3} + \mathcal{O}\left(\frac{1}{c^5}\right) \, , \end{aligned} \tag{B.1.13}$$

$$g_{ij} = \left(1 - 2\gamma \frac{\phi_N}{c^2}\right) \delta_{ij} + \mathcal{O}\left(\frac{1}{c^4}\right) \, . \tag{B.1.14}$$

The Eddington–Robertson–Schiff parameters γ and β are used to describe the classical tests of General Relatively, and therefore probably the most important ones. They can be physically interpreted as how much curvature is produced by a unit rest-mass (γ), and how much non-linearity appears in the law of gravity (β). Preferred-location effects are indicated by a nonzero value of the parameter ξ, whereas preferred-frame effects are captured by nonzero values of the parameters α_1, α_2, and α_3. Lastly, violations of global conservation laws for the total momentum are measured by α_3, ζ_1, ζ_2, ζ_3, and ζ_4.

Note that in this section the Post-Newtonian gauge has been adopted. More generally, there will also be the potential

$$\mathbb{X}(\mathbf{x},t) = G_N \int \mathrm{d}^3x' \, \rho_0(\mathbf{x}',t) \, |\mathbf{x}-\mathbf{x}'| \, , \tag{B.1.15}$$

which obeys the relations

$$\nabla^2 \mathbb{X} = -2\phi_N \, , \qquad \partial_t \partial_i \mathbb{X} = W_i - V_i \, , \tag{B.1.16}$$

that we use in the next section.

B.2 PPN in Degenerate Hořava Gravity

In order to calculate the PPN parameters, we follow [242] and consider a general perturbed flat metric in Cartesian coordinates $(x^0 = ct, x^i)$

$$\begin{aligned} g_{00} &= -1 - \frac{2}{c^2}\phi - \frac{2}{c^4}\phi_{(2)} + \mathcal{O}\left(\frac{1}{c^6}\right) \, , \\ g_{0i} &= \frac{w_i}{c^3} + \frac{\partial_i \omega}{c^3} + \mathcal{O}\left(\frac{1}{c^5}\right) \, , \\ g_{ij} &= \left(1 - \frac{2}{c^2}\psi\right)\delta_{ij} + \left(\partial_i\partial_j - \frac{1}{3}\delta_{ij}\nabla^2\right)\frac{\zeta}{c^2} \\ &\quad + \frac{1}{c^2}\partial_{(i}\zeta_{j)} + \frac{\zeta_{ij}}{c^2} + \mathcal{O}\left(\frac{1}{c^4}\right) \, , \end{aligned} \tag{B.2.1}$$

where under transformations of the spatial coordinates, $\psi, \zeta, \omega, \phi, \phi_{(2)}$ transform as scalars, w_i, ζ_i behave as transverse vectors (i.e. $\partial_i w^i = \partial_i \zeta^i = 0$), and ζ_{ij} is a transverse and traceless tensor (i.e. $\partial_i \zeta^{ij} = \zeta^i{}_i = 0$). Since we want to use this ansatz in the field equations in the unitary gauge (equations (5.5.4)–(5.5.6)), we are not allowed to perform a transformation of the time coordinate (which is fixed to coincide with the khronon), but we can perform a gauge transformation of the spatial coordinates to set $\zeta = \zeta_i = 0$ [242].

We supplement this ansatz with an expression for the energy-momentum tensor, which we assume to be given by the perfect fluid form

$$T^{\mu\nu} = \left(\rho + \frac{p}{c^2}\right)u^\mu u^\nu + p g^{\mu\nu}, \tag{B.2.2}$$

where ρ is the matter energy density, p the pressure and $u^\mu = dx^\mu/d\tau$ the four-velocity of the fluid elements (with τ the proper time). In the following, we introduce

a parameter $\eta_{0,1}$ in the action

$$S = \frac{1}{16\pi G}\int \mathrm{d}^3x\,\mathrm{d}t\,N\sqrt{\gamma}\left[-\eta_{0,1}\left(\lambda+\frac{\beta+2}{3}\right)\left(V^2+2\,K\,V\right)\right.$$
$$\left.+(1-\beta)K_{ij}\,K^{ij}-(1+\lambda)K^2+\alpha\,a_i\,a^i+{}^{(3)}R\right]\,, \quad \text{(B.2.3)}$$

in order to distinguish between (non-degenerate) Hořava gravity (which corresponds to $\eta_{0,1}=0$) from its degenerate generalization ($\eta_{0,1}=1$).

Expanding the evolution equation (5.5.6) to lowest order in $1/c$, we find $\zeta_{ij}=\mathcal{O}(1/c^2)$ from the off-diagonal part, while the trace gives

$$\psi = \phi + \mathcal{O}\left(\frac{1}{c^2}\right)\,. \quad \text{(B.2.4)}$$

From this we can write

$$\psi = \phi + \frac{\delta\psi}{c^2} + \mathcal{O}\left(\frac{1}{c^4}\right)\,, \quad \text{(B.2.5)}$$

which we can substitute in the other equations. Using this expression and expanding equation (5.5.4) to lowest order in $1/c$, we obtain the modified Poisson equation

$$\nabla^2\phi_N = 4\pi G_N\rho + \mathcal{O}\left(\frac{1}{c^2}\right)\,, \quad \text{(B.2.6)}$$

where we define the rescaled gravitational constant $G_N = 2G/(2-\alpha)$. Notice that G_N is the gravitational constant measurable by a local experiment, while G is merely the bare gravitational constant appearing in the action.

We can then expand the momentum constraint (5.5.5) to lowest order in $1/c$ to find the 1PN equation for the "frame-dragging" potential w_i:

$$\nabla^2 w_i + 2\left(\frac{\beta+\lambda}{\beta-1}\right)\partial_i\nabla^2\omega = \frac{16\pi G\rho v_i}{1-\beta} - \frac{2(3+\eta_{0,1})}{3}\left(\frac{2+\beta+3\lambda}{\beta-1}\right)\partial_i\partial_t\phi\,. \quad \text{(B.2.7)}$$

This is the first place where one can see a modification with respect to (non-degenerate) Hořava gravity.

One can then expand both the trace of the evolution equation (5.5.6) and the khronon equation (5.5.4) to next-to-leading order in $1/c$, obtaining respectively

$$2\nabla^2\delta\psi = -24\pi G p - 8\pi\rho v^2 - \left(7+\frac{\alpha}{2}\right)\partial_i\phi\partial_i\phi$$
$$-8\phi\nabla^2\phi + (2+\beta+3\lambda)\left(\partial_t\nabla^2\omega + (3+\eta_{0,1})\partial_t^2\phi\right)\,, \quad \text{(B.2.8)}$$

and

$$\vec{\nabla}\cdot\left[\left(1-\frac{\alpha}{2}\right)\vec{\nabla}\left(\phi+\frac{\phi_{(2)}}{c^2}\right)\right]=4\pi G\rho+\frac{1}{c^2}\Big(8\pi G\rho v^2+12\pi G p+(2-\alpha)\vec{\nabla}\phi\cdot\vec{\nabla}\phi \\ -\frac{1}{6}(2+\beta+3\lambda)\left((3+\eta_{0,1})\partial_t\nabla^2\omega+(9+7\eta_{0,1})\partial_t^2\phi\right)\Big). \quad \text{(B.2.9)}$$

We can then take the divergence of equation (B.2.7) and solve it for ω, obtaining

$$\omega=\frac{3\alpha+2\eta_{0,1}+(\beta+3\lambda)(3+\eta_{0,1})}{6(\beta+\lambda)}\partial_t\mathbb{X}\,. \quad \text{(B.2.10)}$$

Replacing this solution again into equation (B.2.7), we obtain

$$w_i=\frac{2-\alpha}{\beta-1}(V_i+W_i)\,. \quad \text{(B.2.11)}$$

This allows us to evaluate g_{0i} as

$$\begin{aligned} g_{0i}&=\frac{w_i}{c^3}+\frac{\partial_i\omega}{c^3}+\mathcal{O}\left(\frac{1}{c^5}\right) \quad \text{(B.2.12)}\\ &=\frac{-\eta_{0,1}(2+3\lambda-\beta)+\beta(\beta+3\lambda)(3+\eta_{0,1})-3\alpha(1+\beta+2\lambda)+3\lambda+9\beta}{6(\beta-1)(\beta+\lambda)}\frac{W_i}{c^3}\\ &+\frac{\eta_{0,1}(2+3\lambda-\beta)-\beta(\beta+3\lambda)(3+\eta_{0,1})+3\alpha(1-3\beta-2\lambda)+21\lambda+15\beta}{6(\beta-1)(\beta+\lambda)}\frac{V_i}{c^3}\\ &+\mathcal{O}\left(\frac{1}{c^5}\right)\,. \end{aligned}$$

We can also solve equation (B.2.9) for $\phi_{(2)}$

$$\phi_{(2)}=\phi_N^2-2\Phi_1-2\Phi_2-3\Phi_4 \\ +\frac{(3\alpha-6\beta+\eta_{0,1}(\alpha-6\beta-4\lambda))(2+\beta+3\lambda)}{6(\alpha-2)(\beta+\lambda)}\partial_t^2\mathbb{X}\,. \quad \text{(B.2.13)}$$

While the solutions that we found completely describe the metric at 1PN order, in order to read off the PPN parameters one needs to transform the metric from the unitary gauge that we used for the calculation to the standard PN gauge [7,164,242]. We do that, following again [242], by performing a gauge transformation $t\to t+\delta t$, where we choose $\delta t\propto\partial_t\mathbb{X}$, with $\eta_{0,1}$ appearing in the transformation. This finally yields

$$g_{00}=-1-2\frac{\phi_N}{c^2}-2\frac{\phi_N^2}{c^4}+4\frac{\Phi_1}{c^4}+4\frac{\Phi_2}{c^4}+6\frac{\Phi_4}{c^4}+\mathcal{O}\left(\frac{1}{c^6}\right)\,, \quad \text{(B.2.14)}$$

$$g_{0i}=-\frac{1}{2}\left(7+\alpha_1-\alpha_2\right)\frac{V_i}{c^3}-\frac{1}{2}\left(1+\alpha_2\right)\frac{W_i}{c^3}+\mathcal{O}\left(\frac{1}{c^5}\right)\,, \quad \text{(B.2.15)}$$

$$g_{ij}=\left(1-2\frac{\phi_N}{c^2}\right)\delta_{ij}+\mathcal{O}\left(\frac{1}{c^4}\right)\,, \quad \text{(B.2.16)}$$

from which we can read off the parameters α_1 and α_2

$$\alpha_1 = \frac{4(\alpha - 2\beta)}{\beta - 1} \,, \tag{B.2.17}$$

$$\alpha_2 = \eta_{0,1} \frac{2(1 - \alpha + 3\beta + 2\lambda)(2 + \beta + 3\lambda)}{3(\alpha - 2)(\beta + \lambda)} + \frac{(\alpha - 2\beta)[-\beta(3 + \beta + 3\lambda) - \lambda + \alpha(1 + \beta + 2\lambda)]}{(\alpha - 2)(\beta - 1)(\beta + \lambda)} \,. \tag{B.2.18}$$

Bibliography

[1] L. ter Haar, M. Bezares, M. Crisostomi, E. Barausse, and C. Palenzuela, "Dynamics of Screening in Modified Gravity," *Phys. Rev. Lett.* **126** no. 9, (2021) 091102, arXiv:2009.03354 [gr-qc].

[2] M. Bezares, L. ter Haar, M. Crisostomi, E. Barausse, and C. Palenzuela, "Kinetic screening in nonlinear stellar oscillations and gravitational collapse," *Phys. Rev. D* **104** no. 4, (2021) 044022, arXiv:2105.13992 [gr-qc].

[3] M. Bezares, R. Aguilera-Miret, L. ter Haar, M. Crisostomi, C. Palenzuela, and E. Barausse, "No Evidence of Kinetic Screening in Simulations of Merging Binary Neutron Stars beyond General Relativity," *Phys. Rev. Lett.* **128** no. 9, (2022) 091103, arXiv:2107.05648 [gr-qc].

[4] E. Barausse, M. Crisostomi, S. Liberati, and L. ter Haar, "Degenerate Hořava gravity," *Class. Quant. Grav.* **38** no. 10, (2021) 105007, arXiv:2101.00641 [hep-th].

[5] S. M. Carroll, *Spacetime and Geometry*. Cambridge University Press, 7, 2019.

[6] R. M. Wald, *General relativity*. Chicago Univ. Press, Chicago, IL, 1984. https://cds.cern.ch/record/106274.

[7] C. M. Will, "The Confrontation between General Relativity and Experiment," *Living Rev. Rel.* **17** (2014) 4, arXiv:1403.7377 [gr-qc].

[8] C. W. Misner, K. S. Thorne, and J. A. Wheeler, *Gravitation*. W. H. Freeman, San Francisco, 1973.

[9] M. Maggiore, *Gravitational Waves. Vol. 1: Theory and Experiments*. Oxford Master Series in Physics. Oxford University Press, 2007.

[10] H. Reall, "General relativity." http://www.damtp.cam.ac.uk/user/hsr1000/part3_gr_lectures.pdf, October, 2021.

[11] D. Tong, "Lectures on general relativity." http://www.damtp.cam.ac.uk/user/tong/gr.html, September, 2019.

[12] L. Rezzolla, "Gravitational waves from perturbed black holes and relativistic stars." http://users.ictp.it/~pub_off/lectures/lns014/Rezzolla/Rezzolla.pdf, June, 2002.

[13] D. Baumann, "Cosmology." http://cosmology.amsterdam/education/cosmology/, December, 2018.

[14] I. Newton, *Philosophiae naturalis principia mathematica*. J. Societatis Regiae ac Typis J. Streater, 1687. https://books.google.nl/books?id=-dVKAQAAIAAJ.

[15] P. Touboul *et al.*, "MICROSCOPE Mission: First Results of a Space Test of the Equivalence Principle," *Phys. Rev. Lett.* **119** no. 23, (2017) 231101, arXiv:1712.01176 [astro-ph.IM].

[16] A. Heger, C. L. Fryer, S. E. Woosley, N. Langer, and D. H. Hartmann, "How massive single stars end their life," *Astrophys. J.* **591** (2003) 288–300, arXiv:astro-ph/0212469.

[17] A. Hewish, S. J. Bell, J. D. H. Pilkington, P. F. Scott, and R. A. Collins, "Observation of a rapidly pulsating radio source," *Nature* **217** (1968) 709–713.

[18] T. Gold, "Rotating neutron stars as the origin of the pulsating radio sources," *Nature* **218** (1968) 731–732.

[19] T. Gold, "Rotating neutron stars and the nature of pulsars," *Nature* **221** (1969) 25–27.

[20] E. Barausse, V. Cardoso, and P. Pani, "Can environmental effects spoil precision gravitational-wave astrophysics?," *Phys. Rev.* **D89** no. 10, (2014) 104059, arXiv:1404.7149 [gr-qc].

[21] B. Bertotti, L. Iess, and P. Tortora, "A test of general relativity using radio links with the Cassini spacecraft," **425** no. 6956, (Sept., 2003) 374–376.

[22] F. Hofmann, J. Müller, and L. Biskupek, "Lunar laser ranging test of the nordtvedt parameter and a possible variation in the gravitational constant," *Astronomy Astrophysics—ASTRON ASTROPHYS* **522** (11, 2010) .

[23] A. Einstein, "Explanation of the Perihelion Motion of Mercury from the General Theory of Relativity," *Sitzungsber. Preuss. Akad. Wiss. Berlin (Math. Phys.)* **1915** (1915) 831–839.

[24] A. Einstein, "On The influence of gravitation on the propagation of light," *Annalen Phys.* **35** (1911) 898–908.

[25] F. W. Dyson, A. S. Eddington, and C. Davidson, "A Determination of the Deflection of Light by the Sun's Gravitational Field, from Observations Made at the Total Eclipse of May 29, 1919," *Phil. Trans. Roy. Soc. Lond. A* **220** (1920) 291–333.

[26] S. S. Shapiro, J. L. Davis, D. E. Lebach, and J. S. Gregory, "Measurement of the Solar Gravitational Deflection of Radio Waves using Geodetic Very-Long-Baseline Interferometry Data, 1979-1999," *Phys. Rev. Lett.* **92** (2004) 121101.

[27] S. B. Lambert and C. Le Poncin-Lafitte, "Determination of the relativistic parameter gamma using very long baseline interferometry," *Astron. Astrophys.* **499** (2009) 331, arXiv:0903.1615 [gr-qc].

[28] I. I. Shapiro, "Fourth test of general relativity," *Phys. Rev. Lett.* **13** (Dec, 1964) 789–791. https://link.aps.org/doi/10.1103/PhysRevLett.13.789.

[29] K. Nordtvedt, "Testing relativity with laser ranging to the moon," *Phys. Rev.* **170** (Jun, 1968) 1186–1187. https://link.aps.org/doi/10.1103/PhysRev.170.1186.

[30] K. Nordtvedt, "Equivalence principle for massive bodies. ii. theory," *Phys. Rev.* **169** (May, 1968) 1017–1025. https://link.aps.org/doi/10.1103/PhysRev.169.1017.

[31] R. A. Hulse and J. H. Taylor, "Discovery of a pulsar in a binary system," *Astrophys. J.* **195** (1975) L51–L53.

[32] **LIGO Scientific, Virgo** Collaboration, B. P. Abbott *et al.*, "Observation of Gravitational Waves from a Binary Black Hole Merger," *Phys. Rev. Lett.* **116** no. 6, (2016) 061102, arXiv:1602.03837 [gr-qc].

[33] **LIGO Scientific, Virgo** Collaboration, B. Abbott *et al.*, "GW170817: Observation of Gravitational Waves from a Binary Neutron Star Inspiral," *Phys. Rev. Lett.* **119** no. 16, (2017) 161101, arXiv:1710.05832 [gr-qc].

[34] **LIGO Scientific, Virgo** Collaboration, B. P. Abbott *et al.*, "GW151226: Observation of Gravitational Waves from a 22-Solar-Mass Binary Black Hole Coalescence," *Phys. Rev. Lett.* **116** no. 24, (2016) 241103, arXiv:1606.04855 [gr-qc].

[35] **LIGO Scientific, VIRGO** Collaboration, B. P. Abbott *et al.*, "GW170104: Observation of a 50-Solar-Mass Binary Black Hole Coalescence at Redshift 0.2," *Phys. Rev. Lett.* **118** no. 22, (2017) 221101, arXiv:1706.01812 [gr-qc]. [Erratum: Phys.Rev.Lett. 121, 129901 (2018)].

[36] **LIGO Scientific, Virgo** Collaboration, B. P. Abbott *et al.*, "GW170814: A Three-Detector Observation of Gravitational Waves from a Binary Black Hole Coalescence," *Phys. Rev. Lett.* **119** no. 14, (2017) 141101, arXiv:1709.09660 [gr-qc].

[37] **LIGO Scientific, Virgo, Fermi-GBM, INTEGRAL** Collaboration, B. Abbott *et al.*, "Gravitational Waves and Gamma-rays from a Binary Neutron Star Merger: GW170817 and GRB 170817A," *Astrophys. J. Lett.* **848** no. 2, (2017) L13, arXiv:1710.05834 [astro-ph.HE].

[38] **LIGO Scientific, Virgo** Collaboration, B. P. Abbott *et al.*, "Tests of general relativity with GW150914," *Phys. Rev. Lett.* **116** no. 22, (2016) 221101, arXiv:1602.03841 [gr-qc]. [Erratum: Phys.Rev.Lett. 121, 129902 (2018)].

[39] **LIGO Scientific, Virgo** Collaboration, B. P. Abbott *et al.*, "Tests of General Relativity with GW170817," *Phys. Rev. Lett.* **123** no. 1, (2019) 011102, arXiv:1811.00364 [gr-qc].

[40] **LIGO Scientific, Virgo** Collaboration, B. Abbott *et al.*, "Tests of General Relativity with the Binary Black Hole Signals from the LIGO-Virgo Catalog GWTC-1," *Phys. Rev. D* **100** no. 10, (2019) 104036, arXiv:1903.04467 [gr-qc].

[41] **LIGO Scientific, Virgo** Collaboration, R. Abbott *et al.*, "Tests of General Relativity with Binary Black Holes from the second LIGO-Virgo Gravitational-Wave Transient Catalog," arXiv:2010.14529 [gr-qc].

[42] **LIGO Scientific, VIRGO, KAGRA** Collaboration, R. Abbott *et al.*, "Tests of General Relativity with GWTC-3," arXiv:2112.06861 [gr-qc].

[43] Z. Carson and K. Yagi, "Testing General Relativity with Gravitational Waves," arXiv:2011.02938 [gr-qc].

[44] C. Bambi, "Testing General Relativity with Black Hole X-Ray Data," *Astron. Rep.* **65** no. 10, (2021) 902–905, arXiv:2010.03793 [gr-qc].

[45] **Event Horizon Telescope** Collaboration, K. Akiyama *et al.*, "First M87 Event Horizon Telescope Results. I. The Shadow of the Supermassive Black Hole," *Astrophys. J. Lett.* **875** (2019) L1, arXiv:1906.11238 [astro-ph.GA].

[46] **Event Horizon Telescope** Collaboration, K. Akiyama *et al.*, "First Sagittarius A* Event Horizon Telescope Results. I. The Shadow of the Supermassive Black Hole in the Center of the Milky Way," *Astrophys. J. Lett.* **930** no. 2, (2022) L12.

[47] E. Newman and R. Penrose, "An Approach to gravitational radiation by a method of spin coefficients," *J. Math. Phys.* **3** (1962) 566–578.

[48] D. M. Eardley, D. L. Lee, and A. P. Lightman, "Gravitational-wave observations as a tool for testing relativistic gravity," *Phys. Rev. D* **8** (Nov, 1973) 3308–3321. https://link.aps.org/doi/10.1103/PhysRevD.8.3308.

[49] A. Einstein and N. Rosen, "On gravitational waves," *Journal of the Franklin Institute* **223** no. 1, (1937) 43–54. https://www.sciencedirect.com/science/article/pii/S0016003237905830.

[50] C. J. Moore, R. H. Cole, and C. P. L. Berry, "Gravitational-wave sensitivity curves," *Class. Quant. Grav.* **32** no. 1, (2015) 015014, arXiv:1408.0740 [gr-qc].

[51] P. Creminelli and F. Vernizzi, "Dark Energy after GW170817 and GRB170817A," *Phys. Rev. Lett.* **119** no. 25, (2017) 251302, arXiv:1710.05877 [astro-ph.CO].

[52] J. M. Ezquiaga and M. Zumalacárregui, "Dark Energy After GW170817: Dead Ends and the Road Ahead," *Phys. Rev. Lett.* **119** no. 25, (2017) 251304, arXiv:1710.05901 [astro-ph.CO].

[53] T. Baker, E. Bellini, P. G. Ferreira, M. Lagos, J. Noller, and I. Sawicki, "Strong constraints on cosmological gravity from GW170817 and GRB 170817A," *Phys. Rev. Lett.* **119** no. 25, (2017) 251301, arXiv:1710.06394 [astro-ph.CO].

[54] M. Crisostomi and K. Koyama, "Self-accelerating universe in scalar-tensor theories after GW170817," *Phys. Rev.* **D97** no. 8, (2018) 084004, arXiv:1712.06556 [astro-ph.CO].

[55] D. Langlois, R. Saito, D. Yamauchi, and K. Noui, "Scalar-tensor theories and modified gravity in the wake of GW170817," *Phys. Rev. D* **97** no. 6, (2018) 061501, arXiv:1711.07403 [gr-qc].

[56] A. Dima and F. Vernizzi, "Vainshtein Screening in Scalar-Tensor Theories before and after GW170817: Constraints on Theories beyond Horndeski," *Phys. Rev. D* **97** no. 10, (2018) 101302, arXiv:1712.04731 [gr-qc].

[57] T. Tomaru, "Large-scale cryogenic gravitational wave telescope: KAGRA," in *50th Rencontres de Moriond on Gravitation: 100 years after GR*, pp. 255–262. 2015.

[58] M. Punturo *et al.*, "The third generation of gravitational wave observatories and their science reach," *Class. Quant. Grav.* **27** (2010) 084007.

[59] D. Reitze *et al.*, "Cosmic Explorer: The U.S. Contribution to Gravitational-Wave Astronomy beyond LIGO," *Bull. Am. Astron. Soc.* **51** no. 7, (2019) 035, arXiv:1907.04833 [astro-ph.IM].

[60] P. Amaro-Seoane, H. Audley, S. Babak, J. Baker, E. Barausse, P. Bender, E. Berti, P. Binetruy, M. Born, D. Bortoluzzi, J. Camp, C. Caprini, V. Cardoso, M. Colpi, J. Conklin, N. Cornish, C. Cutler, K. Danzmann, R. Dolesi, L. Ferraioli, V. Ferroni, E. Fitzsimons, J. Gair, L. G. Bote, D. Giardini, F. Gibert, C. Grimani, H. Halloin, G. Heinzel, T. Hertog, M. Hewitson, K. Holley-Bockelmann, D. Hollington, M. Hueller, H. Inchauspe, P. Jetzer, N. Karnesis, C. Killow, A. Klein, B. Klipstein, N. Korsakova, S. L. Larson, J. Livas, I. Lloro, N. Man, D. Mance, J. Martino, I. Mateos, K. McKenzie, S. T. McWilliams, C. Miller, G. Mueller, G. Nardini, G. Nelemans, M. Nofrarias, A. Petiteau, P. Pivato, E. Plagnol, E. Porter, J. Reiche, D. Robertson, N. Robertson, E. Rossi, G. Russano, B. Schutz, A. Sesana, D. Shoemaker, J. Slutsky, C. F. Sopuerta, T. Sumner, N. Tamanini, I. Thorpe, M. Troebs, M. Vallisneri, A. Vecchio, D. Vetrugno, S. Vitale, M. Volonteri, G. Wanner, H. Ward, P. Wass, W. Weber, J. Ziemer, and P. Zweifel, "Laser interferometer space antenna," 2017.

[61] S. Babak, A. Petiteau, and M. Hewitson, "LISA Sensitivity and SNR Calculations," arXiv:2108.01167 [astro-ph.IM].

[62] **TianQin** Collaboration, J. Luo *et al.*, "TianQin: a space-borne gravitational wave detector," *Class. Quant. Grav.* **33** no. 3, (2016) 035010, arXiv:1512.02076 [astro-ph.IM].

[63] W.-H. Ruan, Z.-K. Guo, R.-G. Cai, and Y.-Z. Zhang, "Taiji program: Gravitational-wave sources," *Int. J. Mod. Phys. A* **35** no. 17, (2020) 2050075, arXiv:1807.09495 [gr-qc].

[64] K. Yagi and N. Seto, "Detector configuration of DECIGO/BBO and identification of cosmological neutron-star binaries," *Phys. Rev. D* **83** (2011) 044011, arXiv:1101.3940 [astro-ph.CO]. [Erratum: Phys.Rev.D 95, 109901 (2017)].

[65] R. N. Manchester, G. Hobbs, M. Bailes, W. A. Coles, W. van Straten, M. J. Keith, R. M. Shannon, N. D. R. Bhat, A. Brown, S. G. Burke-Spolaor, D. J. Champion, A. Chaudhary, R. T. Edwards, G. Hampson, A. W. Hotan, A. Jameson, F. A. Jenet, M. J. Kesteven, J. Khoo, J. Kocz, K. Maciesiak, S. Oslowski, V. Ravi, J. R. Reynolds, J. M. Sarkissian, J. P. W. Verbiest, Z. L. Wen, W. E. Wilson, D. Yardley, W. M. Yan, and X. P. You, "The parkes

pulsar timing array project," *Publications of the Astronomical Society of Australia* **30** (2013) . http://dx.doi.org/10.1017/pasa.2012.017.

[66] M. A. McLaughlin, "The North American Nanohertz Observatory for Gravitational Waves," *Class. Quant. Grav.* **30** (2013) 224008, arXiv:1310.0758 [astro-ph.IM].

[67] M. Kramer and D. J. Champion, "The european pulsar timing array and the large european array for pulsars," *Classical and Quantum Gravity* **30** no. 22, (Nov, 2013) 224009. https://doi.org/10.1088/0264-9381/30/22/224009.

[68] G. Hobbs, A. Archibald, Z. Arzoumanian, D. Backer, M. Bailes, N. D. R. Bhat, M. Burgay, S. Burke-Spolaor, D. Champion, I. Cognard, W. Coles, J. Cordes, P. Demorest, G. Desvignes, R. D. Ferdman, L. Finn, P. Freire, M. Gonzalez, J. Hessels, A. Hotan, G. Janssen, F. Jenet, A. Jessner, C. Jordan, V. Kaspi, M. Kramer, V. Kondratiev, J. Lazio, K. Lazaridis, K. J. Lee, Y. Levin, A. Lommen, D. Lorimer, R. Lynch, A. Lyne, R. Manchester, M. McLaughlin, D. Nice, S. Oslowski, M. Pilia, A. Possenti, M. Purver, S. Ransom, J. Reynolds, S. Sanidas, J. Sarkissian, A. Sesana, R. Shannon, X. Siemens, I. Stairs, B. Stappers, D. Stinebring, G. Theureau, R. van Haasteren, W. van Straten, J. P. W. Verbiest, D. R. B. Yardley, and X. P. You, "The international pulsar timing array project: using pulsars as a gravitational wave detector," *Classical and Quantum Gravity* **27** no. 8, (Apr, 2010) 084013. http://dx.doi.org/10.1088/0264-9381/27/8/084013.

[69] G. Janssen *et al.*, "Gravitational wave astronomy with the SKA," *PoS* **AASKA14** (2015) 037, arXiv:1501.00127 [astro-ph.IM].

[70] H. P. Robertson, "Kinematics and World-Structure," *Astrophys. J.* **82** (1935) 284–301.

[71] A. G. Walker, "On Milne's Theory of World-Structure," *Proceedings of the London Mathematical Society* **42** (Jan., 1937) 90–127.

[72] G. Lemaitre, "A Homogeneous Universe of Constant Mass and Growing Radius Accounting for the Radial Velocity of Extragalactic Nebulae," *Annales Soc. Sci. Bruxelles A* **47** (1927) 49–59.

[73] E. Hubble, "A relation between distance and radial velocity among extra-galactic nebulae," *Proc. Nat. Acad. Sci.* **15** (1929) 168–173.

[74] **Planck** Collaboration, N. Aghanim *et al.*, "Planck 2018 results. VI. Cosmological parameters," *Astron. Astrophys.* **641** (2020) A6, arXiv:1807.06209 [astro-ph.CO]. [Erratum: Astron.Astrophys. 652, C4 (2021)].

[75] **SDSS** Collaboration, D. J. Eisenstein *et al.*, "Detection of the Baryon Acoustic Peak in the Large-Scale Correlation Function of SDSS Luminous Red Galaxies," *Astrophys. J.* **633** (2005) 560–574, arXiv:astro-ph/0501171.

[76] J. Kovac, E. M. Leitch, C. Pryke, J. E. Carlstrom, N. W. Halverson, and W. L. Holzapfel, "Detection of polarization in the cosmic microwave background using DASI," *Nature* **420** (2002) 772–787, arXiv:astro-ph/0209478.

[77] P. Bull *et al.*, "Beyond ΛCDM: Problems, solutions, and the road ahead," *Phys. Dark Univ.* **12** (2016) 56–99, arXiv:1512.05356 [astro-ph.CO].

[78] **LIGO Scientific, Virgo, VIRGO** Collaboration, B. P. Abbott *et al.*, "A Gravitational-wave Measurement of the Hubble Constant Following the Second Observing Run of Advanced LIGO and Virgo," *Astrophys. J.* **909** no. 2, (2021) 218, arXiv:1908.06060 [astro-ph.CO]. [Erratum: Astrophys.J. 923, 279 (2021)].

[79] A. G. Riess, S. Casertano, W. Yuan, L. M. Macri, and D. Scolnic, "Large Magellanic Cloud Cepheid Standards Provide a 1% Foundation for the Determination of the Hubble Constant and Stronger Evidence for Physics beyond ΛCDM," *Astrophys. J.* **876** no. 1, (2019) 85, arXiv:1903.07603 [astro-ph.CO].

[80] E. Abdalla *et al.*, "Cosmology Intertwined: A Review of the Particle Physics, Astrophysics, and Cosmology Associated with the Cosmological Tensions and Anomalies," in *2022 Snowmass Summer Study*. 3, 2022. arXiv:2203.06142 [astro-ph.CO].

[81] **Supernova Cosmology Project** Collaboration, S. Perlmutter *et al.*, "Measurements of Ω and Λ from 42 high redshift supernovae," *Astrophys. J.* **517** (1999) 565–586, arXiv:astro-ph/9812133.

[82] **Supernova Cosmology Project** Collaboration, S. Perlmutter *et al.*, "Measurements of the cosmological parameters Omega and Lambda from the first 7 supernovae at z>=0.35," *Astrophys. J.* **483** (1997) 565, arXiv:astro-ph/9608192.

[83] **Supernova Cosmology Project** Collaboration, S. Perlmutter *et al.*, "Discovery of a supernova explosion at half the age of the Universe and its cosmological implications," *Nature* **391** (1998) 51–54, arXiv:astro-ph/9712212.

[84] **Supernova Search Team** Collaboration, A. G. Riess *et al.*, "Observational evidence from supernovae for an accelerating universe and a cosmological constant," *Astron. J.* **116** (1998) 1009–1038, arXiv:astro-ph/9805201.

[85] **Supernova Search Team** Collaboration, P. M. Garnavich *et al.*, "Constraints on cosmological models from Hubble Space Telescope observations of high z supernovae," *Astrophys. J. Lett.* **493** (1998) L53–57, arXiv:astro-ph/9710123.

[86] **DES** Collaboration, T. M. C. Abbott *et al.*, "Dark Energy Survey year 1 results: Cosmological constraints from galaxy clustering and weak lensing," *Phys. Rev. D* **98** no. 4, (2018) 043526, arXiv:1708.01530 [astro-ph.CO].

[87] P. Coles and F. Lucchin, *Cosmology: The Origin and evolution of cosmic structure*. 1995.

[88] A. Padilla, "Lectures on the Cosmological Constant Problem," arXiv:1502.05296 [hep-th].

[89] S. Weinberg, "The Cosmological Constant Problem," *Rev. Mod. Phys.* **61** (1989) 1–23.

[90] E. Bianchi and C. Rovelli, "Why all these prejudices against a constant?," arXiv:1002.3966 [astro-ph.CO].

[91] G. Lambiase, S. Mohanty, A. Narang, and P. Parashari, "Testing dark energy models in the light of σ_8 tension," *Eur. Phys. J. C* **79** no. 2, (2019) 141, arXiv:1804.07154 [astro-ph.CO].

[92] F. Pretorius, "Evolution of binary black hole spacetimes," *Phys. Rev. Lett.* **95** (2005) 121101, arXiv:gr-qc/0507014.

[93] J. G. Baker, J. Centrella, D.-I. Choi, M. Koppitz, and J. van Meter, "Gravitational wave extraction from an inspiraling configuration of merging black holes," *Phys. Rev. Lett.* **96** (2006) 111102, arXiv:gr-qc/0511103.

[94] M. Campanelli, C. O. Lousto, P. Marronetti, and Y. Zlochower, "Accurate evolutions of orbiting black-hole binaries without excision," *Phys. Rev. Lett.* **96** (2006) 111101, arXiv:gr-qc/0511048.

[95] D. Lovelock, "The Einstein tensor and its generalizations," *J. Math. Phys.* **12** (1971) 498–501.

[96] D. Lovelock, "The four-dimensionality of space and the einstein tensor," *J. Math. Phys.* **13** (1972) 874–876.

[97] N. Yunes and X. Siemens, "Gravitational-Wave Tests of General Relativity with Ground-Based Detectors and Pulsar Timing-Arrays," *Living Rev. Rel.* **16** (2013) 9, arXiv:1304.3473 [gr-qc].

[98] J. Hadamard, "Sur les problèmes aux dérivés partielles et leur signification physique," *Princeton University Bulletin* **13** (1902) 49–52.

[99] H. Friedrich and A. D. Rendall, "The Cauchy problem for the Einstein equations," *Lect. Notes Phys.* **540** (2000) 127–224, arXiv:gr-qc/0002074.

[100] O. A. Reula, "Hyperbolic methods for einstein's equations.," *Living Reviews in Relativity [electronic only]* **1** (1998) Article No. 1998–3. http://eudml.org/doc/223442.

[101] O. Sarbach and M. Tiglio, "Continuum and Discrete Initial-Boundary-Value Problems and Einstein's Field Equations," *Living Rev. Rel.* **15** (2012) 9, arXiv:1203.6443 [gr-qc].

[102] D. Hilditch, "An Introduction to Well-posedness and Free-evolution," *Int. J. Mod. Phys. A* **28** (2013) 1340015, arXiv:1309.2012 [gr-qc].

[103] M. Ostrogradsky, "Mémoires sur les équations différentielles, relatives au problème des isopérimètres," *Mem. Acad. St. Petersbourg* **6** no. 4, (1850) 385–517.

[104] J. Ben Achour, M. Crisostomi, K. Koyama, D. Langlois, K. Noui, and G. Tasinato, "Degenerate higher order scalar-tensor theories beyond Horndeski up to cubic order," *JHEP* **12** (2016) 100, arXiv:1608.08135 [hep-th].

[105] M. Okounkova, L. C. Stein, M. A. Scheel, and D. A. Hemberger, "Numerical binary black hole mergers in dynamical Chern-Simons gravity: Scalar field," *Phys. Rev. D* **96** no. 4, (2017) 044020, arXiv:1705.07924 [gr-qc].

[106] M. Fierz, "On the physical interpretation of P.Jordan's extended theory of gravitation," *Helv. Phys. Acta* **29** (1956) 128–134.

[107] P. Jordan, "The present state of Dirac's cosmological hypothesis," *Z. Phys.* **157** (1959) 112–121.

[108] C. Brans and R. H. Dicke, "Mach's principle and a relativistic theory of gravitation," *Phys. Rev.* **124** (1961) 925–935.

[109] G. W. Horndeski, "Second-order scalar-tensor field equations in a four-dimensional space," *Int. J. Theor. Phys.* **10** (1974) 363–384.

[110] T. Chiba, T. Okabe, and M. Yamaguchi, "Kinetically driven quintessence," *Phys. Rev. D* **62** (2000) 023511, arXiv:astro-ph/9912463.

[111] C. Armendariz-Picon, V. F. Mukhanov, and P. J. Steinhardt, "A Dynamical solution to the problem of a small cosmological constant and late time cosmic acceleration," *Phys. Rev. Lett.* **85** (2000) 4438–4441, arXiv:astro-ph/0004134 [astro-ph].

[112] T. Kobayashi, M. Yamaguchi, and J. Yokoyama, "Generalized G-inflation: Inflation with the most general second-order field equations," *Prog. Theor. Phys.* **126** (2011) 511–529, arXiv:1105.5723 [hep-th].

[113] C. Deffayet, G. Esposito-Farese, and A. Vikman, "Covariant Galileon," *Phys. Rev. D* **79** (2009) 084003, arXiv:0901.1314 [hep-th].

[114] C. de Rham, G. Gabadadze, and A. J. Tolley, "Ghost free Massive Gravity in the Stückelberg language," *Phys. Lett. B* **711** (2012) 190–195, arXiv:1107.3820 [hep-th].

[115] M. Zumalacárregui and J. García-Bellido, "Transforming gravity: from derivative couplings to matter to second-order scalar-tensor theories beyond the Horndeski Lagrangian," *Phys. Rev.* **D89** (2014) 064046, arXiv:1308.4685 [gr-qc].

[116] J. Gleyzes, D. Langlois, F. Piazza, and F. Vernizzi, "Healthy theories beyond Horndeski," *Phys. Rev. Lett.* **114** no. 21, (2015) 211101, arXiv:1404.6495 [hep-th].

[117] D. Langlois and K. Noui, "Degenerate higher derivative theories beyond Horndeski: evading the Ostrogradski instability," *JCAP* **02** (2016) 034, arXiv:1510.06930 [gr-qc].

[118] M. Crisostomi, K. Koyama, and G. Tasinato, "Extended Scalar-Tensor Theories of Gravity," *JCAP* **1604** (2016) 044, arXiv:1602.03119 [hep-th].

[119] G. R. Dvali, G. Gabadadze, and M. Porrati, "4-D gravity on a brane in 5-D Minkowski space," *Phys. Lett. B* **485** (2000) 208–214, arXiv:hep-th/0005016.

[120] P. Creminelli, M. Lewandowski, G. Tambalo, and F. Vernizzi, "Gravitational Wave Decay into Dark Energy," *JCAP* **1812** (2018) 025, arXiv:1809.03484 [astro-ph.CO].

[121] P. Creminelli, G. Tambalo, F. Vernizzi, and V. Yingcharoenrat, "Dark-Energy Instabilities induced by Gravitational Waves," *JCAP* **2005** (2020) 002, arXiv:1910.14035 [gr-qc].

[122] E. Babichev, "Emergence of ghosts in Horndeski theory," *JHEP* **07** (2020) 038, arXiv:2001.11784 [hep-th].

[123] R. R. Caldwell, R. Dave, and P. J. Steinhardt, "Cosmological imprint of an energy component with general equation of state," *Phys. Rev. Lett.* **80** (1998) 1582–1585, arXiv:astro-ph/9708069.

[124] E. Babichev, V. Mukhanov, and A. Vikman, "k-Essence, superluminal propagation, causality and emergent geometry," *JHEP* **02** (2008) 101, arXiv:0708.0561 [hep-th].

[125] C. Bonvin, C. Caprini, and R. Durrer, "A no-go theorem for k-essence dark energy," *Phys. Rev. Lett.* **97** (2006) 081303, arXiv:astro-ph/0606584.

[126] E. Babichev, C. Deffayet, and R. Ziour, "k-Mouflage gravity," *Int. J. Mod. Phys. D* **18** (2009) 2147–2154, arXiv:0905.2943 [hep-th].

[127] K. Koyama, "Cosmological Tests of Modified Gravity," *Rept. Prog. Phys.* **79** no. 4, (2016) 046902, arXiv:1504.04623 [astro-ph.CO].

[128] K. Hinterbichler and J. Khoury, "Symmetron Fields: Screening Long-Range Forces Through Local Symmetry Restoration," *Phys. Rev. Lett.* **104** (2010) 231301, arXiv:1001.4525 [hep-th].

[129] M. Pietroni, "Dark energy condensation," *Phys. Rev. D* **72** (2005) 043535, arXiv:astro-ph/0505615.

[130] K. A. Olive and M. Pospelov, "Environmental dependence of masses and coupling constants," *Phys. Rev. D* **77** (2008) 043524, arXiv:0709.3825 [hep-ph].

[131] P. Brax, C. van de Bruck, A.-C. Davis, B. Li, and D. J. Shaw, "Nonlinear Structure Formation with the Environmentally Dependent Dilaton," *Phys. Rev. D* **83** (2011) 104026, arXiv:1102.3692 [astro-ph.CO].

[132] J. Khoury and A. Weltman, "Chameleon fields: Awaiting surprises for tests of gravity in space," *Phys. Rev. Lett.* **93** (2004) 171104, arXiv:astro-ph/0309300.

[133] J. Khoury and A. Weltman, "Chameleon cosmology," *Phys. Rev. D* **69** (2004) 044026, arXiv:astro-ph/0309411.

[134] C. de Rham and R. H. Ribeiro, "Riding on irrelevant operators," *JCAP* **1411** (2014) 016, arXiv:1405.5213 [hep-th].

[135] P. Brax and P. Valageas, "Quantum field theory of K-mouflage," *Phys. Rev.* **D94** no. 4, (2016) 043529, arXiv:1607.01129 [astro-ph.CO].

[136] A. I. Vainshtein, "To the problem of nonvanishing gravitation mass," *Phys. Lett. B* **39** (1972) 393–394.

[137] E. Babichev and C. Deffayet, "An introduction to the Vainshtein mechanism," *Class. Quant. Grav.* **30** (2013) 184001, arXiv:1304.7240 [gr-qc].

[138] D. Colladay and V. A. Kostelecky, "Lorentz violating extension of the standard model," *Phys. Rev. D* **58** (1998) 116002, arXiv:hep-ph/9809521.

[139] V. A. Kostelecky and N. Russell, "Data Tables for Lorentz and CPT Violation," arXiv:0801.0287 [hep-ph].

[140] D. Mattingly, "Modern tests of Lorentz invariance," *Living Rev. Rel.* **8** (2005) 5, arXiv:gr-qc/0502097.

[141] T. Jacobson and D. Mattingly, "Gravity with a dynamical preferred frame," *Phys. Rev. D* **64** (2001) 024028, arXiv:gr-qc/0007031.

[142] B. Z. Foster and T. Jacobson, "Post-Newtonian parameters and constraints on Einstein-aether theory," *Phys. Rev. D* **73** (2006) 064015, arXiv:gr-qc/0509083.

[143] C. Y. R. Chen, C. de Rham, A. Margalit, and A. J. Tolley, "A cautionary case of casual causality," *JHEP* **03** (2022) 025, arXiv:2112.05031 [hep-th].

[144] C. de Rham, A. J. Tolley, and J. Zhang, "Causality Constraints on Gravitational Effective Field Theories," *Phys. Rev. Lett.* **128** no. 13, (2022) 131102, arXiv:2112.05054 [gr-qc].

[145] P. Horava, "Quantum Gravity at a Lifshitz Point," *Phys. Rev. D* **79** (2009) 084008, arXiv:0901.3775 [hep-th].

[146] T. Jacobson, "Undoing the twist: The Hořava limit of Einstein-aether theory," *Phys. Rev. D* **89** (2014) 081501, arXiv:1310.5115 [gr-qc].

[147] D. Blas, O. Pujolas, and S. Sibiryakov, "Models of non-relativistic quantum gravity: The Good, the bad and the healthy," *JHEP* **04** (2011) 018, arXiv:1007.3503 [hep-th].

[148] A. O. Barvinsky, D. Blas, M. Herrero-Valea, S. M. Sibiryakov, and C. F. Steinwachs, "Renormalization of Hořava gravity," *Phys. Rev. D* **93** no. 6, (2016) 064022, arXiv:1512.02250 [hep-th].

[149] A. O. Barvinsky, D. Blas, M. Herrero-Valea, S. M. Sibiryakov, and C. F. Steinwachs, "Hořava Gravity is Asymptotically Free in 2 + 1 Dimensions," *Phys. Rev. Lett.* **119** no. 21, (2017) 211301, arXiv:1706.06809 [hep-th].

[150] D. Blas, O. Pujolas, and S. Sibiryakov, "Consistent Extension of Horava Gravity," *Phys. Rev. Lett.* **104** (2010) 181302, arXiv:0909.3525 [hep-th].

[151] E. Barausse, T. P. Sotiriou, and I. Vega, "Slowly rotating black holes in Einstein-æther theory," *Phys. Rev. D* **93** no. 4, (2016) 044044, arXiv:1512.05894 [gr-qc].

[152] G. Lara, M. Herrero-Valea, E. Barausse, and S. M. Sibiryakov, "Black holes in ultraviolet-complete Hořava gravity," *Phys. Rev. D* **103** no. 10, (2021) 104007, arXiv:2103.01975 [gr-qc].

[153] M. Bezares, M. Crisostomi, C. Palenzuela, and E. Barausse, "K-dynamics: well-posed 1+1 evolutions in K-essence," *JCAP* **2103** (2021) 072, arXiv:2008.07546 [gr-qc].

[154] A. Lehebel, E. Babichev, and C. Charmousis, "A no-hair theorem for stars in Horndeski theories," *JCAP* **07** (2017) 037, arXiv:1706.04989 [gr-qc].

[155] E. Barausse and K. Yagi, "Gravitation-Wave Emission in Shift-Symmetric Horndeski Theories," *Phys. Rev. Lett.* **115** no. 21, (2015) 211105, arXiv:1509.04539 [gr-qc].

[156] A.-C. Davis and S. Melville, "Scalar Fields Near Compact Objects: Resummation versus UV Completion," arXiv:2107.00010 [gr-qc].

[157] K. Aoki, S. Mukohyama, and R. Namba, "Positivity vs. Lorentz-violation: an explicit example," arXiv:2107.01755 [hep-th].

[158] P. Brax and P. Valageas, "Small-scale Nonlinear Dynamics of K-mouflage Theories," *Phys. Rev.* **D90** no. 12, (2014) 123521, arXiv:1408.0969 [astro-ph.CO].

[159] E. Barausse, C. Palenzuela, M. Ponce, and L. Lehner, "Neutron-star mergers in scalar-tensor theories of gravity," *Phys. Rev. D* **87** (2013) 081506, arXiv:1212.5053 [gr-qc].

[160] C. Palenzuela, E. Barausse, M. Ponce, and L. Lehner, "Dynamical scalarization of neutron stars in scalar-tensor gravity theories," *Phys. Rev. D* **89** no. 4, (2014) 044024, arXiv:1310.4481 [gr-qc].

[161] W. R. Inc., "Mathematica, Version 12.2." https://www.wolfram.com/mathematica. Champaign, IL, 2020.

[162] E. Babichev, C. Deffayet, and R. Ziour, "The Recovery of General Relativity in massive gravity via the Vainshtein mechanism," *Phys. Rev.* **D82** (2010) 104008, arXiv:1007.4506 [gr-qc].

[163] E. Babichev and M. Crisostomi, "Restoring general relativity in massive bigravity theory," *Phys. Rev.* **D88** no. 8, (2013) 084002, arXiv:1307.3640 [gr-qc].

[164] C. M. Will, *Theory and Experiment in Gravitational Physics*. Cambridge University Press, 1993.

[165] M. Shibata, K. Taniguchi, H. Okawa, and A. Buonanno, "Coalescence of binary neutron stars in a scalar-tensor theory of gravity,".

[166] D. Eardley, "Observable effects of a scalar gravitational field in a binary pulsar," *The Astrophysical Journal* **196** (02, 1975) L59–L62.

[167] C. M. Will and H. W. Zaglauer, "Gravitational Radiation, Close Binary Systems, and the Brans-dicke Theory of Gravity," *Astrophys. J.* **346** (1989) 366.

[168] T. Damour and G. Esposito-Farese, "Tensor multiscalar theories of gravitation," *Class. Quant. Grav.* **9** (1992) 2093–2176.

[169] T. Damour and G. Esposito-Farese, "Nonperturbative strong field effects in tensor - scalar theories of gravitation," *Phys. Rev. Lett.* **70** (1993) 2220–2223.

[170] N. Sennett and A. Buonanno, "Modeling dynamical scalarization with a resummed post-Newtonian expansion," *Phys. Rev.* **D93** no. 12, (2016) 124004, arXiv:1603.03300 [gr-qc].

[171] K. Yagi, D. Blas, E. Barausse, and N. Yunes, "Constraints on Einstein-Æther theory and Hořava gravity from binary pulsar observations," *Phys. Rev. D* **89** no. 8, (2014) 084067, arXiv:1311.7144 [gr-qc]. [Erratum: Phys.Rev.D 90, 069902 (2014), Erratum: Phys.Rev.D 90, 069901 (2014)].

[172] K. Yagi, D. Blas, N. Yunes, and E. Barausse, "Strong Binary Pulsar Constraints on Lorentz Violation in Gravity," *Phys. Rev. Lett.* **112** no. 16, (2014) 161101, arXiv:1307.6219 [gr-qc].

[173] S. Mirshekari and C. M. Will, "Compact binary systems in scalar-tensor gravity: Equations of motion to 2.5 post-Newtonian order," *Phys. Rev. D* **87** no. 8, (2013) 084070, arXiv:1301.4680 [gr-qc].

[174] T. Gupta, M. Herrero-Valea, D. Blas, E. Barausse, N. Cornish, K. Yagi, and N. Yunes, "Updated Binary Pulsar Constraints on Einstein-\aether Theory in Light of Gravitational Wave Constraints on the Speed of Gravity," arXiv:2104.04596 [gr-qc].

[175] K. Yagi, L. C. Stein, and N. Yunes, "Challenging the Presence of Scalar Charge and Dipolar Radiation in Binary Pulsars," *Phys. Rev. D* **93** no. 2, (2016) 024010, arXiv:1510.02152 [gr-qc].

[176] E. Barausse, N. Yunes, and K. Chamberlain, "Theory-Agnostic Constraints on Black-Hole Dipole Radiation with Multiband Gravitational-Wave Astrophysics," *Phys. Rev. Lett.* **116** no. 24, (2016) 241104, arXiv:1603.04075 [gr-qc].

[177] H. O. Silva, J. Sakstein, L. Gualtieri, T. P. Sotiriou, and E. Berti, "Spontaneous scalarization of black holes and compact stars from a Gauss-Bonnet coupling," *Phys. Rev. Lett.* **120** no. 13, (2018) 131104, arXiv:1711.02080 [gr-qc].

[178] H. O. Silva, C. F. B. Macedo, T. P. Sotiriou, L. Gualtieri, J. Sakstein, and E. Berti, "Stability of scalarized black hole solutions in scalar-Gauss-Bonnet gravity," *Phys. Rev.* **D99** no. 6, (2019) 064011, arXiv:1812.05590 [gr-qc].

[179] A. Dima, E. Barausse, N. Franchini, and T. P. Sotiriou, "Spin-induced black hole spontaneous scalarization," *Phys. Rev. Lett.* **125** no. 23, (2020) 231101, arXiv:2006.03095 [gr-qc].

[180] P. C. C. Freire, N. Wex, G. Esposito-Farese, J. P. W. Verbiest, M. Bailes, B. A. Jacoby, M. Kramer, I. H. Stairs, J. Antoniadis, and G. H. Janssen, "The relativistic pulsar-white dwarf binary PSR J1738+0333 II. The most stringent

test of scalar-tensor gravity," *Mon. Not. Roy. Astron. Soc.* **423** (2012) 3328, arXiv:1205.1450 [astro-ph.GA].

[181] C. de Rham, A. J. Tolley, and D. H. Wesley, "Vainshtein Mechanism in Binary Pulsars," *Phys. Rev. D* **87** no. 4, (2013) 044025, arXiv:1208.0580 [gr-qc].

[182] C. de Rham, A. Matas, and A. J. Tolley, "Galileon Radiation from Binary Systems," *Phys. Rev. D* **87** no. 6, (2013) 064024, arXiv:1212.5212 [hep-th].

[183] F. Dar, C. D. Rham, J. T. Deskins, J. T. Giblin, and A. J. Tolley, "Scalar Gravitational Radiation from Binaries: Vainshtein Mechanism in Time-dependent Systems," *Class. Quant. Grav.* **36** no. 2, (2019) 025008, arXiv:1808.02165 [hep-th].

[184] S. Gillessen, F. Eisenhauer, S. Trippe, T. Alexander, R. Genzel, F. Martins, and T. Ott, "Monitoring stellar orbits around the Massive Black Hole in the Galactic Center," *Astrophys. J.* **692** (2009) 1075–1109, arXiv:0810.4674 [astro-ph].

[185] J. Cayuso, N. Ortiz, and L. Lehner, "Fixing extensions to general relativity in the nonlinear regime," *Phys. Rev. D* **96** no. 8, (2017) 084043, arXiv:1706.07421 [gr-qc].

[186] G. Allwright and L. Lehner, "Towards the nonlinear regime in extensions to GR: assessing possible options," *Class. Quant. Grav.* **36** no. 8, (2019) 084001, arXiv:1808.07897 [gr-qc].

[187] C. Bona, T. Ledvinka, and C. Palenzuela, "A 3+1 covariant suite of numerical relativity evolution systems," *Phys. Rev.* **D66** (2002) 084013, arXiv:gr-qc/0208087 [gr-qc].

[188] D. Alic, C. Bona, C. Bona-Casas, and J. Masso, "Efficient implementation of finite volume methods in Numerical Relativity," *Phys. Rev.* **D76** (2007) 104007, arXiv:0706.1189 [gr-qc].

[189] C. Bona, L. Lehner, and C. Palenzuela-Luque, "Geometrically motivated hyperbolic coordinate conditions for numerical relativity: Analysis, issues and implementations," *Phys. Rev.* **D72** (2005) 104009, arXiv:gr-qc/0509092 [gr-qc].

[190] A. Bernal, J. Barranco, D. Alic, and C. Palenzuela, "Multi-state Boson Stars," *Phys. Rev.* **D81** (2010) 044031, arXiv:0908.2435 [gr-qc].

[191] S. Valdez-Alvarado, C. Palenzuela, D. Alic, and L. A. Ureña-López, "Dynamical evolution of fermion-boson stars," *Phys. Rev.* **D87** no. 8, (2013) 084040, arXiv:1210.2299 [gr-qc].

[192] C. Bona, C. Palenzuela-Luque, and C. Bona-Casas, *Elements of Numerical Relativity and Relativistic Hydrodynamics: From Einstein' s Equations to Astrophysical Simulations*. Lecture Notes in Physics. Springer Berlin Heidelberg, 2009. https://books.google.nl/books?id=KgPGHaCUaAYC.

[193] C. Bona, J. Masso, E. Seidel, and J. Stela, "A New formalism for numerical relativity," *Phys. Rev. Lett.* **75** (1995) 600–603, arXiv:gr-qc/9412071.

[194] Y. Foures-Bruhat, "Theoreme d'existence pour certains systemes derivees partielles non lineaires," *Acta Mat.* **88** (1952) 141–225.

[195] G. Lara, M. Bezares, and E. Barausse, "UV completions, fixing the equations, and nonlinearities in k-essence," *Phys. Rev. D* **105** no. 6, (2022) 064058, arXiv:2112.09186 [gr-qc].

[196] J. L. Ripley and F. Pretorius, "Hyperbolicity in Spherical Gravitational Collapse in a Horndeski Theory," *Phys. Rev. D* **99** no. 8, (2019) 084014, arXiv:1902.01468 [gr-qc].

[197] L. Bernard, L. Lehner, and R. Luna, "Challenges to global solutions in Horndeski's theory," *Phys. Rev. D* **100** no. 2, (2019) 024011, arXiv:1904.12866 [gr-qc].

[198] R. Cayuso and L. Lehner, "Nonlinear, noniterative treatment of EFT-motivated gravity," *Phys. Rev. D* **102** no. 8, (2020) 084008, arXiv:2005.13720 [gr-qc].

[199] W. Israel and J. M. Stewart, "Transient relativistic thermodynamics and kinetic theory," *Annals Phys.* **118** (1979) 341–372.

[200] M. Bezares, M. Bošković, S. Liebling, C. Palenzuela, P. Pani, and E. Barausse, "Gravitational waves and kicks from the merger of unequal mass, highly

compact boson stars," *Phys. Rev. D* **105** no. 6, (2022) 064067, arXiv:2201.06113 [gr-qc].

[201] G. Raposo, P. Pani, M. Bezares, C. Palenzuela, and V. Cardoso, "Anisotropic stars as ultracompact objects in General Relativity," *Phys. Rev. D* **99** no. 10, (2019) 104072, arXiv:1811.07917 [gr-qc].

[202] A. Dima, M. Bezares, and E. Barausse, "Dynamical chameleon neutron stars: Stability, radial oscillations, and scalar radiation in spherical symmetry," *Phys. Rev. D* **104** no. 8, (2021) 084017, arXiv:2107.04359 [gr-qc].

[203] C. Bona, C. Palenzuela-Luque, and C. Bona-Casas, eds., *Elements of Numerical Relativity and Relativistic Hydrodynamics*, vol. 783 of *Lecture Notes in Physics, Berlin Springer Verlag*. 2009.

[204] C. Palenzuela, B. Miñano, D. Viganò, A. Arbona, C. Bona-Casas, A. Rigo, M. Bezares, C. Bona, and J. Massó, "A Simflowny-based finite-difference code for high-performance computing in numerical relativity," *Class. Quant. Grav.* **35** no. 18, (2018) 185007, arXiv:1806.04182 [physics.comp-ph].

[205] J. Novak, "Spherical neutron star collapse in tensor - scalar theory of gravity," *Phys. Rev. D* **57** (1998) 4789–4801, arXiv:gr-qc/9707041.

[206] D. Gerosa, U. Sperhake, and C. D. Ott, "Numerical simulations of stellar collapse in scalar-tensor theories of gravity," *Class. Quant. Grav.* **33** no. 13, (2016) 135002, arXiv:1602.06952 [gr-qc].

[207] R. Rosca-Mead, U. Sperhake, C. J. Moore, M. Agathos, D. Gerosa, and C. D. Ott, "Core collapse in massive scalar-tensor gravity," *Phys. Rev. D* **102** no. 4, (2020) 044010, arXiv:2005.09728 [gr-qc].

[208] P. Figueras and T. França, "Gravitational Collapse in Cubic Horndeski Theories," *Class. Quant. Grav.* **37** no. 22, (2020) 225009, arXiv:2006.09414 [gr-qc].

[209] A. Adams, N. Arkani-Hamed, S. Dubovsky, A. Nicolis, and R. Rattazzi, "Causality, analyticity and an IR obstruction to UV completion," *JHEP* **10** (2006) 014, arXiv:hep-th/0602178.

[210] L. Hui and A. Nicolis, "No-Hair Theorem for the Galileon," *Phys. Rev. Lett.* **110** (2013) 241104, arXiv:1202.1296 [hep-th].

[211] T. P. Sotiriou and S.-Y. Zhou, "Black hole hair in generalized scalar-tensor gravity," *Phys. Rev. Lett.* **112** (2014) 251102, arXiv:1312.3622 [gr-qc].

[212] M. Punturo *et al.*, "The Einstein Telescope: A third-generation gravitational wave observatory," *Class. Quant. Grav.* **27** (2010) 194002.

[213] **LISA** Collaboration, P. Amaro-Seoane *et al.*, "Laser Interferometer Space Antenna," arXiv:1702.00786 [astro-ph.IM].

[214] ESA, "Lisa science requirements document https://dms.cosmos.esa.int/COSMOS/doc_fetch.php?id=3752747.".

[215] D. Alic, C. Bona-Casas, C. Bona, L. Rezzolla, and C. Palenzuela, "Conformal and covariant formulation of the Z4 system with constraint-violation damping," *Phys. Rev. D* **85** (2012) 064040, arXiv:1106.2254 [gr-qc].

[216] M. Bezares, C. Palenzuela, and C. Bona, "Final fate of compact boson star mergers," *Phys. Rev. D* **95** no. 12, (2017) 124005, arXiv:1705.01071 [gr-qc].

[217] C. Gundlach, J. M. Martin-Garcia, G. Calabrese, and I. Hinder, "Constraint damping in the Z4 formulation and harmonic gauge," *Class. Quant. Grav.* **22** (2005) 3767–3774, arXiv:gr-qc/0504114.

[218] M. Alcubierre, B. Bruegmann, P. Diener, M. Koppitz, D. Pollney, E. Seidel, and R. Takahashi, "Gauge conditions for long term numerical black hole evolutions without excision," *Phys. Rev. D* **67** (2003) 084023, arXiv:gr-qc/0206072.

[219] S. L. Liebling, C. Palenzuela, and L. Lehner, "Toward fidelity and scalability in non-vacuum mergers," *Class. Quant. Grav.* **37** no. 13, (2020) 135006, arXiv:2002.07554 [gr-qc].

[220] M. Bezares and C. Palenzuela, "Gravitational Waves from Dark Boson Star binary mergers," *Class. Quant. Grav.* **35** no. 23, (2018) 234002, arXiv:1808.10732 [gr-qc].

[221] A. Arbona, A. Artigues, C. Bona-Casas, J. Massó, B. Miñano, A. Rigo, M. Trias, and C. Bona, "Simflowny: A general-purpose platform for the management of physical models and simulation problems," *Computer Physics Communications* **184** no. 10, (2013) 2321–2331. https://www.sciencedirect.com/science/article/pii/S0010465513001471.

[222] A. Arbona, B. Miñano, A. Rigo, C. Bona, C. Palenzuela, A. Artigues, C. Bona-Casas, and J. Massó, "Simflowny 2: An upgraded platform for scientific modelling and simulation," *Computer Physics Communications* **229** (2018) 170–181. https://www.sciencedirect.com/science/article/pii/S0010465518300870.

[223] "Simflowny project website.," 2021. https://bitbucket.org/iac3/simflowny/wiki/Home.

[224] R. D. Hornung and S. R. Kohn, "Managing application complexity in the samrai object-oriented framework," *Concurrency and Computation: Practice and Experience* **14** no. 5, (2002) 347–368. http://dx.doi.org/10.1002/cpe.652.

[225] B. T. Gunney and R. W. Anderson, "Advances in patch-based adaptive mesh refinement scalability," *Journal of Parallel and Distributed Computing* **89** (2016) 65 – 84. http://www.sciencedirect.com/science/article/pii/S0743731515002129.

[226] "Samrai project website.," 2021. https://computation.llnl.gov/project/SAMRAI/.

[227] S. L. Liebling, C. Palenzuela, and L. Lehner, "Effects of high density phase transitions on neutron star dynamics," *Classical and Quantum Gravity* **38** no. 11, (May, 2021) 115007. https://doi.org/10.1088/1361-6382/abf898.

[228] "Lorene home page." http://www.lorene.obspm.fr/, 2010.

[229] M. Kramer *et al.*, "Tests of general relativity from timing the double pulsar," *Science* **314** (2006) 97–102, arXiv:astro-ph/0609417 [astro-ph].

[230] A. Noutsos *et al.*, "Understanding and improving the timing of PSR J0737−3039B," *Astron. Astrophys.* **643** (2020) A143, arXiv:2011.02357 [astro-ph.HE].

[231] M. Kramer *et al. in prep.* (2021) .

[232] R. Arnowitt, S. Deser, and C. W. Misner, "Dynamical structure and definition of energy in general relativity," *Phys. Rev.* **116** (Dec, 1959) 1322–1330. https://link.aps.org/doi/10.1103/PhysRev.116.1322.

[233] A. O. Barvinsky, D. Blas, M. Herrero-Valea, S. M. Sibiryakov, and C. F. Steinwachs, "Renormalization of gauge theories in the background-field approach," *JHEP* **07** (2018) 035, arXiv:1705.03480 [hep-th].

[234] D. Blas, O. Pujolas, and S. Sibiryakov, "On the Extra Mode and Inconsistency of Horava Gravity," *JHEP* **10** (2009) 029, arXiv:0906.3046 [hep-th].

[235] K. Koyama and F. Arroja, "Pathological behaviour of the scalar graviton in Horava-Lifshitz gravity," *JHEP* **03** (2010) 061, arXiv:0910.1998 [hep-th].

[236] X. Gao and Z.-B. Yao, "Spatially covariant gravity with velocity of the lapse function: the Hamiltonian analysis," *JCAP* **1905** (2019) 024, arXiv:1806.02811 [gr-qc].

[237] A. De Felice, D. Langlois, S. Mukohyama, K. Noui, and A. Wang, "Generalized instantaneous modes in higher-order scalar-tensor theories," *Phys. Rev.* **D98** no. 8, (2018) 084024, arXiv:1803.06241 [hep-th].

[238] D. Langlois, K. Noui, and H. Roussille, "Quadratic DHOST theories revisited," arXiv:2012.10218 [gr-qc].

[239] M. Alcubierre, *Introduction to 3+1 Numerical Relativity*. 2008.

[240] T. W. Baumgarte and S. L. Shapiro, *Numerical Relativity: Solving Einstein's Equations on the Computer*. 2010.

[241] L. Blanchet and S. Marsat, "Modified gravity approach based on a preferred time foliation," *Phys. Rev. D* **84** (2011) 044056, arXiv:1107.5264 [gr-qc].

[242] M. Bonetti and E. Barausse, "Post-Newtonian constraints on Lorentz-violating gravity theories with a MOND phenomenology," *Phys. Rev.* **D91** (2015) 084053, arXiv:1502.05554 [gr-qc]. [Erratum: Phys. Rev.D93,029901(2016)].

[243] T. P. Sotiriou, M. Visser, and S. Weinfurtner, "Quantum gravity without Lorentz invariance," *JHEP* **10** (2009) 033, arXiv:0905.2798 [hep-th].

[244] T. Jacobson, "Extended Horava gravity and Einstein-aether theory," *Phys. Rev.* **D81** (2010) 101502, arXiv:1001.4823 [hep-th]. [Erratum: Phys. Rev.D82,129901(2010)].

[245] J. Ben Achour, D. Langlois, and K. Noui, "Degenerate higher order scalar-tensor theories beyond Horndeski and disformal transformations," *Phys. Rev.* **D93** no. 12, (2016) 124005, arXiv:1602.08398 [gr-qc].

[246] D. Langlois and K. Noui, "Hamiltonian analysis of higher derivative scalar-tensor theories," *JCAP* **1607** (2016) 016, arXiv:1512.06820 [gr-qc].

[247] M. Crisostomi, M. Hull, K. Koyama, and G. Tasinato, "Horndeski: beyond, or not beyond?," *JCAP* **1603** (2016) 038, arXiv:1601.04658 [hep-th].

[248] H. Motohashi, K. Noui, T. Suyama, M. Yamaguchi, and D. Langlois, "Healthy degenerate theories with higher derivatives," *JCAP* **1607** (2016) 033, arXiv:1603.09355 [hep-th].

[249] R. Klein and D. Roest, "Exorcising the Ostrogradsky ghost in coupled systems," *JHEP* **07** (2016) 130, arXiv:1604.01719 [hep-th].

[250] M. Crisostomi, R. Klein, and D. Roest, "Higher Derivative Field Theories: Degeneracy Conditions and Classes," *JHEP* **06** (2017) 124, arXiv:1703.01623 [hep-th].

[251] J. D. Bekenstein, "The Relation between physical and gravitational geometry," *Phys. Rev.* **D48** (1993) 3641–3647, arXiv:gr-qc/9211017 [gr-qc].

[252] B. Z. Foster, "Metric redefinitions in Einstein-Aether theory," *Phys. Rev.* **D72** (2005) 044017, arXiv:gr-qc/0502066 [gr-qc].

[253] D. Blas and H. Sanctuary, "Gravitational Radiation in Horava Gravity," *Phys. Rev.* **D84** (2011) 064004, arXiv:1105.5149 [gr-qc].

[254] A. Emir Gumrukcuoglu, M. Saravani, and T. P. Sotiriou, "Hořava gravity after GW170817," *Phys. Rev.* **D97** no. 2, (2018) 024032, arXiv:1711.08845 [gr-qc].

[255] O. Ramos and E. Barausse, "Constraints on Hořava gravity from binary black hole observations," *Phys. Rev.* **D99** no. 2, (2019) 024034, arXiv:1811.07786 [gr-qc].

[256] E. Barausse, "Neutron star sensitivities in Horava gravity after GW170817," *Phys. Rev. D* **100** no. 8, (2019) 084053, arXiv:1907.05958 [gr-qc].

[257] S. Mukohyama, "Dark matter as integration constant in Horava-Lifshitz gravity," *Phys. Rev. D* **80** (2009) 064005, arXiv:0905.3563 [hep-th].

[258] C. Clarkson, G. Ellis, J. Larena, and O. Umeh, "Does the growth of structure affect our dynamical models of the universe? The averaging, backreaction and fitting problems in cosmology," *Rept. Prog. Phys.* **74** (2011) 112901, arXiv:1109.2314 [astro-ph.CO].

[259] R. L. Arnowitt, S. Deser, and C. W. Misner, "Dynamical Structure and Definition of Energy in General Relativity," *Phys. Rev.* **116** (1959) 1322–1330.

[260] R. L. Arnowitt, S. Deser, and C. W. Misner, "The Dynamics of general relativity," *Gen. Rel. Grav.* **40** (2008) 1997–2027, arXiv:gr-qc/0405109.